





RECEIVED: February 7, 2024

REVISED: April 30, 2024

ACCEPTED: June 25, 2024

PUBLISHED: July 10, 2024

Jettiness formulation of the MINNLO_{PS} method

Markus Ebert ^a, Luca Rottoli ^b, Marius Wiesemann ^a, Giulia Zanderighi ^{a,c}
and Silvia Zanolì ^{a,d}

^aMax-Planck-Institut für Physik,
Boltzmannstr. 8 D-85748 Garching, Germany

^bUniversity of Zurich,
Winterthurerstrasse 190, 8057 Zurich, Switzerland

^cPhysik-Department, Technische Universität München,
James-Frank-Strasse 1, 85748 Garching, Germany

^dRudolf Peierls Centre for Theoretical Physics, Clarendon Laboratory, University of Oxford,
Parks Road, Oxford OX1 3PU, U.K.

E-mail: ebert@mpp.mpg.de, luca.rottoli@uzh.ch,
marius.wiesemann@mpp.mpg.de, zanderi@mpp.mpg.de,
silvia.zanoli@physics.ox.ac.uk

ABSTRACT: We present a new formulation of the MINNLO_{PS} method to match NNLO QCD calculations with parton showers by using jettiness as a resummation variable. The full derivation for colour-singlet processes is presented using 0-jettiness starting from the NNLL' resummation formula. We show phenomenological results for Drell-Yan and Higgs-boson production at the LHC and compare our predictions to ATLAS and CMS data. Differences to the original MINNLO_{PS} formulation using the transverse momentum of the colour singlet as resummation variable are discussed. We further present a comparison of MINNLO_{PS} predictions with GENEVA. Finally, we extend the formulation of the MINNLO_{PS} method to 1-jettiness which is applicable to processes with a colour singlet plus one jet in the final state.

KEYWORDS: Higher-Order Perturbative Calculations, Parton Shower, Resummation

ARXIV EPRINT: [2402.00596](https://arxiv.org/abs/2402.00596)

Contents

1	Introduction	1
2	MINNLO_{PS} in a nutshell	3
3	Formulation of the MINNLO_{PS} method using 0-jettiness	5
3.1	Review of \mathcal{T}_0 factorization and evolution	5
3.2	Making contact with the MINNLO _{PS} method	9
3.3	Derivation of the MINNLO _{PS} master formula for \mathcal{T}_0	13
3.4	Matching with the shower	16
4	Validation and phenomenological results	17
4.1	Setup	18
4.2	Comparison and validation against MINNLO _{PS} - p_T results	19
4.3	Comparison to GENEVA results for Drell-Yan production	24
4.4	Comparison against ATLAS and CMS data for Drell-Yan production	26
5	Conclusions	29
A	Explicit formulae for MINNLO_{PS}-\mathcal{T}_0	30
B	Phase space parametrisation for the $D^{(\geq 3)}[\mathcal{T}_0]$ term	33
B.1	Evaluation of F_ℓ^{corr}	34
B.2	Analytic solution of the phase-space constraints	36
B.3	Application to p_T	38
C	MINNLO_{PS} for colour-singlet plus jet production using 1-jettiness	39
C.1	Review of \mathcal{T}_1 factorization and evolution	39
C.2	MINNLO _{PS} formalism based on \mathcal{T}_1	45

1 Introduction

Accurate simulations have become the theoretical cornerstone of many physics analyses at the Large Hadron Collider (LHC) today. They are mandatory not only in the context of precise Standard-Model (SM) measurements, but also instrumental for new-physics searches, especially when looking for small deviations or when providing cross-section limits on beyond-SM (BSM) signatures.

The last ten years have seen an enormous progress in the development of hadron-level event generators that include already corrections up to next-to-next-to-leading order (NNLO) in QCD perturbation theory. To this end, several methods have been developed to match NNLO QCD calculations with parton showers (NNLO+PS). The two main approaches today are the MINNLO_{PS} [1, 2] and GENEVA [3–5] ones. Among the existing NNLO+PS methods

the MINNLO_{PS} one is a notable exception, as it was not only applied to several complex colour-singlet processes [6–13], but it was also extended to the case of heavy-quark pair production [14–16], i.e. processes with colour charges both in the initial and in the final state. Nevertheless, there are several other classes of processes for which NNLO+PS predictions are becoming absolutely crucial in view of the vast progression of the LHC data taking by the experiments. One important class of processes is the one that includes light jets in the final state, such as colour-singlet plus jet production. Although NNLO predictions have been known for this type of processes for several years, in particular for Higgs+jet [17–20], V +jet [21–25], VH +jet [26] (V being a vector boson), and even $\gamma\gamma$ +jet [27], the consistent combination with parton showers is still an open problem.

Current NNLO+PS approaches, such as MINNLO_{PS} [1, 2] or GENEVA [3–5], rely on a suitable jet-resolution variable to separate events at the respective Born level from those with one extra radiation, similar to those NNLO approaches that perform a slicing in such jet-resolution variable to reach NNLO accuracy, like q_T subtraction [28] or N -jettiness subtraction [29, 30], or the more recent subtraction based on p_T -veto [31]. In order to formulate an NNLO(+PS) method, the resummation ingredients of the jet-resolution variable need to be known to a sufficiently large order in the logarithmic expansion. In principle, there is a suitable jet-resolution variable for colour-singlet plus jet processes, namely 1-jettiness (\mathcal{T}_1), for which a factorization theorem has been derived using soft-collinear effective theory (SCET) [32–36] and whose resummation is known at N³LL [37], using the resummation ingredients obtained in refs. [30, 38–41]. In fact, \mathcal{T}_1 has already been used to obtain NNLO predictions through slicing for this class of processes [17, 18, 21, 24, 25]. Although the use of jettiness-like observables in the context of a fully exclusive Monte-Carlo simulation poses some challenges, especially related to preserving the parton shower accuracy, at the moment \mathcal{T}_1 is the only observable for which all the resummation ingredients for an NNLO+PS matching are currently available. Therefore, it provides our best chance to obtain NNLO+PS predictions for colour-singlet plus jet production in a relatively short time period.

As a first step, it is instructive to derive an NNLO+PS approach for inclusive colour-singlet production based on the 0-jettiness (\mathcal{T}_0) variable. This variable has been used to achieve NNLO+PS accuracy within the GENEVA formalism for a variety of processes [42–48]. In this paper, we reformulate the MINNLO_{PS} method in terms of \mathcal{T}_0 as an alternative to the transverse momentum of the colour-singlet final state (p_T), and obtain a new implementation for Higgs-boson and vector-boson production at NNLO+PS accuracy. Our results can be compared directly to the previous MINNLO_{PS} generators that were built using p_T resummation [1, 2]. We will show that, despite the fact that for MINNLO_{PS}- \mathcal{T}_0 the leading logarithmic accuracy in our showered predictions is not fully preserved, we find remarkable agreement for vector-boson production before and after including parton-shower effects. For Higgs-boson production, on the other hand, only NNLO quantities, i.e. the Higgs rapidity, are in good agreement, while we find larger differences in jet-related quantities (formally described at NLO QCD accuracy). In addition, we also compare our predictions to results obtained using the GENEVA method (both for \mathcal{T}_0 and p_T), finding very good agreement in all NNLO quantities. The development of a MINNLO_{PS} framework for \mathcal{T}_1 closely parallels our derivation for \mathcal{T}_0 , and we provide the corresponding derivation and formulae in appendix C.

The result for \mathcal{T}_1 introduces additional complications due to the extra radiation, which generates logarithmic terms that are absent in the cases of \mathcal{T}_0 or p_T .

This paper is organized as follows: First, we briefly recall the MINNLO_{PS} formalism based on p_T in section 2. Then, we derive a new formulation of MINNLO_{PS} using \mathcal{T}_0 in section 3, where we review the factorization/resummation formula for \mathcal{T}_0 (section 3.1), recast it into a form suitable for the MINNLO_{PS} approach (section 3.2), obtain the MINNLO_{PS} master formula for \mathcal{T}_0 (section 3.3) and discuss the shower accuracy (section 3.4). In section 4, after presenting our setup (section 4.1), we compare our new MINNLO_{PS}- \mathcal{T}_0 results against MINNLO_{PS}- p_T predictions (section 4.2) for vector-boson and Higgs-boson production, study the difference between MINNLO_{PS} and GENEVA predictions using both resummation variables for vector-boson production (section 4.3) and present a comparison to ATLAS and CMS data (section 4.4). We summarize our findings in section 5. In appendix A all relevant resummation ingredients for \mathcal{T}_0 are provided, in appendix B we discuss how higher-order resummation terms are spread over the inclusive phase space, and in appendix C we present the derivation of the MINNLO_{PS} approach for \mathcal{T}_1 .

2 MINNLO_{PS} in a nutshell

The MINNLO_{PS} method [1, 2] formulates a fully differential calculation in the Born phase space Φ_F at NNLO QCD accuracy of a produced final state F with invariant mass Q and combines it consistently with multi-parton radiation effects from parton shower. MINNLO_{PS} has been formulated thus far for colour-singlet production [1, 2] and for heavy-quark pair production [14, 15], based on the transverse momentum (p_T) of F as a matching variable in both cases. Here, we focus on the colour-singlet case and, when specific to the original formulation based on p_T resummation, we will refer to it as MINNLO_{PS}- p_T from now on.

MINNLO_{PS} starts from a differential description of the production of the colour singlet and a jet (FJ) at NLO matched to parton showers, which is obtained via the POWHEG approach [49–51] as

$$\frac{d\sigma}{d\Phi_{FJ}} = \bar{B}(\Phi_{FJ}) \times \left\{ \Delta_{\text{pwg}}(\Lambda_{\text{pwg}}) + \int d\Phi_{\text{rad}} \Delta_{\text{pwg}}(p_{T,\text{rad}}) \frac{R(\Phi_{FJ}, \Phi_{\text{rad}})}{B(\Phi_{FJ})} \right\}, \quad (2.1)$$

where MINNLO_{PS} modifies the content of the MINLO' $\bar{B}(\Phi_{FJ})$ function [52], which generates the first radiation (inclusive over the second one), to achieve NNLO QCD accuracy. By contrast, the content of the curly brackets, which describes the exclusive generation of the second radiation according to the POWHEG method, is not modified by the MINNLO_{PS} procedure. Here, Φ_{FJ} denotes the FJ phase space, and B and R are the squared tree-level matrix elements for FJ and FJJ production, respectively. Δ_{pwg} is the usual POWHEG Sudakov form factor [49] (with a lower cutoff of $\Lambda_{\text{pwg}} = 0.89 \text{ GeV}$) and the phase space (transverse momentum) of the second radiation is denoted as $\Phi_{\text{rad}}(p_{T,\text{rad}})$. Extra radiation beyond the second one is added by the consistent matching to the parton shower achieved through POWHEG.

The modification of the $\bar{B}(\Phi_{FJ})$ function is the central ingredient of MINNLO_{PS}. For MINNLO_{PS}- p_T , its derivation [1] stems from the description of the NNLO cross section

differential in the p_T of the colour singlet and in the Born phase space Φ_F , which can be expressed as

$$\frac{d\sigma}{d\Phi_F dp_T} = \frac{d}{dp_T} \left\{ \exp[-\tilde{\mathcal{S}}(p_T)] \mathcal{L}(p_T) \right\} + R_f(p_T) = \exp[-\tilde{\mathcal{S}}(p_T)] \left\{ D(p_T) + \frac{R_f(p_T)}{\exp[-\tilde{\mathcal{S}}(p_T)]} \right\}, \quad (2.2)$$

where R_f contains the non-singular terms in the $p_T \rightarrow 0$ limit, and

$$D(p_T) \equiv -\frac{d\tilde{\mathcal{S}}(p_T)}{dp_T} \mathcal{L}(p_T) + \frac{d\mathcal{L}(p_T)}{dp_T}. \quad (2.3)$$

$\tilde{\mathcal{S}}(p_T)$ represents the Sudakov form factor in p_T , while $\mathcal{L}(p_T)$ contains the parton luminosities, the squared hard matrix elements for the underlying F production process up to two loops as well as the collinear coefficient functions at NNLO (see ref. [1] for further details). A crucial feature of the MINNLO_{PS- p_T} procedure is that the renormalization and factorization scales are set to $\mu_R \sim \mu_F \sim p_T$.

Let us introduce the NLO differential cross section for FJ production as

$$\frac{d\sigma_{\text{FJ}}^{(\text{NLO})}}{d\Phi_F dp_T} = \frac{\alpha_s(p_T)}{2\pi} \left[\frac{d\sigma_{\text{FJ}}}{d\Phi_F dp_T} \right]^{(1)} + \left(\frac{\alpha_s(p_T)}{2\pi} \right)^2 \left[\frac{d\sigma_{\text{FJ}}}{d\Phi_F dp_T} \right]^{(2)}, \quad (2.4)$$

with $[X]^{(i)}$ being the coefficient of the i -th term in the perturbative expansion of the quantity X , so that we can write the non-singular terms as

$$R_f = \frac{d\sigma_{\text{FJ}}^{(\text{NLO})}}{d\Phi_F dp_T} - \frac{\alpha_s(p_T)}{2\pi} \left[\exp[-\tilde{\mathcal{S}}(p_T)] D(p_T) \right]^{(1)} - \left(\frac{\alpha_s(p_T)}{2\pi} \right)^2 \left[\exp[-\tilde{\mathcal{S}}(p_T)] D(p_T) \right]^{(2)}. \quad (2.5)$$

Now, we can rewrite eq. (2.2) as

$$\begin{aligned} \frac{d\sigma}{d\Phi_F dp_T} = \exp[-\tilde{\mathcal{S}}(p_T)] & \left\{ \frac{\alpha_s(p_T)}{2\pi} \left[\frac{d\sigma_{\text{FJ}}}{d\Phi_F dp_T} \right]^{(1)} \left(1 + \frac{\alpha_s(p_T)}{2\pi} [\tilde{\mathcal{S}}(p_T)]^{(1)} \right) \right. \\ & + \left(\frac{\alpha_s(p_T)}{2\pi} \right)^2 \left[\frac{d\sigma_{\text{FJ}}}{d\Phi_F dp_T} \right]^{(2)} + \left[D(p_T) - \frac{\alpha_s(p_T)}{2\pi} [D(p_T)]^{(1)} - \left(\frac{\alpha_s(p_T)}{2\pi} \right)^2 [D(p_T)]^{(2)} \right] \\ & \left. + \text{regular terms of } \mathcal{O}(\alpha_s^3) \right\}. \end{aligned} \quad (2.6)$$

This formula includes all relevant terms needed to reach NNLO QCD accuracy. In particular, upon integration over p_T from scales of the order of the Landau pole Λ to the kinematic upper bound, it reproduces the fully differential NNLO cross section up to terms beyond accuracy.

Each term of eq. (2.6) contributes to the integrated cross section with scales $\mu_R \sim \mu_F \sim Q$ according to the power counting formula

$$\int_{\Lambda}^Q dp_T \frac{1}{p_T} \alpha_s^m(p_T) \ln^n \frac{Q}{p_T} \exp(-\tilde{\mathcal{S}}(p_T)) \approx \mathcal{O} \left(\alpha_s^{m - \frac{n+1}{2}}(Q) \right). \quad (2.7)$$

Here, it is crucial to understand that for MINNLO_{PS- p_T} at most an extra single logarithm appears in the formula due to the choice $\mu_R \sim \mu_F \sim p_T$, therefore $n \leq 1$. As a consequence,

the truncation of (2.6) beyond second order, i.e. all terms including those up to $\alpha_s^2(p_T)$, is NLO accurate in the Φ_F phase space, which corresponds to MINLO' [52] accuracy, while the terms at third order in $\alpha_s(p_T)$ and beyond in the square brackets are the crucial ingredients to reach NNLO accuracy in Φ_F . Moreover, one can expand the square bracket in the second line of eq. (2.6) and neglect terms that produce N³LO corrections or beyond upon integration over p_T , to any inclusive observable in Φ_F . One can therefore, in principle, truncate the second line of eq. (2.6) to third order in $\alpha_s(p_T)$

$$\begin{aligned}
 D^{(\geq 3)}(p_T) &= D(p_T) - \frac{\alpha_s(p_T)}{2\pi} [D(p_T)]^{(1)} - \left(\frac{\alpha_s(p_T)}{2\pi}\right)^2 [D(p_T)]^{(2)} \\
 &= \left(\frac{\alpha_s(p_T)}{2\pi}\right)^3 [D(p_T)]^{(3)} + \mathcal{O}(\alpha_s^4(p_T)).
 \end{aligned}
 \tag{2.8}$$

Nevertheless, in order to preserve the full total derivative of our starting equation eq. (2.2), and to keep terms beyond accuracy generated by the total derivative, it is preferable not to perform such a truncation, although formally valid, as pointed out in ref. [2].

The MINNLO_{PS- p_T} procedure can be applied directly at the fully differential level in the Φ_{FJ} phase space to the $\bar{B}(\Phi_{FJ})$ function in eq. (2.1) [1]:

$$\begin{aligned}
 \bar{B}(\Phi_{FJ}) &\equiv \exp[-\tilde{\mathcal{S}}(p_T)] \left\{ \frac{\alpha_s(p_T)}{2\pi} \left[\frac{d\sigma_{FJ}}{d\Phi_{FJ}} \right]^{(1)} \left(1 + \frac{\alpha_s(p_T)}{2\pi} [\tilde{\mathcal{S}}(p_T)]^{(1)} \right) \right. \\
 &\quad \left. + \left(\frac{\alpha_s(p_T)}{2\pi}\right)^2 \left[\frac{d\sigma_{FJ}}{d\Phi_{FJ}} \right]^{(2)} + D^{(\geq 3)}(p_T) F^{\text{corr}}(\Phi_{FJ}) \right\},
 \end{aligned}
 \tag{2.9}$$

where the factor $F^{\text{corr}}(\Phi_{FJ})$ encodes a suitable function needed to spread the correction $D^{(\geq 3)}(p_T)$, which intrinsically depends only on p_T and Φ_F , on the full Φ_{FJ} phase space, as discussed in detail in section 3 of ref. [1].

3 Formulation of the MINNLO_{PS} method using 0-jettiness

In this section, we derive the MINNLO_{PS} master formula for colour-singlet production using \mathcal{T}_0 factorization and resummation as formulated in SCET. From now on, we will refer to this new formulation of the MINNLO_{PS} method as MINNLO_{PS- \mathcal{T}_0} . Our derivation follows the strategy of the MINNLO_{PS} method based on p_T . In order to perform the MINNLO_{PS- \mathcal{T}_0} derivation we start by reviewing \mathcal{T}_0 factorization and resummation as formulated in SCET in section 3.1. Then, in section 3.2, we bring it into a form that makes it suitable to make contact with the MINNLO_{PS} approach and we derive the MINNLO_{PS- \mathcal{T}_0} master formula in section 3.3. Finally, we discuss the accuracy of the parton shower in section 3.4.

3.1 Review of \mathcal{T}_0 factorization and evolution

We begin by reviewing the SCET resummation formalism for 0-jettiness (\mathcal{T}_0), also known as beam thrust. The infrared-safe 0-jet resolution variable \mathcal{T}_0 was originally introduced in ref. [53], and extended to N -jet processes in ref. [54]. Following the notation of ref. [55], it is defined as

$$\mathcal{T}_0 = \sum_k \min \left\{ \frac{2q_a \cdot p_k}{Q_a}, \frac{2q_b \cdot p_k}{Q_b} \right\}.
 \tag{3.1}$$

Here, the sum runs over all hadronic final states (excluding decay products of the identified colour-singlet final state), p_k are their momenta, and q_a and q_b are the momenta of the colliding partons. Aligning the incoming hadrons along the directions

$$n^\mu = (1, 0, 0, 1), \quad \bar{n}^\mu = (1, 0, 0, -1), \quad (3.2)$$

the incoming parton momenta can be written as

$$q_a^\mu = Q e^Y \frac{n^\mu}{2}, \quad q_b^\mu = Q e^{-Y} \frac{\bar{n}^\mu}{2}, \quad (3.3)$$

where Q and Y are the invariant mass and rapidity of the colour-singlet final state, respectively. Finally, $Q_{a,b}$ in eq. (3.1) are normalization factors giving rise to different definitions of \mathcal{T}_0 . The most common choices are [53, 54]

$$\begin{aligned} \text{leptonic } \mathcal{T}_0 : \quad & Q_a = Q_b = Q, \quad \mathcal{T}_0^{\text{lep}} = \sum_k \min\{e^{+Y} n \cdot p_k, e^{-Y} \bar{n} \cdot p_k\}, \\ \text{hadronic } \mathcal{T}_0 : \quad & Q_{a,b} = Q e^{\pm Y}, \quad \mathcal{T}_0^{\text{cm}} = \sum_k \min\{n \cdot p_k, \bar{n} \cdot p_k\}. \end{aligned} \quad (3.4)$$

It has been shown that the power corrections to the hadronic definition are exponentially enhanced in Y [56–58]. This is compensated for in the leptonic definition by the explicit $e^{\pm Y}$ factors, which is thus the preferred choice and which we will use throughout this paper.

In the kinematic limit $\mathcal{T}_0 \rightarrow 0$, all hadronic momenta p_k must be either soft or collinear to the incoming partons to yield a negligible contribution to the sum in eq. (3.1). Based on this observation, a factorization formula¹ was derived in refs. [53, 54] using SCET. It can be written as

$$\begin{aligned} \frac{d\sigma}{d\Phi_F d\mathcal{T}_0} &= \frac{d\sigma^{\text{sing}}}{d\Phi_F d\mathcal{T}_0} \times [1 + \mathcal{O}((\mathcal{T}_0/Q)^m)], \\ \frac{d\sigma^{\text{sing}}}{d\Phi_F d\mathcal{T}_0} &= \sum_{a,b} \frac{d|\mathcal{M}_{ab}|^2}{d\Phi_F} H_{ab}(Q, \mu) \int dt_a dt_b B_a(t_a, x_a, \mu) B_b(t_b, x_b, \mu) S\left(\mathcal{T}_0 - \frac{t_a}{Q_a} - \frac{t_b}{Q_b}, \mu\right), \end{aligned} \quad (3.5)$$

where we are differential both in \mathcal{T}_0 and in the Born phase space Φ_F . As indicated, the factorization holds up to power corrections in \mathcal{T}_0/Q , with $m = 1$ for inclusive processes without any cuts and $m = 1/2$ for selection cuts which break azimuthal symmetry, see for instance ref. [60]. The sum runs over all flavour combinations a and b contributing to the Born process, where \mathcal{M}_{ab} is the corresponding matrix element and the hard function H_{ab} encodes virtual corrections to it. The beam functions $B_{a,b}$ encode the effect of radiation close the incoming protons, and they are convolved (integral over t_a and t_b) against the soft function S encoding soft radiation. The soft function differs between quark and gluon-induced processes, which is kept implicit in eq. (3.5), but it is independent of the quark flavour in the massless case. Finally, $x_{a,b} = Q e^{\pm Y} / E_{\text{cm}}$ are the Bjorken variables in the Born kinematics, and the renormalization and factorization scales are denoted by μ . Note that all perturbative ingredients depend on the process under consideration (quark versus gluon initiated), but the form of the equations is the same, therefore we leave this dependence implicit.²

¹Starting at $\mathcal{O}(\alpha_s^4)$, the factorization is violated by Glauber contributions [59].

²In the case of p_T factorization there are additional collinear correlation functions [61] for gluon-initiated processes starting at NNLO, which are absent in the case of \mathcal{T}_0 due to the scalar nature of this observable.

While it is standard in the literature to discuss \mathcal{T}_0 in momentum space, here we perform a Fourier transform with respect to $y = y - i0$ to turn the convolution in eq. (3.5) into a simple product, similar to the usual treatment in p_T factorization. This yields

$$\frac{d\sigma^{\text{sing}}}{d\Phi_F d\mathcal{T}_0} = \sum_{a,b} \frac{d|\mathcal{M}_{ab}|^2}{d\Phi_F} H_{ab}(Q, \mu) \int \frac{dy}{2\pi} e^{iy\mathcal{T}_0} B_a\left(\frac{y}{Q_a}, x_a, \mu\right) B_b\left(\frac{y}{Q_b}, x_b, \mu\right) S(y, \mu), \quad (3.6)$$

where the Fourier transformed beam and soft functions are defined as

$$B_j(y, x, \mu) = \int dt e^{-ity} B_j(t, x, \mu), \quad S(y, \mu) = \int d\mathcal{T} e^{-i\mathcal{T}y} S(\mathcal{T}, \mu). \quad (3.7)$$

Note that the arguments of B_j and S have different mass dimensions due to geometric measures, which in eq. (3.6) we have put back into the arguments of the beam functions.

In Fourier space, the hard, beam and soft functions obey the following renormalization group equations (RGEs):³

$$\begin{aligned} \frac{d}{d \ln \mu} \ln H_{ab}(Q, \mu) = \gamma_H(Q^2, \mu) &= 2\Gamma_C[\alpha_s(\mu)] \ln \frac{Q^2}{\mu^2} + \gamma_H[\alpha_s(\mu)], \\ \frac{d}{d \ln \mu} \ln B_i\left(\frac{y}{Q_i}, x, \mu\right) = \gamma_B\left(\frac{y}{Q_i}, \mu\right) &= 2\Gamma_C[\alpha_s(\mu)] \ln \frac{y\mu^2}{y_0 Q_i} + \gamma_B[\alpha_s(\mu)], \\ \frac{d}{d \ln \mu} \ln S(y, \mu) = \gamma_S(y, \mu) &= -4\Gamma_C[\alpha_s(\mu)] \ln \frac{y\mu}{y_0} + \gamma_S[\alpha_s(\mu)]. \end{aligned} \quad (3.8)$$

Here, Γ_C is the cusp anomalous dimension, and $\gamma_{H,B,S}$ are the hard, beam and soft non-cusp anomalous dimensions, respectively. For brevity, we also defined the constant

$$y_0 = -ie^{-\gamma_E} \quad (3.9)$$

appearing in the logarithms, where γ_E is the Euler-Mascheroni constant. Note that due to the Fourier transform, the beam anomalous dimension explicitly depends on the measure Q_i , which in momentum space only appears in the convolution in eq. (3.5). Finally, the overall μ independence implies that

$$\gamma_H(\alpha_s) + 2\gamma_B(\alpha_s) + \gamma_S(\alpha_s) = 0, \quad (3.10)$$

as well as $Q_a Q_b = Q^2$, which is fulfilled for both hadronic and leptonic \mathcal{T}_0 .

It is clear from eq. (3.8) that the hard, beam and soft functions contain large logarithms that can be minimized using the scale choices

$$\mu_H = Q, \quad \mu_B = \sqrt{\frac{Qy_0}{y}} = \sqrt{\mu_H \mu_S}, \quad \mu_S = \frac{y_0}{y}, \quad (3.11)$$

for H , B and S , respectively. Note that for generic measures $Q_a \neq Q_b$, this would leave potentially large logarithms $\ln(Q/Q_i)$ in the individual beam functions B_i , which however is absent for our preferred choice $\mathcal{T}_0^{\text{lep}}$. By solving eq. (3.8), we can evolve all functions

³For processes such as Higgs production, \mathcal{M}_{ab} also carries a scale dependence, which would be compensated by changing γ_H accordingly. Alternatively, which shall be our default choice in this work, one can always simultaneously evolve $|\mathcal{M}_{ab}|^2$ and H_{ab} , which leaves γ_H unchanged.

appearing in eq. (3.6) from their natural scales in eq. (3.11) to a common scale μ , which resums large logarithms $\ln(Q/\mathcal{T}_0)$ appearing in the cross section. The resummed cross section is then given by

$$\begin{aligned} \frac{d\sigma^{\text{sing}}}{d\Phi_{\text{F}} d\mathcal{T}_0} &= \int \frac{dy}{2\pi} e^{iy\mathcal{T}_0} \sum_{a,b} \frac{d|\mathcal{M}_{ab}|^2}{d\Phi_{\text{F}}} H_{ab}(Q, \mu_H) B_a\left(\frac{y}{Q_a}, x_a, \mu_B\right) B_b\left(\frac{y}{Q_b}, x_b, \mu_B\right) S(y, \mu_S) \\ &\times \exp\left\{-\int_{\mu_B}^{\mu_H} \frac{d\mu'}{\mu'} \left[2\Gamma_{\text{C}}[\alpha_s(\mu')] \ln \frac{Q^2}{\mu'^2} + \gamma_H[\alpha_s(\mu')]\right]\right\} \\ &\times \exp\left\{-\int_{\mu_B}^{\mu_S} \frac{d\mu'}{\mu'} \left[-4\Gamma_{\text{C}}[\alpha_s(\mu')] \ln \frac{y\mu'}{y_0} + \gamma_S[\alpha_s(\mu')]\right]\right\}, \end{aligned} \quad (3.12)$$

where the two exponentials evolve the hard and soft functions from their natural scales μ_H and μ_S to the beam scale μ_B , respectively.

To bring this into a form suitable for the MINNLO_{PS} method, we first notice that for the hard and soft functions, using their natural scales, the coefficients in the perturbative expansion are constant,⁴ i.e.

$$\begin{aligned} \bar{H}_{ab}(Q) &\equiv H_{ab}(Q, \mu_H = Q) = \sum_{n=0}^{\infty} \left[\frac{\alpha_s(Q)}{2\pi}\right]^n H_{ab}^{(n)}, \\ \bar{S}(y_0/y) &\equiv S(y, \mu_S = y_0/y) = \sum_{n=0}^{\infty} \left[\frac{\alpha_s(y_0/y)}{2\pi}\right]^n S^{(n)}. \end{aligned} \quad (3.13)$$

We introduced the barred notation to define the series expansion of the hard and soft functions evaluated at their canonical scales, where the dependence on the scale is entirely contained in the running coupling. We can then express the first line in eq. (3.12) at a common scale, as used in the MINNLO_{PS} method. Since the beam scale μ_B enters the nonperturbative parton distribution functions (PDFs), it is natural to choose μ_B as this common scale. Thus, with some abuse of notation ($\bar{H}_{ab}(Q) \equiv \bar{H}_{ab}[\alpha_s(Q)]$ and $S(y_0/y) \equiv \bar{S}[\alpha_s(y_0/y)]$), we rewrite eq. (3.13) as

$$\begin{aligned} \bar{H}_{ab}(Q) &= \bar{H}_{ab}(\mu_B) \exp\left[\int_{\mu_B}^Q \frac{d\mu'}{\mu'} \gamma_{\bar{H}}[\alpha_s(\mu')]\right], \\ \bar{S}(y_0/y) &= \bar{S}(\mu_B) \exp\left[\int_{\mu_B}^{y_0/y} \frac{d\mu'}{\mu'} \gamma_{\bar{S}}[\alpha_s(\mu')]\right], \end{aligned} \quad (3.14)$$

where the induced anomalous dimensions are given by

$$\gamma_{\bar{F}}(\alpha_s) = 2\beta(\alpha_s) \frac{d \ln \bar{F}(\alpha_s)}{d\alpha_s} = -4\pi\beta_0 \frac{F^{(1)}}{F^{(0)}} \left(\frac{\alpha_s}{2\pi}\right)^2 + \mathcal{O}(\alpha_s^3), \quad (3.15)$$

for $\bar{F} = \bar{H}_{ab}$ or $\bar{F} = \bar{S}$. $\beta(\alpha_s)$ represents the QCD β function as defined in (A.1), and β_0 its first order coefficient given in (A.2). The beam functions can be related to the PDFs as

$$B_i\left(\frac{y}{Q_i}, x, \mu\right) = \sum_j \int_x^1 \frac{dx'}{x'} \mathcal{C}_{ij}\left(\frac{y}{Q_i}, x', \mu\right) f_j\left(\frac{x}{x'}, \mu\right) \equiv (\mathcal{C} \otimes f)_i\left(\frac{y}{Q_i}, x, \mu\right) z, \quad (3.16)$$

⁴For $2 \rightarrow 2$ or more complicated processes, the hard function constants actually have a nontrivial dependence on Φ_{F} , which we keep implicit.

where the \mathcal{C}_{ij} are perturbatively calculable coefficients. At their canonical scale, they read

$$\bar{\mathcal{C}}_{ij} \left(\frac{y}{Q_i}, x \right) \equiv \mathcal{C}_{ij} \left(\frac{y}{Q_i}, x, \mu_B \right) = \sum_{n=0}^{\infty} \left[\frac{\alpha_s(\mu_B)}{2\pi} \right]^n \mathcal{C}_{ij}^{(n)}(x), \quad (3.17)$$

with all dependence on y arising through $\alpha_s(\mu_B)$. Similar to the treatment commonly used in p_T resummation, where the beam and soft functions are combined into a transverse-momentum dependent PDF (TMDPDF), we absorb the \mathcal{T}_0 soft function with the beam function, and define

$$\bar{\mathcal{C}}_{ij} \left(\frac{y}{Q_i}, x \right) \equiv \bar{\mathcal{C}}_{ij} \left(\frac{y}{Q_i}, x, \mu_B \right) \sqrt{S(\mu_B)}. \quad (3.18)$$

Using eqs. (3.14)–(3.18) to rewrite eq. (3.12), we arrive at our final expression

$$\frac{d\sigma^{\text{sing}}}{d\Phi_F d\mathcal{T}_0} = \int \frac{dy}{2\pi} e^{iy\mathcal{T}_0} \mathcal{L}(y_0/y) e^{-S(y_0/y)}, \quad (3.19)$$

where the luminosity and Sudakov factor are defined as

$$\begin{aligned} \mathcal{L}(y_0/y) &= \sum_{a,b} \frac{d|\mathcal{M}_{ab}|^2}{d\Phi_F} \bar{H}_{ab}(\mu_B) (\bar{C} \otimes f)_a(x_a, \mu_B) (\bar{C} \otimes f)_b(x_b, \mu_B), \\ \mathcal{S}(y_0/y) &= 2 \int_{\mu_B}^{\mu_H} \frac{d\mu'}{\mu'} \left[A[\alpha_s(\mu')] \ln \frac{Q^2}{\mu'^2} + B_H[\alpha_s(\mu')] \right] \\ &\quad + 2 \int_{\mu_B}^{\mu_S} \frac{d\mu'}{\mu'} \left[A[\alpha_s(\mu')] \ln \frac{(y_0/y)^2}{\mu'^2} + B_S[\alpha_s(\mu')] \right]. \end{aligned} \quad (3.20)$$

In what follows, we will keep the dependence of the PDFs on the momentum fractions x_a and x_b and on μ_B implicit. Following the standard naming conventions in MINNLO_{PS}, the anomalous dimensions are labeled as A and B . They are related to the anomalous dimensions in eq. (3.8) by

$$A(\alpha_s) = \Gamma_C(\alpha_s), \quad B_F(\alpha_s) = \frac{1}{2} \gamma_F(\alpha_s) - \beta(\alpha_s) \frac{d \ln \bar{F}(\alpha_s)}{d\alpha_s}, \quad (3.21)$$

where $\bar{F} = \bar{H}$ for the hard function and $\bar{F} = \bar{S}$ for the soft function. Note that the structure of \mathcal{S} contains two distinct evolution kernels, and as such its structure differs from the Sudakov for p_T resummation, which can be written as a single kernel.

We expand the coefficients in eq. (3.21) as

$$A(\alpha_s) = \sum_{n=1}^{\infty} A^{(n)} \left(\frac{\alpha_s}{2\pi} \right)^n, \quad B_F(\alpha_s) = \sum_{n=1}^{\infty} B_F^{(n)} \left(\frac{\alpha_s}{2\pi} \right)^n. \quad (3.22)$$

Explicit results for all required coefficients are collected in appendix A.

3.2 Making contact with the MINNLO_{PS} method

We have already brought the \mathcal{T}_0 resummation formula into a form that is suitable to make contact with the MINNLO_{PS} method, see eqs. (3.19) and (3.20). We begin by taking the cumulant of eq. (3.19),

$$\frac{d\sigma^{\text{sing}}(\mathcal{T}_0)}{d\Phi_F} = \int_0^{\mathcal{T}_0} d\mathcal{T}'_0 \int \frac{dy}{2\pi} e^{iy\mathcal{T}'_0} \mathcal{L}(y_0/y) e^{-S(y_0/y)}, \quad (3.23)$$

which we expand around $y_0/y \sim \mathcal{T}_0$ in order to evaluate analytically the Fourier transform over dy . More precisely, we define our expansion through

$$L_y = \ln \frac{\mathcal{T}_0 y}{y_0} \ll 1. \quad (3.24)$$

Expanding the luminosity and Sudakov yields

$$\begin{aligned} \mathcal{L}(y_0/y) &= \mathcal{L}(\mathcal{T}_0) + L_y \mathcal{L}'(\mathcal{T}_0) + \frac{1}{2} L_y^2 \mathcal{L}''(\mathcal{T}_0) + \dots, \\ e^{-S(y_0/y)} &= e^{-S(\mathcal{T}_0) - L_y S'(\mathcal{T}_0)} \left[1 - \frac{1}{2} L_y^2 S''(\mathcal{T}_0) - \frac{1}{6} L_y^3 S'''(\mathcal{T}_0) + \dots \right], \end{aligned} \quad (3.25)$$

where the derivatives of an arbitrary function f are defined as

$$f^{(n)} = \frac{d^n f}{d^n \ln(1/\mathcal{T}_0)} = (-1)^n \frac{d^n f}{d^n \ln \mathcal{T}_0}, \quad \text{with } f' \equiv f^{(1)}, f'' \equiv f^{(2)}, f''' \equiv f^{(3)}, \dots \quad (3.26)$$

By evaluating the integral of the cumulant using

$$\int_0^{\mathcal{T}_0} d\mathcal{T}' \int \frac{dy}{2\pi} e^{i\mathcal{T}'_0 y} L_y^n e^{-S' L_y} = (-1)^n \partial_{S'}^n \frac{e^{-\gamma_E S'}}{\Gamma(1+S')}, \quad (3.27)$$

and by truncating eq. (3.23) at NNLO accuracy, we obtain

$$\begin{aligned} \frac{d\sigma^{\text{sing}}(\mathcal{T}_0)}{d\Phi_F} &= e^{-S(\mathcal{T}_0)} \left[\mathcal{L}(\mathcal{T}_0) \left(1 - \frac{1}{2} \partial_{S'}^2 S'' + \frac{1}{6} \partial_{S'}^3 S''' + \frac{1}{8} \partial_{S'}^4 (S'')^2 \right) \right. \\ &\quad \left. + \mathcal{L}'(\mathcal{T}_0) \left(-\partial_{S'} + \frac{1}{2} \partial_{S'}^3 S'' \right) + \frac{1}{2} \partial_{S'}^2 \mathcal{L}''(\mathcal{T}_0) + \mathcal{O}(\alpha_s^3) \right] \frac{e^{-\gamma_E S'}}{\Gamma(1+S')}. \end{aligned} \quad (3.28)$$

Here we used that the power counting in terms of the strong coupling constant is given by:

$$S' = \mathcal{O}(\alpha_s), \quad S'' = \mathcal{O}(\alpha_s), \quad S''' = \mathcal{O}(\alpha_s^2), \quad \mathcal{L}' = \mathcal{O}(\alpha_s), \quad \mathcal{L}'' = \mathcal{O}(\alpha_s^2). \quad (3.29)$$

Expanding also the Gamma factor in eq. (3.28) and taking the partial derivatives with respect to S' , we arrive at

$$\begin{aligned} \frac{d\sigma^{\text{sing}}(\mathcal{T}_0)}{d\Phi_F} &= e^{-S(\mathcal{T}_0)} \left[\mathcal{L}(\mathcal{T}_0) \left(1 - \frac{\zeta_2}{2} [(S')^2 - S''] - \zeta_3 S' S'' + \frac{3\zeta_4}{16} (S'')^2 + \frac{\zeta_3}{3} S''' \right) \right. \\ &\quad \left. + \mathcal{L}'(\mathcal{T}_0) (\zeta_2 S' + \zeta_3 S'') - \frac{\zeta_2}{2} \mathcal{L}''(\mathcal{T}_0) + \mathcal{O}(\alpha_s^3) \right]. \end{aligned} \quad (3.30)$$

The terms in square brackets are to be understood as an expansion in $\alpha_s(\mu_B)$ with $\mu_B = \sqrt{Q\mathcal{T}_0}$, since μ_B defined in eq. (3.11) has also been expanded around \mathcal{T}_0 .

Before proceeding, we note that eq. (3.30) has a much richer structure than its counterpart in $\text{MINNLO}_{\text{PS-}p_T}$. The reason is that the analog of eq. (3.27) in p_T has a much simpler expansion itself. Most notably, for $\text{MINNLO}_{\text{PS-}p_T}$ one does not encounter the \mathcal{L}'' term, which will have a significant impact on our final formula, and there are fewer S' terms in the coefficients of \mathcal{L} and \mathcal{L}' .

Our goal is to write eq. (3.30) in the form

$$\frac{d\sigma^{\text{sing}}(\mathcal{T}_0)}{d\Phi_F} = \tilde{\mathcal{L}}(\mathcal{T}_0) e^{-S(\mathcal{T}_0)}, \quad (3.31)$$

which has the same structure as the singular part of the starting formula in eq. (2.2) of the MINNLO_{PS-p_T} method. Thus, bringing the \mathcal{T}_0 resummation formula into that form allows us to follow the same subsequent steps when deriving the MINNLO_{PS- \mathcal{T}_0} formalism. Similar to MINNLO_{PS-p_T} this can be achieved by absorbing the additional terms in square brackets in eq. (3.30) into a redefinition of the Sudakov factor and the luminosity. Evaluating the derivatives of \mathcal{S} in eq. (3.30), we obtain the expression

$$\begin{aligned} \frac{d\sigma^{\text{sing}}(\mathcal{T}_0)}{d\Phi_{\text{F}}} = e^{-\mathcal{S}(\mathcal{T}_0)} & \left\{ \mathcal{L}(\mathcal{T}_0) \left[1 + \frac{\alpha_s}{2\pi} c_{1,0} + \left(\frac{\alpha_s}{2\pi} \right)^2 (c_{2,2} L_{\mathcal{T}}^2 + c_{2,1} L_{\mathcal{T}} + c_{2,0}) \right] \right. \\ & + \mathcal{L}'(\mathcal{T}_0) \left[\frac{\alpha_s}{2\pi} (c'_{1,1} L_{\mathcal{T}} + c'_{1,0}) \right] \\ & \left. + \mathcal{L}''(\mathcal{T}_0) c''_{0,0} + \mathcal{O}(\alpha_s^3) \right\}. \end{aligned} \quad (3.32)$$

Here and in the following, we always use the abbreviations

$$\alpha_s = \alpha_s(\sqrt{Q\mathcal{T}_0}), \quad L_{\mathcal{T}} = \frac{1}{2} \ln \frac{Q}{\mathcal{T}_0}. \quad (3.33)$$

The constants appearing in eq. (3.32) are given by

$$\begin{aligned} c_{1,0} &= A^{(1)} \zeta_2, \\ c_{2,2} &= -8[A^{(1)}]^2 \zeta_2, \\ c_{2,1} &= -8[A^{(1)}]^2 \zeta_3 + 4A^{(1)} \zeta_2 (B_S^{(1)} - B_H^{(1)}) + 8\pi\beta_0 A^{(1)} \zeta_2 \\ &= -4A^{(1)} (c'_{1,0} - 2\pi\beta_0 \zeta_2), \\ c_{2,0} &= \zeta_2 A^{(2)} + \frac{3}{4}[A^{(1)}]^2 \zeta_4 + 2A^{(1)} \zeta_3 (B_S^{(1)} - B_H^{(1)}) - \frac{\zeta_2}{2} (B_S^{(1)} - B_H^{(1)})^2 \\ &+ \pi\beta_0 [4A^{(1)} \zeta_3 + \zeta_2 (B_H^{(1)} - 3B_S^{(1)})] \\ &= A^{(2)} \zeta_2 + [A^{(1)}]^2 \left(\frac{3}{4} \zeta_4 + \frac{2\zeta_3^2}{\zeta_2} \right) - \frac{(c'_{1,0})^2}{2\zeta_2} + 2\pi\beta_0 \left(A^{(1)} \zeta_3 - B_S^{(1)} \zeta_2 + \frac{1}{2} c'_{1,0} \right), \\ c'_{1,0} &= 2A^{(1)} \zeta_3 + \zeta_2 (B_H^{(1)} - B_S^{(1)}), \\ c'_{1,1} &= 4A^{(1)} \zeta_2, \\ c''_{0,0} &= -\frac{\zeta_2}{2}. \end{aligned} \quad (3.34)$$

Furthermore, we require the first and second derivative of \mathcal{L} up to α_s and α_s^2 , respectively. They are given by

$$\mathcal{L}'(\mathcal{T}_0) = \sum_{a,b} \frac{d|\mathcal{M}_{ab}|^2}{d\Phi_{\text{F}}} [-\hat{P} \otimes f)_a f_b + (a \leftrightarrow b)] + \mathcal{O}(\alpha_s^2), \quad (3.35)$$

$$\begin{aligned} \mathcal{L}''(\mathcal{T}_0) &= \sum_{a,b} \frac{d|\mathcal{M}_{ab}|^2}{d\Phi_{\text{F}}} [\{(\hat{P} \otimes f)_a (\hat{P} \otimes f)_b - (\hat{P}' \otimes f)_a f_b \\ &+ (\hat{P} \otimes \hat{P} \otimes f)_a f_b\} + (a \leftrightarrow b)] + \mathcal{O}(\alpha_s^3), \end{aligned} \quad (3.36)$$

where the regularised splitting function \hat{P}_{ij} can be expanded as

$$\hat{P}_{ij}(x, \alpha_s) = \sum_{n=0}^{\infty} \hat{P}_{ij}^{(n)}(x) \left(\frac{\alpha_s}{2\pi}\right)^{n+1}, \quad (3.37)$$

and its derivative is given by

$$\hat{P}'_{ij}(x, \alpha_s(\mu_B)) = -\frac{d}{d \ln \mathcal{T}_0} \hat{P}_{ij}(x, \alpha_s(\mu_B)) = \left(\frac{\alpha_s(\mu_B)}{2\pi}\right)^2 2\pi\beta_0 \hat{P}_{ij}^{(0)}(x) + \mathcal{O}(\alpha_s^3). \quad (3.38)$$

It is possible to absorb all terms in the first line of eq. (3.32) into a redefinition of the Sudakov and the luminosity. However, the $\alpha_s L_{\mathcal{T}}$ term in the second line of eq. (3.32) can not be absorbed into a redefinition of the Sudakov without reintroducing such a term in the first line as well. Similarly, the first term in eq. (3.36) can not be factorized such that it can be absorbed into a redefinition of the beam function matching kernels \bar{C}_{ij} . Therefore, we can express our final result as

$$\frac{d\sigma^{\text{sing}}(\mathcal{T}_0)}{d\Phi_{\text{F}}} = e^{-S(\mathcal{T}_0)} \tilde{\mathcal{L}}(\mathcal{T}_0), \quad (3.39)$$

by defining the final luminosity factor through

$$\begin{aligned} \tilde{\mathcal{L}}(\mathcal{T}_0) &= \sum_{a,b} \frac{d|\mathcal{M}_{ab}|^2}{d\Phi_{\text{F}}} \tilde{H}_{ab}(\mu_B) \left[(\tilde{C} \otimes f)_a (\tilde{C} \otimes f)_b + 2c''_{0,0} (\hat{P} \otimes f)_a (\hat{P} \otimes f)_b \right] \\ &\quad - \sum_{a,b} \frac{d|\mathcal{M}_{ab}|^2}{d\Phi_{\text{F}}} \left(\frac{\alpha_s}{2\pi}\right)^2 c'_{1,1} L_{\mathcal{T}} \left[(\hat{P}^{(0)} \otimes f)_a f_b + f_a (\hat{P}^{(0)} \otimes f)_b \right] + \mathcal{O}(\alpha_s^3). \end{aligned} \quad (3.40)$$

Here, the second line arises from the corresponding term in eq. (3.36), and can not be absorbed into a redefinition of the kernels \bar{C}_{ij} , while the last line contains an explicit $L_{\mathcal{T}}$ term. All non-logarithmic terms in eq. (3.32) are absorbed into the modified hard function and matching kernels, which are given by

$$\tilde{H}_{ab}(\mu_B) = \bar{H}_{ab}(\mu_B) \left[1 + \frac{\alpha_s}{2\pi} c_{1,0} + \left(\frac{\alpha_s}{2\pi}\right)^2 c_{2,0} + \mathcal{O}(\alpha_s^3) \right], \quad (3.41)$$

$$\begin{aligned} \tilde{C}_{ij}(x, \mu_B) &= \bar{C}_{ij}(x, \mu_B) \\ &\quad - \left(\frac{\alpha_s}{2\pi}\right)^2 \left[-c''_{0,0} (\hat{P}^{(0)} \otimes \hat{P}^{(0)})_{ij}(x) + (c'_{1,0} + 2c''_{0,0}\pi\beta_0) \hat{P}_{ij}^{(0)}(x) \right] + \mathcal{O}(\alpha_s^3). \end{aligned} \quad (3.42)$$

In the original MINNLO_{PS-p_T} implementation, the remaining terms appearing in the equivalent of eq. (3.32) were absorbed into a redefinition of the Sudakov form factor (specifically, by redefining the B coefficients). In our default implementation of MINNLO_{PS- \mathcal{T}_0} we do not perform such a redefinition.

Finally, we note that for the practical implementation it is convenient to combine the two integrals in eq. (3.20) into a single integral,

$$\begin{aligned} S(\mathcal{T}_0) &= 2 \int_0^{\ln \sqrt{Q/\mathcal{T}_0}} d\ell \left\{ 2A[\alpha_s(Qe^{-\ell})] \ell + 2A[\alpha_s(\mathcal{T}_0 e^{\ell})] \ell \right. \\ &\quad \left. + B_H[\alpha_s(Qe^{-\ell})] - B_S[\alpha_s(\mathcal{T}_0 e^{\ell})] \right\}. \end{aligned} \quad (3.43)$$

For completeness, we also quote the expansion of the Sudakov,

$$\begin{aligned}
\mathcal{S}(\mathcal{T}_0) &= \frac{\alpha_s(\mu_B)}{2\pi} \left[4A^{(1)}L_{\mathcal{T}}^2 + 2L_{\mathcal{T}}(B_H^{(1)} - B_S^{(1)}) \right] \\
&+ \left[\frac{\alpha_s(\mu_B)}{2\pi} \right]^2 \left[4L_{\mathcal{T}}^2 \left(A^{(2)} - \pi\beta_0(B_H^{(1)} + B_S^{(1)}) \right) + 2L_{\mathcal{T}}(B_H^{(2)} - B_S^{(2)}) \right] \\
&+ \left[\frac{\alpha_s(\mu_B)}{2\pi} \right]^3 \left[\frac{2}{3}(4\pi\beta_0)^2 [A^{(1)}L_{\mathcal{T}}^4 + L_{\mathcal{T}}^3(B_H^{(1)} - B_S^{(1)})] \right. \\
&\quad \left. + L_{\mathcal{T}}^2 \left[4A^{(3)} - 8\pi^2\beta_1(B_H^{(1)} + B_S^{(1)}) - 8\pi\beta_0(B_H^{(2)} + B_S^{(2)}) \right] \right. \\
&\quad \left. + 2L_{\mathcal{T}}(B_H^{(3)} - B_S^{(3)}) \right] + \mathcal{O}(\alpha_s^4). \tag{3.44}
\end{aligned}$$

We note that the MINNLO_{PS} formulation contains the same ingredients as those entering in a NNLL' computation, but does not need to retain its formal logarithmic accuracy in order to guarantee that the final result is NNLO accurate.

3.3 Derivation of the MINNLO_{PS} master formula for \mathcal{T}_0

With the resummation formula in a suitable form we are now ready to derive the MINNLO_{PS}- \mathcal{T}_0 master formula. We start from the resummed cumulative cross section in eq. (3.31),

$$\frac{d\sigma^{\text{sing}}(\mathcal{T}_0)}{d\Phi_{\text{F}}} = \tilde{\mathcal{L}}(\mathcal{T}_0)e^{-\mathcal{S}(\mathcal{T}_0)}, \tag{3.45}$$

where all the ingredients have been derived in detail in the previous section. We obtain the NNLO cross section differential in \mathcal{T}_0 and in the Born phase space Φ_{F} by taking the total derivative and then matching the ensuing differential cross section at small \mathcal{T}_0 with the fixed-order cross section valid at large \mathcal{T}_0

$$\begin{aligned}
\frac{d\sigma}{d\Phi_{\text{F}}d\mathcal{T}_0} &= \frac{d}{d\mathcal{T}_0} \left\{ \exp[-\mathcal{S}(\mathcal{T}_0)] \tilde{\mathcal{L}}(\mathcal{T}_0) \right\} + R_f(\mathcal{T}_0) \\
&= \exp[-\mathcal{S}(\mathcal{T}_0)] \left\{ D(\mathcal{T}_0) + \frac{R_f(\mathcal{T}_0)}{\exp[-\mathcal{S}(\mathcal{T}_0)]} \right\}. \tag{3.46}
\end{aligned}$$

Here, R_f contains terms that are non-singular in the $\mathcal{T}_0 \rightarrow 0$ limit, and we have defined

$$D(\mathcal{T}_0) \equiv -\frac{d\mathcal{S}(\mathcal{T}_0)}{d\mathcal{T}_0} \tilde{\mathcal{L}}(\mathcal{T}_0) + \frac{d\tilde{\mathcal{L}}(\mathcal{T}_0)}{d\mathcal{T}_0}. \tag{3.47}$$

A central feature of the MINNLO_{PS} method is that the renormalization and factorization scales are evaluated at the low scale, i.e. the typical scale of the resummation.⁵ For \mathcal{T}_0 resummation there are two relevant low scales, namely $\mu_S = \mathcal{T}_0$ and $\mu_B = \sqrt{\mathcal{T}_0}Q$, as discussed above. We select $\mu_{\text{R}} \sim \mu_{\text{F}} \sim \mu_B$ as the common low scale at which to evaluate all terms in eq. (3.46), especially because the PDFs are naturally evaluated at that scale. The logarithms

⁵Note that this is not a strict requirement of the MINNLO_{PS} method and other choices are possible in general, but it has been introduced as the default setting within the MINNLO_{PS} approach so far.

to be resummed are then given by either $\ln(Q/\mu_B) = \ln\sqrt{Q/\mathcal{T}_0}$ or $\ln(\mathcal{T}_0/\mu_B) = \ln\sqrt{\mathcal{T}_0/Q}$. To simplify the notation in the following, we will always use

$$\mu_B = \sqrt{Q\mathcal{T}_0} = Qe^{-L_{\mathcal{T}}}, \quad L_{\mathcal{T}} = \frac{1}{2} \ln \frac{Q}{\mathcal{T}_0}, \quad (3.48)$$

which is the natural extension of eq. (3.33) to the \mathcal{T}_0 spectrum. In particular, we express all derivatives w.r.t. \mathcal{T}_0 as derivatives w.r.t. $L_{\mathcal{T}}$. This induces a Jacobian in eq. (3.47),

$$D(\mathcal{T}_0) = \frac{1}{2\mathcal{T}_0} \left[\frac{d\mathcal{S}(\mathcal{T}_0)}{dL_{\mathcal{T}}} \tilde{\mathcal{L}}(\mathcal{T}_0) - \frac{d\tilde{\mathcal{L}}(\mathcal{T}_0)}{dL_{\mathcal{T}}} \right], \quad (3.49)$$

but simplifies the expressions for derivatives of \mathcal{S} and $\tilde{\mathcal{L}}$ evaluated below.

As in eq. (2.4) for $\text{MINNLO}_{\text{PS-}p_{\text{T}}}$, we introduce the NLO differential cross section for FJ production

$$\frac{d\sigma_{\text{FJ}}^{(\text{NLO})}}{d\Phi_{\text{F}}d\mathcal{T}_0} = \frac{\alpha_s(\mu_B)}{2\pi} \left[\frac{d\sigma_{\text{FJ}}}{d\Phi_{\text{F}}d\mathcal{T}_0} \right]^{(1)} + \left(\frac{\alpha_s(\mu_B)}{2\pi} \right)^2 \left[\frac{d\sigma_{\text{FJ}}}{d\Phi_{\text{F}}d\mathcal{T}_0} \right]^{(2)}, \quad (3.50)$$

so that we can write the finite remainder R_f at this order as

$$R_f = \frac{d\sigma_{\text{FJ}}^{(\text{NLO})}}{d\Phi_{\text{F}}d\mathcal{T}_0} - \frac{\alpha_s(\mu_B)}{2\pi} [\exp[-\mathcal{S}(\mathcal{T}_0)]D(\mathcal{T}_0)]^{(1)} - \left(\frac{\alpha_s(\mu_B)}{2\pi} \right)^2 [\exp[-\mathcal{S}(\mathcal{T}_0)]D(\mathcal{T}_0)]^{(2)}. \quad (3.51)$$

This allows us to rewrite eq. (3.46) as

$$\begin{aligned} \frac{d\sigma}{d\Phi_{\text{F}}d\mathcal{T}_0} &= \exp[-\mathcal{S}(\mathcal{T}_0)] \left\{ \frac{\alpha_s(\mu_B)}{2\pi} \left[\frac{d\sigma_{\text{FJ}}}{d\Phi_{\text{F}}d\mathcal{T}_0} \right]^{(1)} \left(1 + \frac{\alpha_s(\mu_B)}{2\pi} [\mathcal{S}(\mathcal{T}_0)]^{(1)} \right) \right. \\ &\quad \left. + \left(\frac{\alpha_s(\mu_B)}{2\pi} \right)^2 \left[\frac{d\sigma_{\text{FJ}}}{d\Phi_{\text{F}}d\mathcal{T}_0} \right]^{(2)} + \left[D(\mathcal{T}_0) - \frac{\alpha_s(\mu_B)}{2\pi} [D(\mathcal{T}_0)]^{(1)} - \left(\frac{\alpha_s(\mu_B)}{2\pi} \right)^2 [D(\mathcal{T}_0)]^{(2)} \right] \right. \\ &\quad \left. + \text{regular terms of } \mathcal{O}(\alpha_s^3) \right\}. \end{aligned} \quad (3.52)$$

Here, $D(\mathcal{T}_0)$ is the term from eq. (3.46) without any further expansion, while the other terms arise from expanding $R_f/e^{-\mathcal{S}}$ using eq. (3.51).⁶ Using eq. (3.49), the $[D(\mathcal{T}_0)]^{(n)}$ coefficients are given by

$$\begin{aligned} [D(\mathcal{T}_0)]^{(1)} &= \frac{1}{2\mathcal{T}_0} \left\{ \left[\frac{d\mathcal{S}(\mathcal{T}_0)}{dL_{\mathcal{T}}} \right]^{(1)} [\tilde{\mathcal{L}}(\mathcal{T}_0)]^{(0)} - \left[\frac{d\tilde{\mathcal{L}}(\mathcal{T}_0)}{dL_{\mathcal{T}}} \right]^{(1)} \right\}, \\ [D(\mathcal{T}_0)]^{(2)} &= \frac{1}{2\mathcal{T}_0} \left\{ \left[\frac{d\mathcal{S}(\mathcal{T}_0)}{dL_{\mathcal{T}}} \right]^{(2)} [\tilde{\mathcal{L}}(\mathcal{T}_0)]^{(0)} + \left[\frac{d\mathcal{S}(\mathcal{T}_0)}{dL_{\mathcal{T}}} \right]^{(1)} [\tilde{\mathcal{L}}(\mathcal{T}_0)]^{(1)} - \left[\frac{d\tilde{\mathcal{L}}(\mathcal{T}_0)}{dL_{\mathcal{T}}} \right]^{(2)} \right\}. \end{aligned} \quad (3.53)$$

⁶Note that, when deriving $D(\mathcal{T}_0)$ all resummation ingredients need to be included to an order such that the cumulative cross section in eq. (3.45) is accurate at relative $\mathcal{O}(\alpha_s^2)$, in particular that means two-loop order in the hard, beam and the soft functions. This is necessary to ensure NNLO accuracy of the $\text{MINNLO}_{\text{PS}}$ approach.

The expansion of the derivative of the Sudakov form factor with respect to $L_{\mathcal{T}}$ are given by

$$\begin{aligned} \left[\frac{d\mathcal{S}}{dL_{\mathcal{T}}} \right]^{(1)} &= 2(4A^{(1)}L_{\mathcal{T}} + B_H^{(1)} - B_S^{(1)}), \\ \left[\frac{d\mathcal{S}}{dL_{\mathcal{T}}} \right]^{(2)} &= 2 \left[4A^{(2)}L_{\mathcal{T}} + B_H^{(2)} - B_S^{(2)} + 8\pi\beta_0(A^{(1)}L_{\mathcal{T}}^2 - B_S^{(1)}L_{\mathcal{T}}) \right], \end{aligned} \quad (3.54)$$

while the fixed-order terms of $\tilde{\mathcal{L}}(\mathcal{T}_0)$ and their derivatives follow from eq. (3.40),

$$\begin{aligned} [\tilde{\mathcal{L}}(\mathcal{T}_0)]^{(0)} &= \sum_{a,b} \frac{d|\mathcal{M}_{ab}|^2}{d\Phi_{\mathbb{F}}} f_a f_b, \\ [\tilde{\mathcal{L}}(\mathcal{T}_0)]^{(1)} &= \sum_{a,b} \frac{d|\mathcal{M}_{ab}|^2}{d\Phi_{\mathbb{F}}} \left\{ \tilde{H}^{(1)} f_a f_b + (\tilde{C}^{(1)} \otimes f)_a f_b + f_a (\tilde{C}^{(1)} \otimes f)_b \right\}, \\ [\tilde{\mathcal{L}}(\mathcal{T}_0)]^{(2)} &= \sum_{a,b} \frac{d|\mathcal{M}_{ab}|^2}{d\Phi_{\mathbb{F}}} \left\{ \tilde{H}^{(1)} \left[(\tilde{C}^{(1)} \otimes f)_a f_b + f_a (\tilde{C}^{(1)} \otimes f)_b \right] + \tilde{H}^{(2)} f_a f_b \right. \\ &\quad + (\tilde{C}^{(2)} \otimes f)_a f_b + f_a (\tilde{C}^{(2)} \otimes f)_b \\ &\quad + (\tilde{C}^{(1)} \otimes f)_a (\tilde{C}^{(1)} \otimes f)_b - \zeta_2 (\hat{P}^{(0)} \otimes f)_a (\hat{P}^{(0)} \otimes f)_b \\ &\quad \left. - c'_{1,1} L_{\mathcal{T}} \left[(\hat{P}^{(0)} \otimes f)_a f_b + f_a (\hat{P}^{(0)} \otimes f)_b \right] \right\}, \\ \left[\frac{d\tilde{\mathcal{L}}(\mathcal{T}_0)}{dL_{\mathcal{T}}} \right]^{(1)} &= \sum_{a,b} \frac{d|\mathcal{M}_{ab}|^2}{d\Phi_{\mathbb{F}}} (-2) \left\{ (\hat{P}^{(0)} \otimes f)_a f_b + f_a (\hat{P}^{(0)} \otimes f)_b \right\}, \\ \left[\frac{d\tilde{\mathcal{L}}(\mathcal{T}_0)}{dL_{\mathcal{T}}} \right]^{(2)} &= \sum_{a,b} \frac{d|\mathcal{M}_{ab}|^2}{d\Phi_{\mathbb{F}}} (-2) \left\{ (\hat{P}^{(1)} \otimes f)_a f_b + f_a (\hat{P}^{(1)} \otimes f)_b \right. \\ &\quad + \left(\tilde{H}^{(1)} + \frac{c'_{1,1}}{2} \right) \left[(\hat{P}^{(0)} \otimes f)_a f_b + f_a (\hat{P}^{(0)} \otimes f)_b \right] \\ &\quad + (\hat{P}^{(0)} \otimes f)_a (\tilde{C}^{(1)} \otimes f)_b + (\tilde{C}^{(1)} \otimes f)_a (\hat{P}^{(0)} \otimes f)_b \\ &\quad + (\tilde{C}^{(1)} \otimes \hat{P}^{(0)} \otimes f)_a f_b + f_a (\tilde{C}^{(1)} \otimes \hat{P}^{(0)} \otimes f)_b \\ &\quad \left. - 2\pi\beta_0 \left[\tilde{H}^{(1)} f_a f_b + (C^{(1)} \otimes f)_a f_b + f_a (C^{(1)} \otimes f)_b \right] \right\}. \end{aligned} \quad (3.55)$$

The scale dependence is implemented as in appendix D of ref. [1], which directly generalizes from the p_T to the \mathcal{T}_0 case up to the required accuracy, as we have made sure that our starting equation has the identical structure. We note that $[D(\mathcal{T}_0)]^{(1)}$ does not depend on the renormalization and factorization scale factors K_R and K_F , while for $[D(\mathcal{T}_0)]^{(2)}$ one has

$$[D(\mathcal{T}_0)]^{(2)}(K_F, K_R) = [D(\mathcal{T}_0)]^{(2)} - 2\beta_0\pi \left[\frac{d\tilde{\mathcal{L}}(\mathcal{T}_0)}{d\mathcal{T}_0} \right]^{(1)} \ln \frac{K_F^2}{K_R^2}. \quad (3.56)$$

By construction, eq. (3.52) yields the NNLO cross section fully differential in $\Phi_{\mathbb{F}}$ when integrating over \mathcal{T}_0 , which can be understood as follows: Our starting equation eq. (3.46) is computed at exactly that accuracy, provided that we take into account all relevant contributions up to two-loop level in the computation of the cumulant in eq. (3.45). Given

that we have not expanded $D(\mathcal{T}_0)$ in eq. (3.52) the total derivative w.r.t. \mathcal{T}_0 in eq. (3.46), and therefore in $D(\mathcal{T}_0)$, is kept intact. As a result, eq. (3.52) retains NNLO accuracy in Φ_{F} (when integrating over \mathcal{T}_0). By contrast, if we were to truncate $D(\mathcal{T}_0)$ beyond $\mathcal{O}(\alpha_s^3)$, for instance, we would neglect large logarithmic terms proportional to $L_{\mathcal{T}}^n$ at higher orders. Depending on their power n , these missing logarithmic terms could spoil the NNLO accuracy upon integration over \mathcal{T}_0 . In the case of $\text{MINNLO}_{\text{PS-}p_{\text{T}}}$ expanding $D(p_{\text{T}})$ up to $\mathcal{O}(\alpha_s^3)$ would be sufficient to retain NNLO accuracy, but in the case of \mathcal{T}_0 higher powers n of the logarithms appear, which would require an expansion even beyond $\mathcal{O}(\alpha_s^3)$. This renders it crucial to keep the full unexpanded $D(\mathcal{T}_0)$ for $\text{MINNLO}_{\text{PS-}\mathcal{T}_0}$.

We can now apply the $\text{MINNLO}_{\text{PS-}\mathcal{T}_0}$ procedure directly at the fully differential level in the Φ_{FJ} phase space to the POWHEG FJ calculation, as given in eq. (2.1), by replacing the corresponding $\bar{B}(\Phi_{\text{FJ}})$ function through

$$\begin{aligned} \bar{B}(\Phi_{\text{FJ}}) \equiv \exp[-\mathcal{S}(\mathcal{T}_0)] & \left\{ \frac{\alpha_s(\sqrt{Q\mathcal{T}_0})}{2\pi} \left[\frac{d\sigma_{\text{FJ}}}{d\Phi_{\text{FJ}}} \right]^{(1)} \left(1 + \frac{\alpha_s(\sqrt{Q\mathcal{T}_0})}{2\pi} [\mathcal{S}(\mathcal{T}_0)]^{(1)} \right) \right. \\ & \left. + \left(\frac{\alpha_s(\sqrt{Q\mathcal{T}_0})}{2\pi} \right)^2 \left[\frac{d\sigma_{\text{FJ}}}{d\Phi_{\text{FJ}}} \right]^{(2)} + D^{(\geq 3)}(\mathcal{T}_0) F^{\text{corr}}(\Phi_{\text{FJ}}) \right\}. \end{aligned} \quad (3.57)$$

The factor $F^{\text{corr}}(\Phi_{\text{FJ}})$ encodes a suitable function to spread the correction $D^{(\geq 3)}(\mathcal{T}_0)$, which intrinsically depends only \mathcal{T}_0 and Φ_{F} , on the full Φ_{FJ} phase space, as discussed in detail in appendix B.

3.4 Matching with the shower

So far, we presented how to reach NNLO accuracy within the $\text{MINNLO}_{\text{PS}}$ method using \mathcal{T}_0 as a resolution variable. We now discuss how to match our $\text{MINNLO}_{\text{PS-}\mathcal{T}_0}$ predictions with a parton shower. In both $\text{MINNLO}_{\text{PS-}p_{\text{T}}}$ and $\text{MINNLO}_{\text{PS-}\mathcal{T}_0}$, the matching with the parton shower relies on the POWHEG formalism. In particular, the non-emission probability associated to the first and to the second emissions are encoded in the $\text{MINNLO}_{\text{PS}}$ and POWHEG Sudakov form factors, given in eq. (3.43) for $\text{MINNLO}_{\text{PS-}\mathcal{T}_0}$ (eq. (2.9) of [1] for $\text{MINNLO}_{\text{PS-}p_{\text{T}}}$) and eq. (2.1), respectively. In the original $\text{MINNLO}_{\text{PS-}p_{\text{T}}}$ formulation, these Sudakov form factors are both associated to transverse-momentum like observables, and they match the leading-logarithmic structure of a transverse-momentum ordered parton shower. This implies that, as long as the emissions generated by the shower are ordered in transverse momentum and vetoed according to the POWHEG procedure, the leading-logarithmic accuracy of the shower is preserved. In this case, the corresponding Lund plane [62] is filled without leaving any empty areas and without covering the same area twice, which would constitute a leading-logarithmic violation. By contrast, in the $\text{MINNLO}_{\text{PS-}\mathcal{T}_0}$ approach the $\text{MINNLO}_{\text{PS}}$ Sudakov form factor is associated to a different variable, \mathcal{T}_0 , whose resummation has a different leading-logarithmic structure. Thus, the matching with a parton shower becomes a delicate point. Filling correctly the Lund plane is now highly non trivial, since applying the standard POWHEG formalism can lead to empty areas or regions that are accounted for two times (thus wrongly suppressed).

To address these issues, one should modify the POWHEG mapping (for instance extending the mapping described in ref. [63] to deal initial state) and/or rely on a truncated-

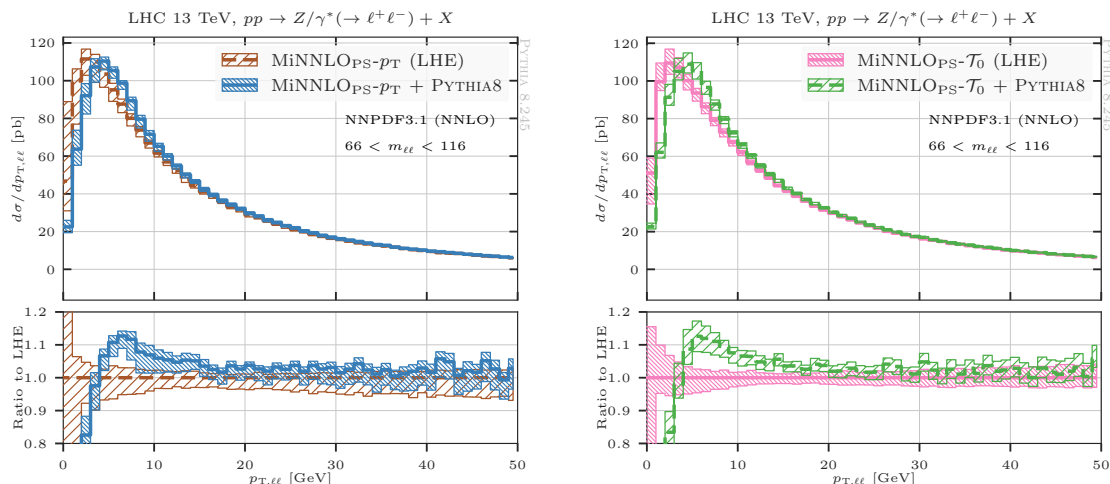


Figure 1. Transverse-momentum distribution of the lepton pair in Drell-Yan production. Left plot: comparison of $\text{MiNNLO}_{\text{PS-}p_T}$ at LHE level (brown, dashed) and after parton showering (blue, solid); right plot: comparison of $\text{MiNNLO}_{\text{PS-}\mathcal{T}_0}$ at LHE level (pink, solid) and after parton showering (green, dashed). The ratio plots show the relative effect of the parton shower.

vetoed shower [49] to properly fill the Lund plane. More concretely, this implies a substantial modification of the POWHEG code. We note that analogue modifications would be needed to implement a matching with NLL-accurate parton showers, which are being actively developed at the time of writing [64–71]. Since the main goal of this paper is to define the theoretical framework of the new $\text{MiNNLO}_{\text{PS}}$ formalism based on jettiness-like observables, we prefer to postpone a detailed discussion on the matching to a future paper. We believe that studying this problem in a separate work would be optimal, in view of the construction of an NNLO Monte Carlo event generator consistently matched to an NLL parton shower. Therefore, in this paper we do not implement these modifications, which means that in our matched results the accuracy of the parton shower is not fully preserved. However, in section 4.2, we will show more quantitatively that the numerical effect of this choice is rather small by comparing our $\text{MiNNLO}_{\text{PS-}\mathcal{T}_0}$ and $\text{MiNNLO}_{\text{PS-}p_T}$ results after showering. This comparison provides us with an estimate of the size of the neglected terms needed to formally preserve the shower accuracy. Moreover, the impact of the parton shower is almost identical for $\text{MiNNLO}_{\text{PS-}p_T}$ and $\text{MiNNLO}_{\text{PS-}\mathcal{T}_0}$. This can be observed from the two ratio panels of figure 1 that show the showered result divided by the Les-Houches-Event (LHE) level one for the example case of the transverse momentum distribution of the Z boson in Drell-Yan production. We find an analogous behaviour for all distributions we considered in Higgs-boson and Drell-Yan production. In conclusion, despite the fact that the logarithmic accuracy of the parton shower is not formally preserved in the $\text{MiNNLO}_{\text{PS-}\mathcal{T}_0}$ case, its effect in the two $\text{MiNNLO}_{\text{PS}}$ formulations is almost identical.

4 Validation and phenomenological results

In this section we present phenomenological results for Drell-Yan production ($pp \rightarrow \ell^+\ell^-$) and on-shell Higgs-boson production ($pp \rightarrow H$) in the heavy-top limit. For our practical

implementation we use as a starting point the $\text{MINNLO}_{\text{PS-}p_{\text{T}}}$ generators in POWHEG-BOX-V2 developed in refs. [1, 2], which are based on the POWHEG computations of $H+\text{jet}$ [72] and $Z+\text{jet}$ [73] production, and we apply the $\text{MINNLO}_{\text{PS-}\mathcal{T}_0}$ formalism discussed in the previous section. The relevant input parameters are discussed in section 4.1. First, we validate our $\text{MINNLO}_{\text{PS-}\mathcal{T}_0}$ predictions against the $\text{MINNLO}_{\text{PS-}p_{\text{T}}}$ ones [1, 2] in section 4.2. Then, we present the first comparison between results from the $\text{MINNLO}_{\text{PS}}$ and GENEVA [4] generators in section 4.3. Finally, we compare our predictions against high-precision data from ATLAS [74] and CMS [75] for Drell-Yan production at 13 TeV in section 4.4.

4.1 Setup

We consider proton-proton collisions at the LHC with a center-of-mass energy of 13 TeV. We use the G_μ scheme with $\cos^2\theta_W = m_W^2/m_Z^2$ and $\alpha = \sqrt{2}G_\mu m_W^2 \sin^2\theta_W/\pi$ and we set the electroweak (EW) inputs to their PDG [76] values: $G_F = 1.16639 \times 10^{-5} \text{ GeV}^{-2}$, $m_W = 80.385 \text{ GeV}$, $\Gamma_W = 2.0854 \text{ GeV}$, $m_Z = 91.1876 \text{ GeV}$, $\Gamma_Z = 2.4952 \text{ GeV}$, $m_H = 125 \text{ GeV}$. We set the on-shell top-quark mass to $m_t = 173.2 \text{ GeV}$. Our choice for the parton densities is the NNLO set of NNPDF3.1 [77] with $\alpha_s = 0.118$, which is obtained via the LHAPDF interface [78]. The PDFs are read by LHAPDF and evolved internally through HOPPET [79] as described in ref. [1]. The central factorization and renormalization scales are set following the $\text{MINNLO}_{\text{PS}}$ procedure, as described before. For Higgs-boson production the overall two powers of the strong coupling are evaluated at the scale $\mu_R^{(0)} = m_H$. We estimate the uncertainties due to missing higher-order corrections through the usual variations of μ_F and μ_R around their central value by a factor of two in each direction with the constraint $0.5 \leq \mu_R/\mu_F \leq 2$ while keeping the minimal and maximal values of the cross section. Resummation effects at large \mathcal{T}_0 are switched off by replacing the nominal logarithm $L_{\mathcal{T}}$ with the modified logarithm $\tilde{L}_{\mathcal{T}} = 1/p \ln(1 + (\sqrt{Q/\mathcal{T}})^p)$. For our predictions, we set $p = 6$, to ensure that they vanish sufficiently fast. We have checked that our final predictions depend only mildly on the value of p used. For all predictions presented in this paper we make use of the PYTHIA8 parton shower [80] and we employ a variation of the MONASH tune [81] adapted by CMS to improve the description of the Drell-Yan transverse-momentum spectrum.⁷

We validate our $\text{MINNLO}_{\text{PS-}\mathcal{T}_0}$ implementation for Drell-Yan and Higgs production against reference predictions from the $\text{MINNLO}_{\text{PS-}p_{\text{T}}}$ generators developed in refs. [1, 2] using the identical input settings. Moreover, we present a first comparison between $\text{MINNLO}_{\text{PS}}$ and GENEVA predictions for Drell-Yan production. The GENEVA results correspond to those presented in ref. [4], and we refer the reader to that paper for the respective input parameters and settings. Finally, we compare our predictions with experimental measurements by both the ATLAS [74] and the CMS collaboration [75]. In order to provide the most realistic comparison to experimental data, our showered predictions always include effects from hadronization and multi-particle interactions (MPI). We do not require any lepton dressing, as we do not include any QED showering effects.

⁷We thank Kenneth Long for providing us with the settings.

	$pp \rightarrow H$ (on-shell)		$pp \rightarrow Z \rightarrow \ell^+\ell^-$	
	σ [pb]	$\sigma/\sigma_{\text{NNLO}}$	σ [fb]	$\sigma/\sigma_{\text{NNLO}}$
NNLO	$40.32(2)_{-10.4\%}^{+10.7\%}$	1.000	$1919(1)_{-1.1\%}^{+0.9\%}$	1.000
MINNLO _{PS-p_T}	$39.33(1)_{-11.0\%}^{+12.2\%}$	0.975	$1907(2)_{-1.2\%}^{+1.1\%}$	0.994
MINNLO _{PS-\mathcal{T}_0}	$41.56(2)_{-10.1\%}^{+9.4\%}$	1.031	$1925(1)_{-1.2\%}^{+1.2\%}$	1.003

Table 1. Predictions of the total inclusive cross section for Higgs-boson production and the DY process at NNLO obtained with MATRIX [82], and using the MINNLO_{PS- p_T} and MINNLO_{PS- \mathcal{T}_0} implementations. The second and fourth columns show the ratio to the NNLO cross section.

4.2 Comparison and validation against MINNLO_{PS- p_T} results

We start the presentation of the phenomenological results by comparing our MINNLO_{PS- \mathcal{T}_0} predictions with MINNLO_{PS- p_T} ones. The MINNLO_{PS- p_T} generators have been tested extensively against fixed-order predictions in ref. [2]. They therefore serve us as reference predictions to validate our MINNLO_{PS- \mathcal{T}_0} implementations in this section.

4.2.1 Total cross section

Table 1 compares MINNLO_{PS- \mathcal{T}_0} and MINNLO_{PS- p_T} predictions for the total inclusive cross sections for Higgs-boson production and for Drell-Yan production (with an invariant-mass window of $66 \text{ GeV} < m_{\ell\ell} < 116 \text{ GeV}$). One should bear in mind that, despite both being NNLO accurate, these predictions differ by terms beyond NNLO accuracy. This is the case as they use different matching observables in their expansion and different scale settings. As a result, those predictions should agree within the quoted perturbative uncertainties. Indeed, as one can see, the predicted rates from MINNLO_{PS- \mathcal{T}_0} and MINNLO_{PS- p_T} are fully consistent with each other within the uncertainties from scale variation.

4.2.2 NNLO accuracy in distributions of the colour-singlet final states

We continue by considering differential distributions of the colour-singlet final states in Higgs-boson and Drell-Yan production. Since the results at Les Houches event (LHE) level are similar to the showered ones for all the distributions discussed in this section, we only show results including shower effects as well as hadronisation and multi-parton interactions (MPI). For on-shell Higgs-boson production the only formally NNLO-accurate observable is the rapidity of the Higgs boson, whose distribution is shown in figure 2. The predictions from the MINNLO_{PS- \mathcal{T}_0} (green, dashed) and MINNLO_{PS- p_T} (blue, solid) generators are in complete agreement within the given uncertainty bands. This is a numerical confirmation of the NNLO accuracy of our new MINNLO_{PS- \mathcal{T}_0} implementation for Higgs boson production. Similarly, we present a validation of NNLO-accurate observables in the phase space of the final-state leptons in Drell-Yan production in figure 3. In particular, the distributions in the rapidity ($y_{\ell\ell}$) and invariant-mass ($m_{\ell\ell}$) of the lepton pair, as well as the rapidity (y_{ℓ^+}) and the transverse-momentum (p_{T,ℓ^+}) of the positively charged lepton are shown. In all cases, we find a remarkable agreement between the MINNLO_{PS- \mathcal{T}_0} and MINNLO_{PS- p_T}

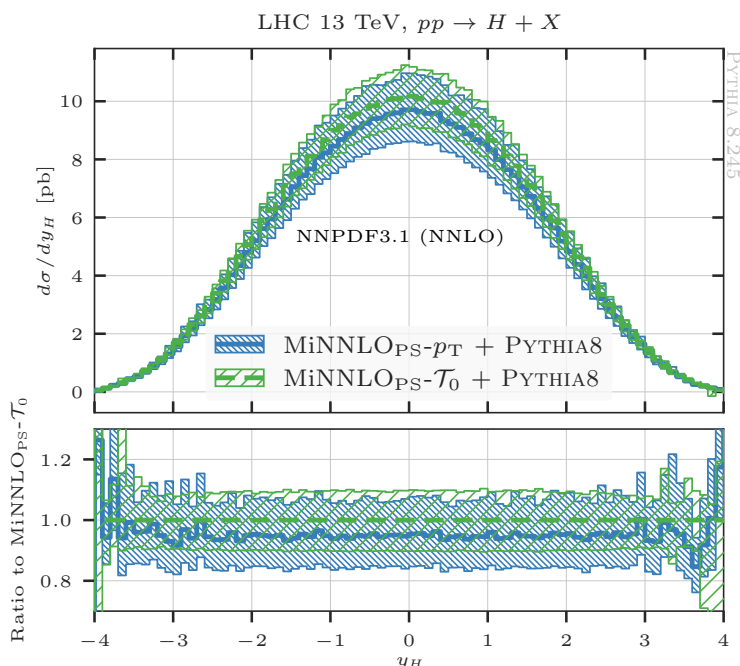


Figure 2. Comparison of MiNNLO_{PS}- \mathcal{T}_0 (green, dashed) and MiNNLO_{PS}- p_T (blue, solid) predictions for the rapidity distribution of the Higgs boson.

results, especially considering the very small scale uncertainties of this process, which are of order $\sim 1\%$. Only for $p_{T,\ell^+} \gtrsim m_Z/2$ the uncertainty bands increase to 5–10% and the two predictions differ by about 5% from each other (i.e. again within those uncertainties). This behaviour is well understood and can be traced back to a phase-space effect [83], which requires the two (back-to-back) leptons at LO to share the available energy of $m_{\ell\ell} \sim m_Z$ among them, effectively restricting their transverse momentum spectra to $p_{T,\ell} \lesssim m_Z/2$. As a result, the p_{T,ℓ^+} distribution, even in an NNLO calculation, becomes formally only NLO accurate above the $m_Z/2$ threshold, which explains both the increased uncertainty band and the larger differences between the MiNNLO_{PS}- \mathcal{T}_0 and MiNNLO_{PS}- p_T predictions.

4.2.3 NLO accuracy in exclusive distributions in the one-jet phase space

We finish the validation of our MiNNLO_{PS}- \mathcal{T}_0 implementation by considering distributions that require the presence of at least one jet in the final state. Such distributions, by construction, are only NLO accurate, and accordingly MiNNLO_{PS} predictions have the same formal accuracy as MiNLO' ones. However, since the kinematical origin of the NNLO corrections added through the MiNNLO_{PS} procedure corresponds to that of the Born phase space without any extra jets, building a consistent NNLO+PS generator requires some form of spreading of these distributions in one-jet phase space. Indeed, such spreading is implemented in the MiNNLO_{PS} method for both the p_T and the \mathcal{T}_0 matching, see $F^{\text{corr}}(\Phi_{\text{FJ}})$ in eq. (2.9) and eq. (3.57), respectively. It is obvious that such spreading for MiNNLO_{PS}- p_T and MiNNLO_{PS}- \mathcal{T}_0 may have different effects in the one-jet phase space. Nevertheless, the predictions are expected to be in reasonable agreement with each other and with the MiNLO'

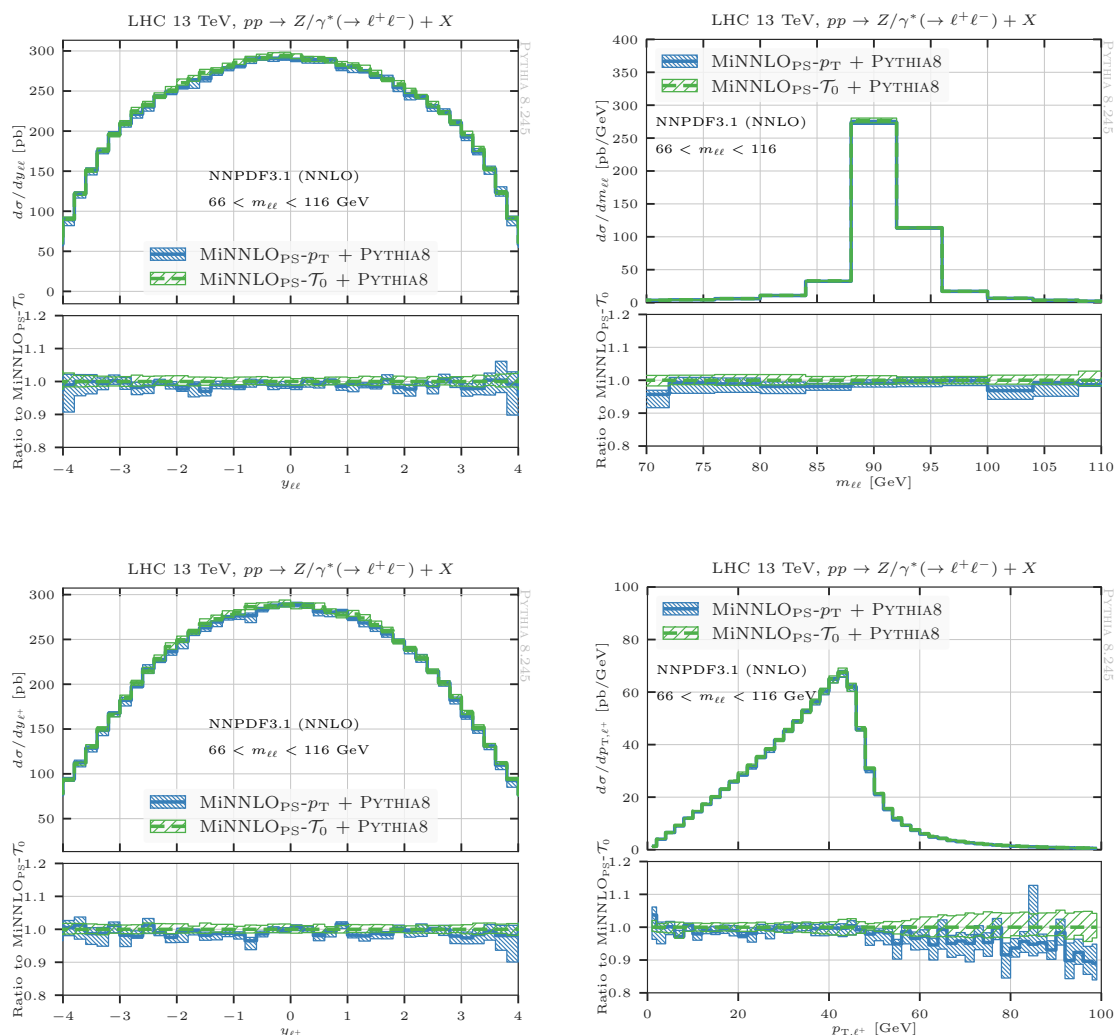


Figure 3. Comparison of $\text{MiNNLO}_{\text{PS}}\text{-}\mathcal{T}_0$ (green, dashed) and $\text{MiNNLO}_{\text{PS}}\text{-}p_T$ (blue, solid) predictions for differential distributions in the phase-space of the leptons in Drell-Yan production.

ones within the respective scale uncertainties. While such validation has been performed (for various processes) for the $\text{MiNNLO}_{\text{PS}}\text{-}p_T$ implementation by comparing to MINLO' results, here we need to perform such validation also for our new $\text{MiNNLO}_{\text{PS}}\text{-}\mathcal{T}_0$ implementation.

To this end, we compare $\text{MiNNLO}_{\text{PS}}\text{-}\mathcal{T}_0$ predictions to $\text{MiNNLO}_{\text{PS}}\text{-}p_T$ ones for distributions in the one-jet phase space in figure 4 for both Higgs-boson production and Drell-Yan production. In both cases, we also show predictions at NNLO accuracy obtained using MATRIX . In particular, we show the distribution in the transverse momentum (p_{T,j_1}) and rapidity (y_{j_1}) of the leading jet. The results for Higgs and Drell-Yan production turn out to be rather different. While for Drell-Yan, by and large, $\text{MiNNLO}_{\text{PS}}\text{-}\mathcal{T}_0$ and $\text{MiNNLO}_{\text{PS}}\text{-}p_T$ are consistent with each other within uncertainties, with acceptable (and not unexpected) differences in terms of shape, for Higgs-boson production we observe much larger differences between the two predictions. These different behaviours can be qualitatively explained by the fact that relative size of the cross-section which is spread in the one-jet phase space is much

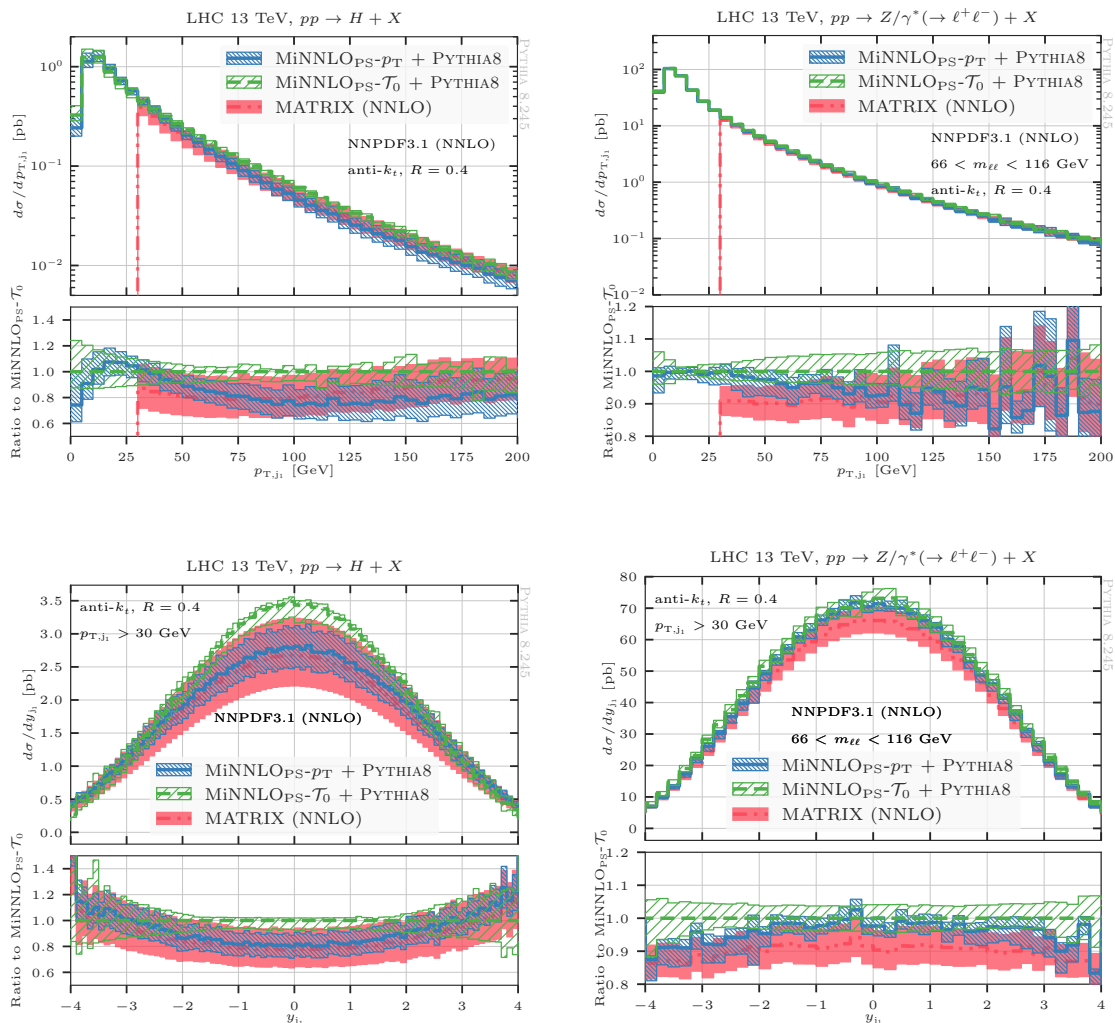


Figure 4. Comparison of $\text{MiNNLO}_{\text{PS-}\mathcal{T}_0}$ (green, dashed) and $\text{MiNNLO}_{\text{PS-}p_T}$ (blue, solid) predictions for differential distributions involving the hardest jet for Higgs (left) and Drell-Yan (right) production. For reference, we also include predictions at NNLO accuracy obtained with MATRIX (red, dot-dashed).

larger in the Higgs case, thus enhancing the differences between the two formulations. In particular, we observe that the $\text{MiNNLO}_{\text{PS-}\mathcal{T}_0}$ prediction is about 20% larger at $p_{T,j_1} > 70$ GeV and at central rapidities of the leading jet. Those differences are not fully covered by the scale uncertainty bands, which are at the 10% level, and they are already present at the LHE level, i.e. before shower effects are included. We found that modifying the spreading function of the inclusive NNLO correction for $\text{MiNNLO}_{\text{PS-}\mathcal{T}_0}$ in the one-jet phase space can have an impact on those distributions in the case of Higgs-boson production. However, while variations of the spreading function partially mitigate the differences with $\text{MiNNLO}_{\text{PS-}p_T}$, they do not eliminate them completely. For reference, we also show predictions obtained with MATRIX both in Drell-Yan and in Higgs production. In the case of p_{T,j_1} we see that $\text{MiNNLO}_{\text{PS-}p_T}$ results approach the NLO-accurate predictions earlier than the corresponding $\text{MiNNLO}_{\text{PS-}\mathcal{T}_0}$ result, although by $p_{T,j_1} \gtrsim 150$ GeV the three results are in broad agreement within their respective uncertainties. In the case of the jet rapidity we observe a qualitatively

better agreement between the shape of the MATRIX predictions and those of $\text{MiNNLO}_{\text{PS-}p_T}$, especially in the Higgs case. In the Drell-Yan case the MATRIX result is about 10% lower than both the $\text{MiNNLO}_{\text{PS-}p_T}$ and the $\text{MiNNLO}_{\text{PS-}\mathcal{T}_0}$ ones at central rapidity. At larger jet rapidities the MATRIX prediction gets progressively close to the $\text{MiNNLO}_{\text{PS-}p_T}$ one, while maintaining an $\mathcal{O}(10\%)$ difference with respect to the $\text{MiNNLO}_{\text{PS-}\mathcal{T}_0}$ result.

We would like to stress that as far as NNLO accuracy is concerned, the $\text{MiNNLO}_{\text{PS-}\mathcal{T}_0}$ implementation provides correct results also for Higgs-boson production. However, since our aim is a full fledged NNLO+PS Monte-Carlo generator, the issues observed in jet-related quantities of the $\text{MiNNLO}_{\text{PS-}\mathcal{T}_0}$ matching pose a certain level of concern for Higgs-boson production. Nevertheless, we reckon that the new results for Drell-Yan production are very encouraging and make a $\text{MiNNLO}_{\text{PS}}$ implementation based on jettiness worthwhile, also in view of moving towards higher jet multiplicities. Moreover, one should bear in mind that the present paper should be considered a first step towards NNLO+PS matching for processes with an extra jet in the final state. Eventually, the relevant ingredients for NNLO matching for new one-jet resolution variables will become available, which renders the present and forthcoming studies crucial.

4.2.4 Results for the \mathcal{T}_0 distribution

Finally, in this section we compare the results obtained for the \mathcal{T}_0 distribution between $\text{MiNNLO}_{\text{PS-}\mathcal{T}_0}$ and $\text{MiNNLO}_{\text{PS-}p_T}$. The results are shown in figure 5 at NNLO+PS level. We stress that despite the $\text{MiNNLO}_{\text{PS-}\mathcal{T}_0}$ results are obtained starting from a NNLO+PS formulation which contains the ingredients entering a NNLL' resummation for \mathcal{T}_0 they do not retain any formal accuracy, even before showering the results. We recall that at NNLO+PS level our predictions always include effects from hadronization and multi-particle interactions (MPI), which are particularly large for N -jettiness observables, see [59]. In particular, the inclusion of MPI distorts significantly the shape of the distribution with respect to the results at parton level, broadening it and shifting the peak of the distribution towards higher values of \mathcal{T}_0 . We observe an overall reasonable agreement between the results of $\text{MiNNLO}_{\text{PS-}\mathcal{T}_0}$ and those of $\text{MiNNLO}_{\text{PS-}p_T}$, both for the Higgs case and for the Drell-Yan case; in both cases, the spectrum obtained with $\text{MiNNLO}_{\text{PS-}\mathcal{T}_0}$ is slightly harder, with $\mathcal{O}(10\%)$ ($\mathcal{O}(20\%)$) differences for the Drell-Yan (Higgs) case. Let us now focus on the large \mathcal{T}_0 region, where we expect the two predictions to agree as the effect of resummation decreases. In the Drell-Yan case, the two predictions are indeed in good agreement starting from $\mathcal{T}_0 \gtrsim 200$ GeV. In the Higgs case, the agreement between $\text{MiNNLO}_{\text{PS-}\mathcal{T}_0}$ and the $\text{MiNNLO}_{\text{PS-}p_T}$ distributions at large \mathcal{T}_0 is delayed, with the two predictions getting closer to each other only for $\mathcal{T}_0 \gtrsim 300$ GeV. We observe very good agreement from $\mathcal{T}_0 \gtrsim 150$ GeV between the predictions when removing MPI and hadronization effects, indicating that the behaviour in figure 5 in the Higgs case is an interplay of the different scale choices in the two calculations (p_T -based or \mathcal{T}_0 -based) with MPI and hadronization effects. We finally observe that the $\text{MiNNLO}_{\text{PS-}p_T}$ scale uncertainty band is rather symmetric in the whole range, while the $\text{MiNNLO}_{\text{PS-}\mathcal{T}_0}$ one presents some degree of shrinking and is more asymmetric, especially in the Higgs case.

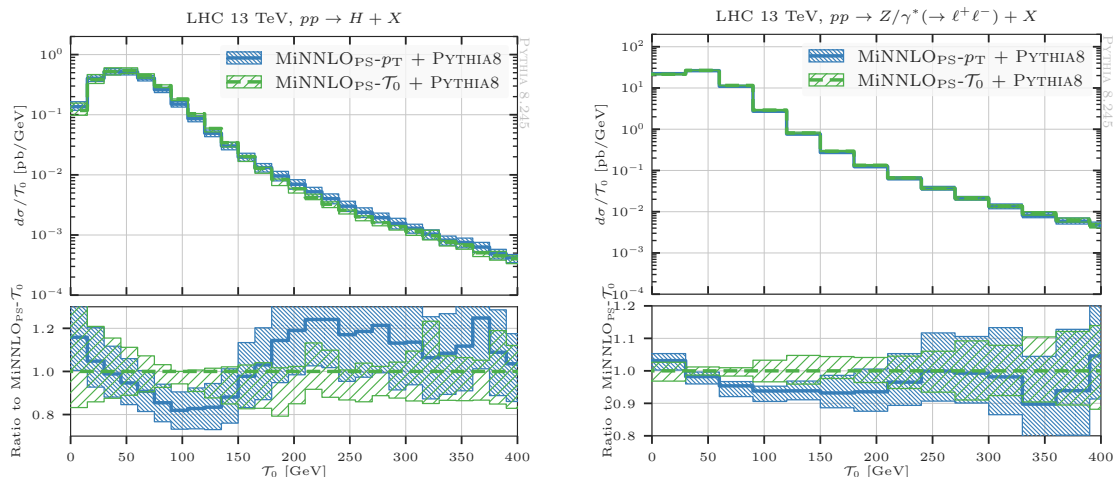


Figure 5. Comparison of $\text{MiNNLO}_{\text{PS}}-\mathcal{T}_0$ (green, dashed) and $\text{MiNNLO}_{\text{PS}}-p_T$ (blue, solid) predictions for the \mathcal{T}_0 distribution for Higgs (left) and Drell-Yan (right) production.

4.3 Comparison to GENEVA results for Drell-Yan production

We continue our study of phenomenological results by presenting a first direct comparison between the predictions from our $\text{MiNNLO}_{\text{PS}}$ generators to the ones from the GENEVA generators [3, 4]. Also in the case of the GENEVA method there exist two different implementations for the Drell-Yan process, one using \mathcal{T}_0 as the matching variable (the default choice for GENEVA predictions so far) [3] and one using p_T as the matching variable. The $\text{GENEVA}-p_T$ implementation employs the resummed p_T spectrum obtained through RADISH [84, 85] by means of an interpolation of a grid fully differential in the degrees of freedom of the Born phase space as well as in p_T .

Figures 6 and 7 show the comparison of $\text{MiNNLO}_{\text{PS}}$ and GENEVA predictions in the phase space of the two final-state leptons using as matching variables \mathcal{T}_0 and p_T , respectively. Given that $\text{MiNNLO}_{\text{PS}}$ and GENEVA treat terms beyond accuracy differently, we do not expect a one-to-one correspondence between their results, but rather that their NNLO predictions agree within the associated scale uncertainties. Indeed, we observe for both the \mathcal{T}_0 and p_T results that $\text{MiNNLO}_{\text{PS}}$ and GENEVA predictions are in full agreement within uncertainties. Note that for Born-level observables the public version of $\text{GENEVA}-\mathcal{T}_0$ allows one to calculate the uncertainty only with a three-scale variation as described in ref. [42], which explains why the $\text{GENEVA}-\mathcal{T}_0$ uncertainties are somewhat smaller than the $\text{MiNNLO}_{\text{PS}}-\mathcal{T}_0$ ones. Similarly to before, the largest relative differences appear for $p_{T,\ell^+} > m_Z/2$, with a visible shape distortion around the threshold, which is sensitive to soft-gluon effects and therefore to the specific matching scheme. We recall that these differences as well as the widening of the uncertainty bands for $p_{T,\ell^+} > m_Z/2$ is expected, since the accuracy of the predictions is effectively reduced to NLO.

Finally, in figure 8 we perform a comparison between the results obtained with $\text{MiNNLO}_{\text{PS}}$ and GENEVA for the \mathcal{T}_0 distribution. In order to not overcrowd the plots, we show on the left panel the comparison between the two NNLO+PS computations using \mathcal{T}_0 as resolution variable and on the right plot a comparison between the two results using p_T .

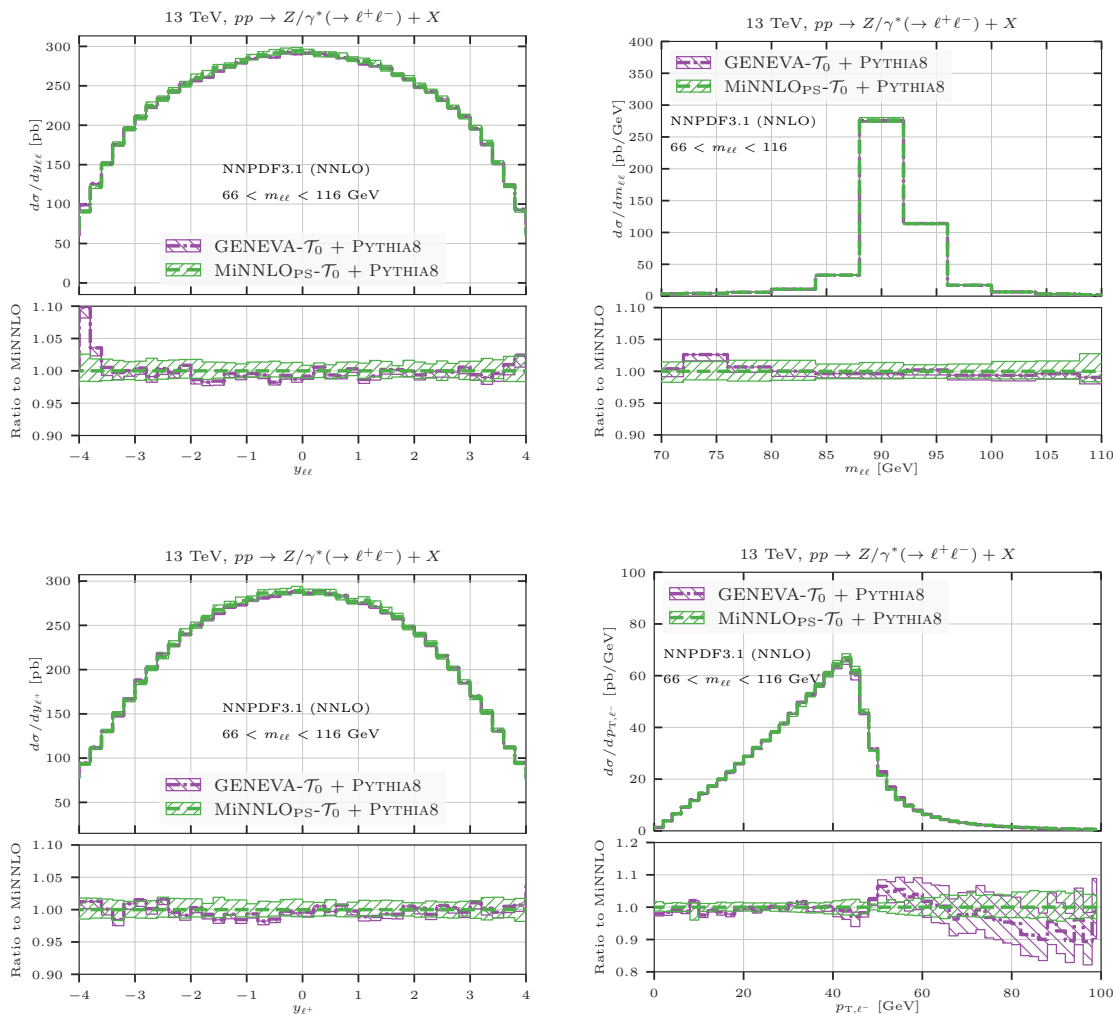


Figure 6. Comparison of $\text{MINNLO}_{\text{PS}}\mathcal{T}_0$ (green, dashed) and $\text{GENEVA}\mathcal{T}_0$ (purple, dot-dashed) predictions for differential distributions in the phase-space of the leptons in Drell-Yan production.

In the left panel we also show, as reference, the result at NNLO+NNLL' accuracy obtained using GENEVA [42]. As discussed in section 4.2.4, the inclusion of MPI has a substantial effect on the \mathcal{T}_0 distribution, which at NNLO+PS level has a completely different shape with respect to the parton-level NNLO+NNLL' results. After the inclusion of MPI effects the results of $\text{MINNLO}_{\text{PS}}$ and GENEVA are qualitatively in agreement, but retain important differences both at low and at relatively large \mathcal{T}_0 values. The peak of the $\text{MINNLO}_{\text{PS}}$ distribution is shifted towards larger values of \mathcal{T}_0 with respect to the GENEVA predictions. Differences persist also at larger values of \mathcal{T}_0 , which are however partially driven by the different choice of scales in the two calculations; in particular, the GENEVA predictions used here [4] employ renormalization and factorization scales sensitive to the transverse momentum of the radiation, which are responsible for lowering the tail of the distribution. We finally note that the shape of the \mathcal{T}_0 distribution after the matching with the shower is largely driven by the tune used in the parton shower, which is not the same in the two calculations. We have checked that by using the same settings as in the GENEVA predictions

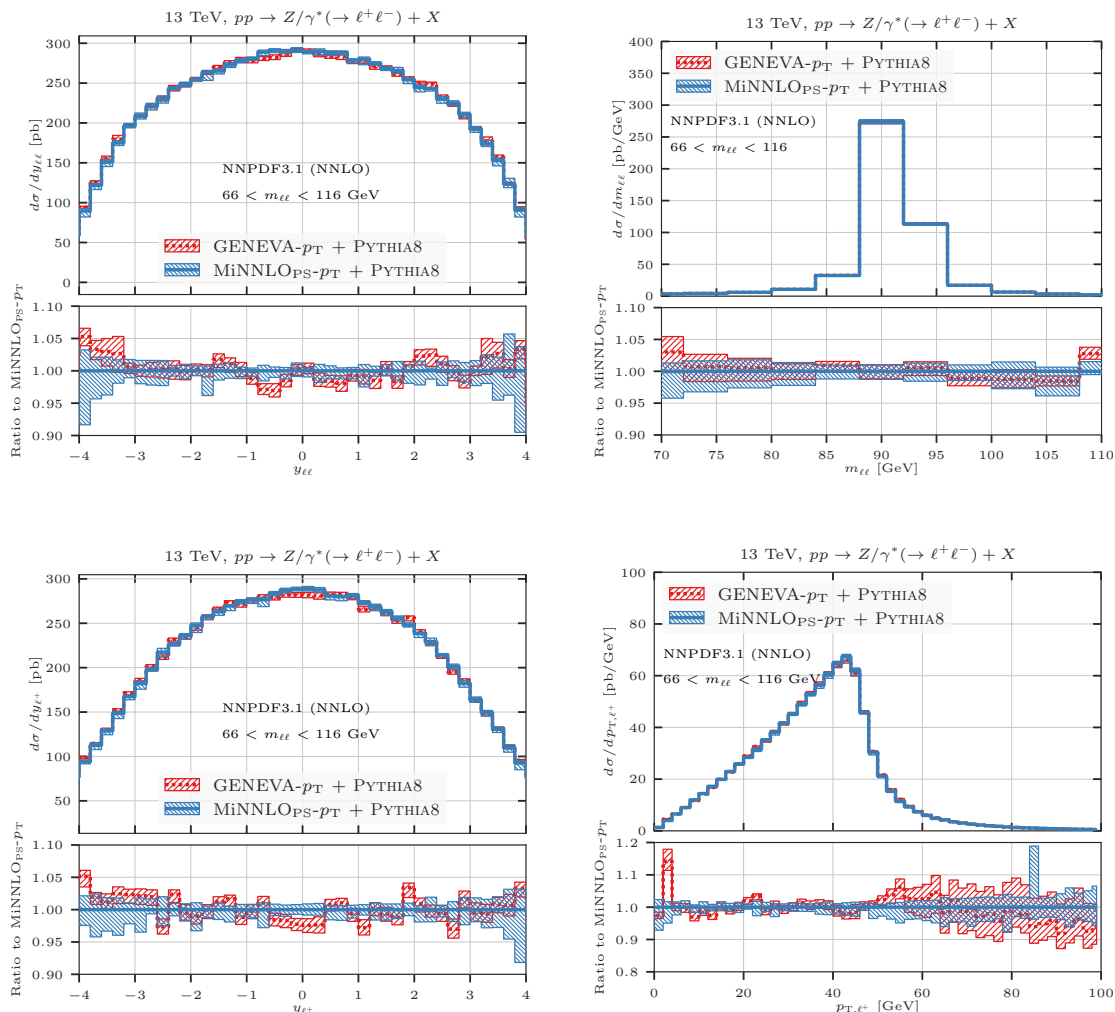


Figure 7. Comparison of MINNLO_{PS-p_T} (blue, solid) and GENEVA-p_T (red, dotted) predictions for differential distributions in the phase-space of the leptons in Drell-Yan production.

the peak of the MINNLO_{PS} one shifts towards smaller values of \mathcal{T}_0 , improving significantly the agreement of the two predictions.

4.4 Comparison against ATLAS and CMS data for Drell-Yan production

In this section we compare our MINNLO_{PS} predictions for Drell-Yan production against ATLAS and CMS data. We consider the recent ATLAS analysis presented in ref. [74], where results for the transverse momentum of the dilepton system ($p_{T,\ell\ell}$) and a variation of the Collins-Soper angle (ϕ^*) are shown. The angle ϕ^* is defined as

$$\phi^* = \tan\left(\frac{\pi - \Delta\phi}{2}\right) \sin(\theta^*), \quad \cos(\theta^*) = \tanh\left(\frac{\Delta\eta}{2}\right), \quad (4.1)$$

where $\Delta\eta$ and $\Delta\phi$ are the differences in pseudorapidity and azimuthal angle between the two leptons. As for the CMS data, we consider the analysis presented in ref. [75] where, besides results for $p_{T,\ell\ell}$ and ϕ^* , also the rapidity distribution of the dilepton system ($y_{\ell\ell}$) is

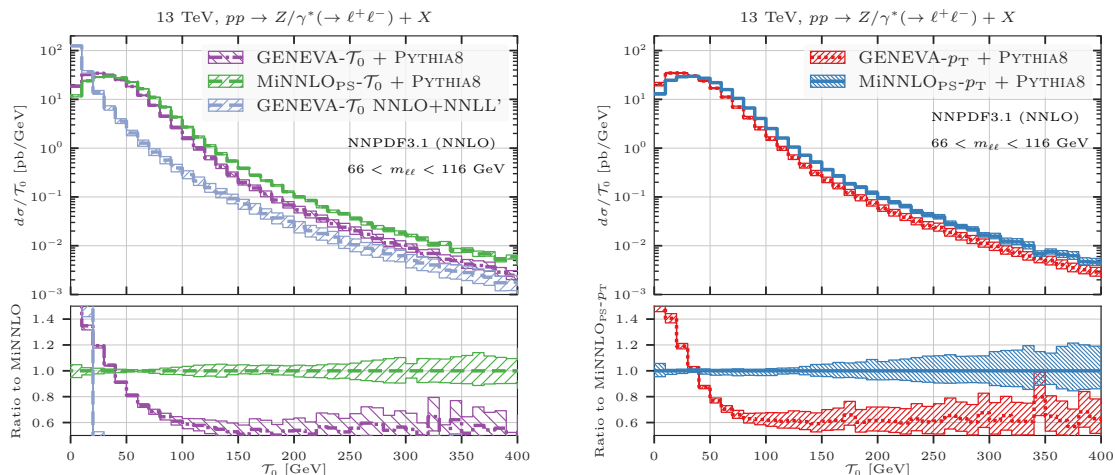


Figure 8. Comparison between $\text{MiNNLO}_{\text{PS}}$ and GENEVA predictions for the \mathcal{T}_0 distribution. Left panel: comparison of $\text{MiNNLO}_{\text{PS}}\text{-}\mathcal{T}_0$ (green, dashed) and GENEVA- \mathcal{T}_0 (purple, dot-dashed), as well as a parton-level NNLO+NNLL' curve. Right panel: Comparison between $\text{MiNNLO}_{\text{PS}}\text{-}p_T$ (blue, solid) and GENEVA- p_T (red, dotted) predictions.

ATLAS [74]	CMS [75]
$p_{T,\ell} > 27 \text{ GeV}$	$p_{T,\ell} > 25 \text{ GeV}$
$ \eta_\ell < 2.5$	$ \eta_\ell < 2.4$
$66 \text{ GeV} < m_{\ell\ell} < 116 \text{ GeV}$	$ m_{\ell\ell} - m_Z \text{ GeV} < 15 \text{ GeV}$

Table 2. Fiducial cuts used in the ATLAS and CMS analyses.

shown. The two analyses use similar fiducial cuts, which are reported in table 2. In figure 9 we present a comparison between $\text{MiNNLO}_{\text{PS}}\text{-}p_T$ (blue, solid) and $\text{MiNNLO}_{\text{PS}}\text{-}\mathcal{T}_0$ (green, dashed) predictions with ATLAS data. As for the transverse momentum of the dilepton system, our $\text{MiNNLO}_{\text{PS}}$ predictions are in good agreement with data throughout the entire spectrum. For very small values of $p_{T,\ell\ell}$ ($p_{T,\ell\ell} < 10 \text{ GeV}$), we observe a slight difference in shape between the $\text{MiNNLO}_{\text{PS}}$ curves and data, which is however not unexpected as this region is sensitive to soft-collinear radiation and requires an accurate resummation of large logarithmic terms. At large $p_{T,\ell\ell}$ values, both generators are NLO accurate only, which is reflected in the enlarged theory uncertainty bands. In this high- $p_{T,\ell\ell}$ region theory predictions tend to overestimate data but the agreement remains good, at 1–2 σ level. As for the angle ϕ^* , we observe that both generators agree rather well with data (1–2 σ level), but data tend to fall more sharply at large ϕ^* values. In figure 10 we present a comparison with CMS data. In this comparison we observe the same relative behaviour as with ATLAS data for both $p_{T,\ell\ell}$ and ϕ^* , so the same conclusions hold. Moreover, we present results for the rapidity distribution of the reconstructed Z boson $y_{\ell\ell}$, for which we observe an excellent description of the data with both $\text{MiNNLO}_{\text{PS}}\text{-}p_T$ and $\text{MiNNLO}_{\text{PS}}\text{-}\mathcal{T}_0$, with a discrepancy of a few percent only, relatively flat across the whole rapidity range.

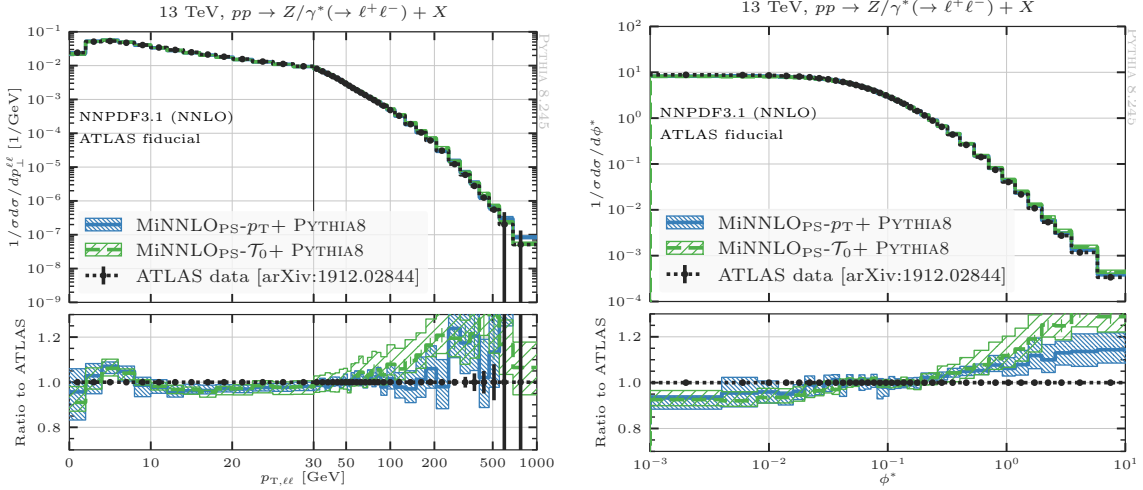


Figure 9. Comparison of MiNNLO_{PS}- p_T (blue, solid) and MiNNLO_{PS}- \mathcal{T}_0 (green, dashed) against ATLAS data from ref. [74] for the transverse momentum of the lepton pair (left) and the Collins-Soper angle ϕ^* (right), as defined in the main text.

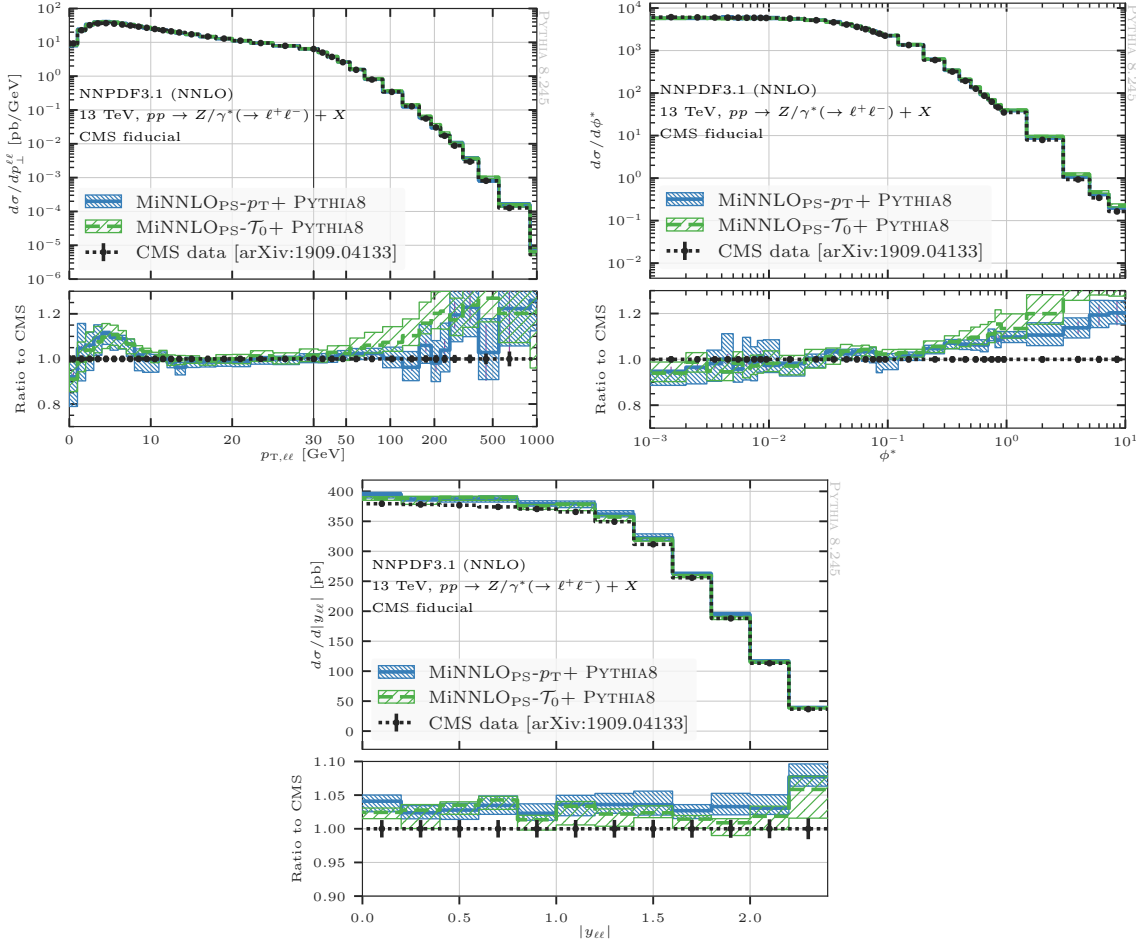


Figure 10. Comparison of MiNNLO_{PS}- p_T (blue, solid) and MiNNLO_{PS}- \mathcal{T}_0 (green, dashed) against CMS data from ref. [75] for the transverse momentum of the lepton pair (upper left) and the Collins-Soper angle ϕ^* (upper right), as defined in the main text, and the Z boson rapidity distribution (bottom plot).

5 Conclusions

We have presented the derivation of the $\text{MINNLO}_{\text{PS}}$ formalism using jettiness as resummation variable. This calculation opens the door to consider NNLO+PS matching for processes with additional jets in the final state. As a proof-of-concept we have performed a complete implementation of the $\text{MINNLO}_{\text{PS}}$ approach using the 0-jettiness variable for colour-singlet production. Specifically, we have considered Higgs-boson production and Drell-Yan production as a first implementation.

We have validated our $\text{MINNLO}_{\text{PS}}-\mathcal{T}_0$ implementation against the existing $\text{MINNLO}_{\text{PS}}-p_{\text{T}}$ generators, finding excellent agreement among their predictions within uncertainties for NNLO-accurate observables, including the total inclusive cross section and differential distributions, both for Higgs-boson and Drell-Yan production. On the other hand, for jet-related quantities in Higgs-boson production we observe larger differences between $\text{MINNLO}_{\text{PS}}-\mathcal{T}_0$ and $\text{MINNLO}_{\text{PS}}-p_{\text{T}}$ predictions. Those are present both at Les-Houches-Event level and after the inclusion of parton shower effects, but their relative difference remains almost identical before and after showering. The corresponding jet-related results for the Drell-Yan process are in good agreement between the $\text{MINNLO}_{\text{PS}}-\mathcal{T}_0$ and $\text{MINNLO}_{\text{PS}}-p_{\text{T}}$ implementations.

We then continued by presenting the first direct comparison of $\text{MINNLO}_{\text{PS}}$ predictions with existing results from the GENEVA generators for Drell-Yan production. For this process both $\text{MINNLO}_{\text{PS}}$ and GENEVA implementations exist using \mathcal{T}_0 and p_{T} as a matching variable. We have shown that for NNLO-accurate quantities $\text{MINNLO}_{\text{PS}}$ and GENEVA results are in excellent agreement within the respective higher-order uncertainties, which is not unexpected given that both approaches yield NNLO accurate predictions.

Finally, we have compared $\text{MINNLO}_{\text{PS}}-\mathcal{T}_0$ and $\text{MINNLO}_{\text{PS}}-p_{\text{T}}$ predictions to Drell-Yan data recorded by the ATLAS and by the CMS collaboration. By and large, we have found $\text{MINNLO}_{\text{PS}}$ predictions to be in remarkable agreement with the experimental data, with differences mostly within one standard deviation.

This work is a first important step towards NNLO+PS matching for processes with massless partons in the final state, such as Higgs plus jet and vector boson plus jet production, which has not been achieved for any such process to date. The implementation of the $\text{MINNLO}_{\text{PS}}$ approach based on \mathcal{T}_0 has been fully worked out, implemented and validated. We have also fully worked out all necessary formulae to obtain NNLO+PS accurate predictions for colour singlet plus jet production using \mathcal{T}_1 as a resummation variable. All equations are reported in appendix C. The complete implementation for \mathcal{T}_1 and application to a corresponding process, such as Higgs plus jet or Drell-Yan plus jet production, is left to future work.

Acknowledgments

We would like to thank Simone Alioli, Pier Francesco Monni and Paolo Nason for fruitful discussions, and we are grateful to Simone Alioli for comments on the manuscript. We also thank Kenneth Long for providing us details on the PYTHIA tune used for the $\text{MINNLO}_{\text{PS}}$ predictions by CMS and for useful discussion on the experimental analysis. L.R. has been supported by the SNSF under contract PZ00P2 201878. S.Z. has been supported by the

International Max Planck Research School (IMPRS) on “Elementary Particle Physics”. The research of S.Z. has also been supported by the European Research Council (ERC) under the European Union’s Horizon 2020 research and innovation program (grant agreement No. 788223, PanScales, and grant agreement No. 804394, HipQCD) and by the Science and Technology Facilities Council (STFC) under grant ST/T000864/1.

A Explicit formulae for $\text{MiNNLO}_{\text{PS}}\text{-}\mathcal{T}_0$

In this appendix, we collect explicit formulae of relevant perturbative ingredients we used or obtained in the main sections of this paper.

Notation. The QCD β function is expanded in terms of the strong coupling α_s as

$$\beta[\alpha_s(\mu)] = \frac{d\alpha_s(\mu)}{d \ln \mu^2} = -\alpha_s(\mu) \sum_{n=0}^{\infty} \beta_n [\alpha_s(\mu)]^{n+1}, \quad (\text{A.1})$$

where the coefficients β_n are given by [86, 87]

$$\begin{aligned} \beta_0 &= \frac{11C_A - 2n_f}{12\pi}, \\ \beta_1 &= \frac{17C_A^2 - (5C_A + 3C_F)n_f}{24\pi^2}, \\ \beta_2 &= \frac{2857C_A^3 + (54C_F^2 - 615C_A C_F - 1415C_A^2)n_f + (66C_F + 79C_A)n_f^2}{3456\pi^3}. \end{aligned} \quad (\text{A.2})$$

The DGLAP evolution kernels are defined by

$$\frac{\partial f_i(x, \mu)}{\partial \ln \mu^2} = \sum_j \int_x^1 \frac{dx'}{x'} \hat{P}_{ij}[x', \alpha_s(\mu)] f_j\left(\frac{x}{x'}, \mu\right), \quad (\text{A.3})$$

with the expansion of the splitting function given in eq. (3.37). We refer to ref. [1] for explicit expressions for the coefficients $\hat{P}^{(n)}(x)$.

Given a generic function F depending on the renormalization scale μ through the running coupling α_s , we define its perturbative expansion in terms of $\alpha_s/(2\pi)$ as:

$$F(\dots, \mu) = \sum_{n=0}^{\infty} F^{(n)}(\dots) \left[\frac{\alpha_s(\mu)}{2\pi} \right]^n. \quad (\text{A.4})$$

We note that this convention differs from the standard one used in the SCET literature. For a collection of all required ingredients in the standard SCET notation, see e.g. ref. [88].

\mathcal{T}_0 Sudakov form factor. The $\text{MiNNLO}_{\text{PS}}\text{-}\mathcal{T}_0$ Sudakov form factor presented in (3.20) depends on the A and B coefficients defined as in (3.21)

$$A(\alpha_s) = \Gamma_C(\alpha_s), \quad B_F(\alpha_s) = \frac{1}{2} \gamma_F(\alpha_s) - \beta(\alpha_s) \frac{d \ln \bar{F}(\alpha_s)}{d \alpha_s}, \quad (\text{A.5})$$

where \bar{F} can either be related to the hard or the soft functions. These coefficients admit the following perturbative expansion:

$$A(\alpha_s) = \sum_{n=1}^{\infty} A^{(n)} \left(\frac{\alpha_s}{2\pi} \right)^n, \quad B_F(\alpha_s) = \sum_{n=1}^{\infty} B_F^{(n)} \left(\frac{\alpha_s}{2\pi} \right)^n. \quad (\text{A.6})$$

The A coefficient is identical to the cusp anomalous dimension. Up to three loops, its coefficients obey Casimir scaling, i.e. $\Gamma_C^{(n)} \propto C$, where C is the Casimir of the given representation, for any given perturbative order n . Up to the third order, the coefficients $A^{(n)}$ are given by [89–91]

$$\begin{aligned}
 A^{(1)} &\equiv \Gamma_C^{(1)} = 2C, \\
 A^{(2)} &\equiv \Gamma_C^{(2)} = C \left[C_A \left(\frac{67}{9} - 2\zeta_2 \right) - \frac{10}{9} n_f \right], \\
 A^{(3)} &\equiv \Gamma_C^{(3)} = C \left[C_A^2 \left(\frac{245}{12} - \frac{268}{18} \zeta_2 + \frac{22}{6} \zeta_3 + 11\zeta_4 \right) + C_A n_f \left(-\frac{209}{54} + \frac{20}{9} \zeta_2 - \frac{14}{3} \zeta_3 \right) \right. \\
 &\quad \left. + C_F n_f \left(-\frac{55}{12} + 4\zeta_3 \right) - \frac{2}{27} n_f^2 \right], \tag{A.7}
 \end{aligned}$$

where $C = C_F$ for quark-induced processes and $C = C_A$ for gluon-induced processes. Note that $A^{(1)}$ and $A^{(2)}$ agree with the corresponding expressions for p_T resummation given in ref. [1], while the expression of $A^{(3)}$ differs from the one for p_T resummation, as given in ref. [1].

The B coefficient for the hard function reads

$$B_H(\alpha_s) = 2\gamma_H(\alpha_s) - \beta(\alpha_s) \frac{d \ln \bar{H}_{ab}(\alpha_s)}{d\alpha_s}, \tag{A.8}$$

where \bar{H}_{ab} is the hard function and γ_H is the hard anomalous dimension, with $\gamma_H = \gamma_H^q(\gamma_H^g)$ for quarks (gluons). To the required order, they read [92–96]

$$2\gamma_H^{q(1)} = -3C_F, \tag{A.9}$$

$$2\gamma_H^{q(2)} = C_F \left[C_F \left(6\zeta_2 - 12\zeta_3 - \frac{3}{4} \right) + C_A \left(-\frac{11}{2} \zeta_2 + 13\zeta_3 - \frac{961}{108} \right) + n_f \left(\zeta_2 + \frac{65}{54} \right) \right],$$

$$2\gamma_H^{g(1)} = -4\pi\beta_0, \tag{A.10}$$

$$2\gamma_H^{g(2)} = C_A^2 \left(\frac{11}{6} \zeta_2 + \zeta_3 - \frac{346}{27} \right) + C_A n_f \left(\frac{64}{27} - \frac{\zeta_2}{3} \right) + C_F n_f.$$

The fixed-order expansion of eq. (A.8) thus reads

$$\begin{aligned}
 B_H^{(1)} &= 2\gamma_H^{(1)}, \\
 B_H^{(2)} &= 2\gamma_H^{(2)} + 2\pi\beta_0 H^{(1)}, \tag{A.11}
 \end{aligned}$$

where $H^{(1)}$ refers to the one-loop coefficient of the corresponding hard function, which is given below for Higgs-boson and Drell-Yan production.

For the \mathcal{T}_0 soft function, the B coefficient is defined as

$$B_S(\alpha_s) = \frac{1}{2} \gamma_S(\alpha_s) - \beta(\alpha_s) \frac{d \ln \bar{S}(\alpha_s)}{d\alpha_s}, \tag{A.12}$$

where γ_S is the anomalous dimension of the soft function \bar{S} . Up to second order, its expansion coefficients obey Casimir scaling and read

$$\begin{aligned}
 \gamma_S^{(1)} &= 0, \\
 \gamma_S^{(2)} &= C \left[C_A \left(\frac{11}{3} \zeta_2 + 14\zeta_3 - \frac{404}{27} \right) + n_f \left(\frac{56}{27} - \frac{2}{3} \zeta_2 \right) \right]. \tag{A.13}
 \end{aligned}$$

The fixed-order expansion of eq. (A.12) reads

$$\begin{aligned} B_S^{(1)} &= 0, \\ B_S^{(2)} &= C \left[C_A \left(7\zeta_3 - \frac{16}{9} \right) - 2\pi\beta_0 \left(2\zeta_2 + \frac{28}{9} \right) \right]. \end{aligned} \quad (\text{A.14})$$

Here, we used the one-loop result for S given in eq. (A.20).

We now present explicit expressions for the hard, beam and soft functions.

\mathcal{T}_0 hard function. The hard function is defined in eq. (3.13) as

$$\bar{H}_{ab}(Q, \mu = Q) = 1 + \frac{\alpha_s(Q)}{2\pi} H_{ab}^{(1)} + \left[\frac{\alpha_s(Q)}{2\pi} \right]^2 H_{ab}^{(2)} + \mathcal{O}(\alpha_s^3). \quad (\text{A.15})$$

The coefficients $H^{(1)}$ and $H^{(2)}$ for Higgs and Drell-Yan production are identical to those used in ref. [1] without including the shift $\Delta H^{(2)}$ from momentum-space resummation. For completeness, we repeat them here.

The hard function for Higgs production in the $m_t \rightarrow \infty$ limit is obtained by combining the IR-finite gluon form factor, which is known up to three loops [97–102], with the Wilson coefficient from integrating out the top quark, which itself is known up to four loops [103–105]. Here, we only need the results up to two loops, which are given by

$$\begin{aligned} H_{gg}^{(1)} &= C_A \left(5 + \frac{7}{6}\pi^2 \right) - 3C_F, \\ H_{gg}^{(2)} &= \left(\frac{7}{2}C_A^2 - \frac{11}{2}C_A C_F + 2C_F n_f \right) \log \frac{m_H^2}{m_t^2} + C_A^2 \left(\frac{755\pi^2}{72} - \frac{143\zeta_3}{18} + \frac{37\pi^4}{72} + \frac{23827}{648} \right) \\ &\quad + C_A \left[C_F \left(-\frac{145}{6} - \frac{7}{2}\pi^2 \right) + n_f \left(-\frac{23}{9}\zeta_3 - \frac{25}{36}\pi^2 - \frac{2255}{324} \right) - \frac{5}{24} \right] \\ &\quad + C_F \left[9C_F + n_f \left(4\zeta_3 - \frac{41}{6} \right) - \frac{1}{3} \right]. \end{aligned} \quad (\text{A.16})$$

For Drell-Yan, the hard function is obtained from the IR-finite quark vector form factor which is known up to three loops [98–102, 106–109]. Starting at $\mathcal{O}(\alpha_s^2)$ there are also nonvanishing singlet contributions from the axial anomaly, which are known to have a small effect on the cross section [110, 111] and are thus neglected here. (For a detailed discussion of its inclusion in the hard function, see e.g. ref. [112].) The hard function coefficients are

$$\begin{aligned} H_{q\bar{q}}^{(1)} &= C_F \left(\frac{7}{6}\pi^2 - 8 \right), \\ H_{q\bar{q}}^{(2)} &= C_F^2 \left(-\frac{83}{12}\pi^2 - 15\zeta_3 + \frac{67}{120}\pi^4 + \frac{511}{16} \right) + C_A C_F \left(\frac{1061}{216}\pi^2 + \frac{313}{18}\zeta_3 - \frac{2}{45}\pi^4 - \frac{51157}{1296} \right) \\ &\quad + C_F n_f \left(-\frac{91}{108}\pi^2 + \frac{\zeta_3}{9} + \frac{4085}{648} \right). \end{aligned} \quad (\text{A.17})$$

Setting $N_c = 3$ and $n_f = 5$, eqs. (A.16) and (A.17) reproduce eqs. (B.10) and (B.12) in ref. [1].

\mathcal{T}_0 beam functions. The beam functions for leptonic \mathcal{T}_0 are defined in eqs. (3.16) and (3.17) as

$$B_i\left(\frac{y}{Q}, x, \mu_B\right) = \sum_j \int_x^1 \frac{dx'}{x'} \mathcal{C}_{ij}\left(\frac{y}{Q}, x', \mu_B\right) f_j\left(\frac{x}{x'}, \mu_B\right),$$

$$\bar{\mathcal{C}}_{ij}(x, \mu_B) \equiv \mathcal{C}_{ij}\left(\frac{y}{Q}, x, \mu_B\right) = \delta_{ij} \delta(1-z) + \sum_{n=1}^{\infty} \left[\frac{\alpha_s(\mu_B)}{2\pi}\right]^n \mathcal{C}_{ij}^{(n)}(z), \quad (\text{A.18})$$

where $\mu_B = \sqrt{Qy_0/y}$ is fixed to minimize all logarithms in Fourier space. At two loops, the beam functions have been calculated in refs. [39, 40, 95] in momentum space. To obtain the functions $\bar{\mathcal{C}}_{ij}$, one has to first perform the Fourier transform as defined in eq. (3.7), and then choose $\mu_B = \sqrt{Qy_0/y}$ to eliminate explicit logarithms. Alternatively, one can obtain them directly from the results provided in ref. [113] in Fourier space upon setting the logarithm $L_y = 0$ in there.⁸ It is then trivial to combine the results for $\bar{\mathcal{C}}_{ij}$ with the soft function given below to obtain the coefficients \bar{C}_{ij} as defined in eq. (3.18). Since the $\bar{\mathcal{C}}_{ij}$ are rather lengthy and provided as Mathematica files with ref. [113], we do not provide explicit expressions here.

\mathcal{T}_0 soft function. The soft function is defined in eq. (3.13) as

$$\bar{S}(y_0/y) = 1 + \frac{\alpha_s(y_0/y)}{2\pi} S^{(1)} + \left[\frac{\alpha_s(y_0/y)}{2\pi}\right]^2 S^{(2)} + \mathcal{O}(\alpha_s^3). \quad (\text{A.19})$$

The two loop results have been calculated in momentum space in refs. [114–117]. Taking cross terms induced by the Fourier transform into account, we obtain

$$S^{(1)} = -\frac{\pi^2}{2} C, \quad (\text{A.20})$$

$$S^{(2)} = C \left[C_A \left(-\frac{\pi^2}{9} + \frac{7}{30} \pi^4 - \frac{160}{27} \right) + 4\pi\beta_0 \left(-\frac{77}{72} \pi^2 + \frac{13}{6} \zeta_3 - \frac{5}{27} \right) \right] + \frac{\pi^4}{8} C^2,$$

where $C = C_F$ for quark annihilation and $C = C_A$ for gluon fusion.

B Phase space parametrisation for the $D^{(\geq 3)}[\mathcal{T}_0]$ term

In this appendix we discuss the parametrisation of the factor $F^{\text{corr}}(\Phi_{\text{FJ}})$ in eq. (3.57). The starting point is the POWHEG projection of the FJ phase space Φ_{FJ} onto the F phase space Φ_{F} for initial state radiation. The Φ_{FJ} phase space can be expressed in the following factorised form (see 5.1.1 of [50] for additional details)

$$d\Phi_{\text{FJ}} = d\Phi_{\text{F}} d\Phi_{\text{rad}}, \quad d\Phi_{\text{rad}} = \frac{s}{(4\pi)^3} \frac{\xi}{1-\xi} d\xi d\phi dy \quad (\text{B.1})$$

where s is the square of the total incoming energy and we have introduced the variables

$$\xi = \frac{2k^0}{\sqrt{s}}, \quad y = \cos\theta, \quad k_T^2 = \frac{s}{4} \xi^2 (1-y^2), \quad (\text{B.2})$$

⁸Note that the results in ref. [113] are expanded in α_s/π instead of $\alpha_s/(2\pi)$.

where k^0 , θ and ϕ are the energy, the scattering angle and the azimuth of the radiated parton, respectively, defined in the centre-of-mass frame of the FJ system.

For a single real emission the definition of \mathcal{T}_0 in eq. (3.1) yields

$$\mathcal{T}_0 = k_T e^{-|Y-\eta_k|}, \quad (\text{B.3})$$

where η_k is the rapidity of the emission in the laboratory frame. Using the relation

$$\eta_k = \frac{1}{2} \ln \frac{x_1(1+y)}{x_2(1-y)}, \quad (\text{B.4})$$

we obtain

$$\mathcal{T}_0 = k_T e^{-|\Delta Y(y)|}, \quad \Delta Y(y) = \frac{1}{2} \ln \frac{x_1(1+y)}{x_2(1-y)} - Y, \quad (\text{B.5})$$

in terms of the momentum fractions of the two initial-state partons in the Φ_{FJ} phase space $x_{1,2}$ and the rapidity of the colour-singlet system Y . In eq. (B.5), it is important to note that k_T and $x_{1,2}$ themselves depend on ξ and y . Making all of this dependence manifest, we obtain

$$\begin{aligned} \mathcal{T}_0 &= \frac{Q\xi}{2} \frac{\sqrt{1-y^2}}{\sqrt{1-\xi}} e^{-|\Delta Y(\bar{x}_{1,2}, \xi, y)|}, \\ \Delta Y(\bar{x}_{1,2}, \xi, y) &= \frac{1}{2} \ln \frac{1+y}{1-y} \frac{\bar{x}_1}{\bar{x}_2} \frac{2-\xi(1-y)}{2-\xi(1+y)} - Y, \end{aligned} \quad (\text{B.6})$$

where the barred momentum fractions are [50]

$$\bar{x}_1 = x_1 \sqrt{1-\xi} \sqrt{\frac{2-\xi(1+y)}{2-\xi(1-y)}}, \quad \bar{x}_2 = x_2 \sqrt{1-\xi} \sqrt{\frac{2-\xi(1-y)}{2-\xi(1+y)}}, \quad (\text{B.7})$$

and Q is the invariant mass of the colour-singlet system.

B.1 Evaluation of F_ℓ^{corr}

The factor $F^{\text{corr}}(\Phi_{\text{FJ}})$ is defined as

$$F_\ell^{\text{corr}}(\Phi_{\text{FJ}}) = \frac{J_\ell(\Phi_{\text{FJ}})}{\sum_{\ell'} \int d\Phi'_{\text{rad}} J_{\ell'}(\Phi'_{\text{FJ}}) \delta(\mathcal{T}_0 - \mathcal{T}'_0)}, \quad (\text{B.8})$$

where $\bar{\Phi}'_{\text{FJ}} \equiv \Phi'_{\text{FJ}}|_{\Phi'_F = \Phi_F}$, whereas $J_\ell(\Phi_{\text{FJ}})$ is an arbitrary function of Φ_{FJ} . In our implementation we use the expressions (A.13) and (A.14) of ref. [1].

Using eq. (B.5), we then obtain

$$\frac{J_\ell(\Phi_{\text{FJ}})}{F_\ell^{\text{corr}}(\Phi_{\text{FJ}})} = \sum_{\ell'} \int d\xi d\phi dy \frac{s}{(4\pi)^3} \frac{\xi}{1-\xi} J_{\ell'}(\bar{\Phi}'_{\text{FJ}}) \delta\left(\mathcal{T}_0 - \frac{\xi\sqrt{s}}{2} \frac{\sqrt{1-y^2}}{e^{|\Delta Y(y)|}}\right), \quad (\text{B.9})$$

which is the straightforward extension of eq. (A.6) in [1] for \mathcal{T}_0 . After re-arranging the δ function and using eq. (B.6) we have

$$\frac{J_\ell(\Phi_{\text{FJ}})}{F_\ell^{\text{corr}}(\Phi_{\text{FJ}})} = \frac{\mathcal{T}_0}{(2\pi)^2} \sum_{\ell'} \int d\xi dy J_{\ell'}(\bar{\Phi}'_{\text{FJ}}) \frac{\xi}{(1-\xi)^2} \delta\left(\frac{4\mathcal{T}_0^2}{Q^2} - \frac{\xi^2}{1-\xi} \frac{1-y^2}{e^{2|\Delta Y(\bar{x}_{1,2}, \xi, y)|}}\right). \quad (\text{B.10})$$

In order to solve the δ , we change the integration variables from (ξ, y) to (k_T, η_k) using the relations

$$k_T = \frac{Q}{2} \xi \frac{\sqrt{1-y^2}}{\sqrt{1-\xi}}, \quad \eta_k = \frac{1}{2} \ln \left[\frac{\bar{x}_1 (1+y) (2-\xi(1-y))}{\bar{x}_2 (1-y) (2-\xi(1+y))} \right]. \quad (\text{B.11})$$

The Jacobian of this variable transformation is given by

$$d\xi dy = \frac{2(1-\xi)^2}{Q^2 \xi} dk_T^2 d\eta_k. \quad (\text{B.12})$$

In terms of these variables, the FKS radiation phase space reads

$$d\Phi_{\text{rad}} = \frac{s}{(4\pi)^3} \frac{\xi}{1-\xi} d\xi d\phi dy = \frac{2}{(4\pi)^3} dk_T^2 d\eta_k d\phi. \quad (\text{B.13})$$

Applying this together with eq. (B.3) to eq. (B.8), we obtain

$$\begin{aligned} \frac{J_\ell(\Phi_{\text{FJ}})}{F_\ell^{\text{corr}}(\Phi_{\text{FJ}})} &= \sum_{\ell'} \int d\Phi'_{\text{rad}} J_{\ell'}(\bar{\Phi}'_{\text{FJ}}) \delta(\mathcal{T}_0 - k_T e^{-|Y-\eta_k|}) \\ &= \sum_{\ell'} \int \frac{dk_T^2 d\eta_k}{(4\pi)^2} J_{\ell'}(\bar{\Phi}'_{\text{FJ}}) \delta(\mathcal{T}_0 - k_T e^{-|Y-\eta_k|}) \\ &= \sum_{\ell'} \frac{\mathcal{T}_0}{8\pi^2} \int d\eta_k J_{\ell'}(\bar{\Phi}'_{\text{FJ}}) e^{2|Y-\eta_k|}. \end{aligned} \quad (\text{B.14})$$

In order to evaluate $J_{\ell'}$ we now need to find the kinematic bounds of η_k , and express y and ξ as a function of k_T and η_k . To see that the inverse of eq. (B.11) is unique, consider that

$$\frac{d\eta_k}{dy} = \frac{4 - 2\xi(1+y^2)}{4(1-y^2)(1-\xi) + (1-y^2)^2 \xi^2} > 0, \quad (\text{B.15})$$

where the inequality follows since $-1 \leq y \leq 1$ and $0 \leq \xi \leq 1$. It is useful to introduce the parameters

$$\kappa = \frac{\bar{x}_2}{\bar{x}_1} e^{2\eta_k} = e^{2(\eta_k - Y)}, \quad \beta = 2 + \frac{1+\kappa}{\sqrt{\kappa}} \sqrt{1 + \frac{Q^2}{k_T^2}}, \quad (\text{B.16})$$

through which we can express ξ and y as

$$\xi = 1 - \frac{1}{1 + \beta \frac{k_T^2}{Q^2}}, \quad y = \frac{\kappa - 1}{\kappa + 1} \left(1 - \frac{2}{\beta} \right). \quad (\text{B.17})$$

Note that $\kappa \geq 0$ and $\beta \geq 2$, and hence eq. (B.17) always obeys the obvious bounds $0 < \xi < 1$ and $-1 < y < 1$. In order to identify the kinematic bounds on k_T, η_k we insert eq. (B.17) into eq. (B.7),

$$\begin{aligned} x_{1,2} &= \bar{x}_{1,2} \left(\sqrt{1 + \epsilon^2} + \epsilon \kappa^{\pm 1/2} \right) \\ &= \bar{x}_{1,2} \left(\sqrt{1 + \epsilon^2} + \epsilon e^{\pm(\eta_k - Y)} \right), \end{aligned} \quad (\text{B.18})$$

where $\epsilon = k_T/Q$. Eq. (B.18) clearly implies $x_{1,2} \geq \bar{x}_{1,2}$, so we only need to solve for the constraints $x_{1,2} \leq 1$. Since $x_{1,2}$ are monotonically growing with ϵ , we easily find

$$\epsilon = \frac{k_T}{Q} \leq \epsilon_{\max}, \quad \epsilon_{\max} = \min \left\{ \frac{\sqrt{1 - (1 - \kappa)\bar{x}_1^2} - \sqrt{\kappa}}{\bar{x}_1(1 - \kappa)}, (\bar{x}_1 \rightarrow \bar{x}_2, \kappa \rightarrow \kappa^{-1}) \right\}. \quad (\text{B.19})$$

Inserting this constraint into eq. (B.14), we obtain

$$\frac{J_\ell(\Phi_{\text{FJ}})}{F_\ell^{\text{corr}}(\Phi_{\text{FJ}})} = \sum_{\ell'} \frac{\mathcal{T}_0}{8\pi^2} \int d\eta_k J_{\ell'}(\bar{\Phi}'_{\text{FJ}}) e^{2|Y - \eta_k| \Theta} \left(\frac{Q\epsilon_{\max}}{\mathcal{T}_0 e^{|\eta_k - Y|}} - 1 \right). \quad (\text{B.20})$$

B.2 Analytic solution of the phase-space constraints

We can finally derive an analytic solution to this phase space bound. Defining

$$\tau_0 = \frac{\mathcal{T}_0}{Q} = \frac{k_T}{Q} e^{-|\eta_k - Y|}, \quad (\text{B.21})$$

the phase space bound from eq. (B.18) can be written as

$$\begin{aligned} x_1 &= \bar{x}_1 \left(\tau_0 e^{|\eta_k - Y|} e^{+(\eta_k - Y)} + \sqrt{1 + \tau_0^2 e^{2|\eta_k - Y|}} \right) \leq 1, \\ x_2 &= \bar{x}_2 \left(\tau_0 e^{|\eta_k - Y|} e^{-(\eta_k - Y)} + \sqrt{1 + \tau_0^2 e^{2|\eta_k - Y|}} \right) \leq 1. \end{aligned} \quad (\text{B.22})$$

By using $Y = \frac{1}{2} \ln(\bar{x}_1/\bar{x}_2)$, we can write $\bar{x}_{1,2} = \sqrt{\bar{x}_1 \bar{x}_2} e^{\pm Y}$. Thus, we obtain the symmetrical result

$$\tau_0 e^{|\eta_k - Y|} e^{\pm(\eta_k - Y)} + \sqrt{1 + \tau_0^2 e^{2|\eta_k - Y|}} \leq \frac{e^{\mp Y}}{\sqrt{\bar{x}_1 \bar{x}_2}}. \quad (\text{B.23})$$

Defining $s \equiv \text{sgn}(\eta_k - Y)$, the two cases $s = \pm 1$ can be combined as

$$\begin{aligned} \tau_0 e^{2|\eta_k - Y|} + \sqrt{1 + \tau_0^2 e^{2|\eta_k - Y|}} &\leq \frac{e^{-sY}}{\sqrt{\bar{x}_1 \bar{x}_2}} \equiv c(+s), \\ \tau_0 + \sqrt{1 + \tau_0^2 e^{2|\eta_k - Y|}} &\leq \frac{e^{sY}}{\sqrt{\bar{x}_1 \bar{x}_2}} \equiv c(-s). \end{aligned} \quad (\text{B.24})$$

For brevity, we defined $c(s) = (\sqrt{\bar{x}_1 \bar{x}_2} e^{sY})^{-1}$ such that

$$c(+1) = (\sqrt{\bar{x}_1 \bar{x}_2} e^Y)^{-1} = \frac{1}{\bar{x}_1}, \quad c(-1) = (\sqrt{\bar{x}_1 \bar{x}_2} e^{-Y})^{-1} = \frac{1}{\bar{x}_2}. \quad (\text{B.25})$$

Since the constraints in eq. (B.24) are monotonically increasing with $|\eta_k - Y|$, we can solve them fairly easily. We obtain

$$\begin{aligned} |\eta_k - Y| &\leq \Delta Y_{\max}[\text{sgn}(\eta_k - Y)], \\ \Delta Y_{\max}(s) &= \min \left\{ \frac{1}{2} \ln \frac{\tau_0 + 2c(s) - \sqrt{\tau_0^2 + 4c(s)\tau_0 + 4}}{2\tau_0}, \frac{1}{2} \ln \frac{[\tau_0 - c(-s)]^2 - 1}{\tau_0^2} \right\}. \end{aligned} \quad (\text{B.26})$$

For this bound to be positive, we have to impose that

$$c(s) \geq 1 \quad \wedge \quad |\tau_0 - c(-s)| > 1, \quad (\text{B.27})$$

where the first constraint is always fulfilled since $c(\pm 1) = \frac{1}{\bar{x}_{1,2}} \geq 1$. To construct the final solution, consider both cases separately:

$$\begin{aligned} \eta_k > Y : \quad \eta_k - Y &\leq +\Delta Y_{\max}(+1) \quad \Leftrightarrow \quad \eta_k \leq Y + \Delta Y_{\max}(+1), \\ \eta_k < Y : \quad \eta_k - Y &\geq -\Delta Y_{\max}(-1) \quad \Leftrightarrow \quad \eta_k \geq Y - \Delta Y_{\max}(-1). \end{aligned} \quad (\text{B.28})$$

In summary, we obtain that

$$\eta_{\min} \leq \eta_k \leq \eta_{\max}, \quad (\text{B.29})$$

with

$$\eta_{\min} = Y - \Delta Y_{\max}(-1), \quad \eta_{\max} = Y + \Delta Y_{\max}(+1). \quad (\text{B.30})$$

To ensure that the solution is physical, we have to require that

$$\left| \tau_0 - \frac{1}{\bar{x}_{1,2}} \right| > 1 \quad \wedge \quad \eta_{\min} \leq \eta_{\max}. \quad (\text{B.31})$$

For the actual numerical implementation we perform the variable transform

$$t = \tanh(\eta_k - Y), \quad (\text{B.32})$$

which maps $\eta_k \in (-\infty, \infty)$ into the finite range $t \in (-1, 1)$. Taking the Jacobian into account, we find

$$\begin{aligned} \frac{J_\ell(\Phi_{\text{FJ}})}{F_\ell^{\text{corr}}(\Phi_{\text{FJ}})} &= \sum_{\ell'} \frac{\mathcal{T}_0}{8\pi^2} \int_{t_{\min}}^{t_{\max}} \frac{dt}{1-t^2} \frac{1+|t|}{1-|t|} J_{\ell'}(\bar{\Phi}'_{\text{FJ}}) \\ &= \sum_{\ell'} \frac{\mathcal{T}_0}{8\pi^2} \int_{t_{\min}}^{t_{\max}} \frac{dt}{(1-|t|)^2} J_{\ell'}(\bar{\Phi}'_{\text{FJ}}), \end{aligned} \quad (\text{B.33})$$

and the integration bounds are given by

$$\begin{aligned} t_{\min} &= \tanh[-\Delta Y_{\max}(-1)] = \frac{T_{\min} - 1}{T_{\min} + 1}, \\ t_{\max} &= \tanh[+\Delta Y_{\max}(+1)] = \frac{T_{\max} - 1}{T_{\max} + 1}, \end{aligned} \quad (\text{B.34})$$

where $\Delta_{\pm} \equiv \Delta Y_{\max}(\pm 1)$ and

$$\begin{aligned} \frac{1}{T_{\min}} &= e^{2\Delta Y_{\max}(-1)} = \min \left\{ \frac{\tau_0 + 2\bar{x}_2^{-1} - \sqrt{\tau_0^2 + 4\bar{x}_2^{-1}\tau_0 + 4}}{2\tau_0}, \frac{[\tau_0 - \bar{x}_1^{-1}]^2 - 1}{\tau_0^2} \right\}, \\ T_{\max} &= e^{2\Delta Y_{\max}(+1)} = \min \left\{ \frac{\tau_0 + 2\bar{x}_1^{-1} - \sqrt{\tau_0^2 + 4\bar{x}_1^{-1}\tau_0 + 4}}{2\tau_0}, \frac{[\tau_0 - \bar{x}_2^{-1}]^2 - 1}{\tau_0^2} \right\}. \end{aligned} \quad (\text{B.35})$$

The solution is physical if and only if

$$T_{\min} > 0 \quad \wedge \quad T_{\max} > 0 \quad \wedge \quad T_{\min} \leq T_{\max}, \quad (\text{B.36})$$

or equivalently

$$-1 < t_{\min} < -1 \quad \wedge \quad -1 < t_{\max} < -1 \quad \wedge \quad t_{\min} \leq t_{\max}. \quad (\text{B.37})$$

Finally, note that with this change of variables

$$\kappa = e^{2(\eta_k - Y)} = \frac{1+t}{1-t}, \quad (\text{B.38})$$

with which eq. (B.17) becomes

$$\xi = 1 - \frac{1}{1 + \beta\epsilon^2}, \quad y = t \left(1 - \frac{2}{\beta}\right), \quad \beta = 2 + 2t\sqrt{\frac{1+\epsilon^2}{1-t^2}}, \quad (\text{B.39})$$

with

$$\epsilon^2 = \frac{k_T^2}{Q^2} = \tau_0^2 e^{2|\eta_k - Y|} = \tau_0^2 \frac{1+|t|}{1-|t|}. \quad (\text{B.40})$$

B.3 Application to p_T

We finally note that we can obtain a simpler result than the one in appendix A of [1] starting from the relation

$$\begin{aligned} \left[\frac{J_\ell(\Phi_{\text{FJ}})}{F_\ell^{\text{corr}}(\Phi_{\text{FJ}})} \right]_{p_T} &\stackrel{!}{=} e^{-|Y-\eta_k|} \left[\frac{J_\ell(\Phi_{\text{FJ}})}{F_\ell^{\text{corr}}(\Phi_{\text{FJ}})} \right]_{\mathcal{T}_0=p_T e^{-|Y-\eta_k|}} \\ &= \sum_{\ell'} \frac{p_T}{8\pi^2} \int d\eta_k J_{\ell'}(\bar{\Phi}'_{\text{FJ}}) \Theta(Q\epsilon_{\max} - p_T). \end{aligned} \quad (\text{B.41})$$

The Θ constraint is different from the one in eq. (B.14) due to the missing factor $e^{|Y-\eta_k|}$. We can actually solve this bound analytically. Using eq. (B.19), the constraint reads

$$\epsilon \leq \frac{\sqrt{1 - (1-\kappa)\bar{x}_1^2} - \sqrt{\kappa}}{\bar{x}_1(1-\kappa)} \quad \wedge \quad \epsilon \leq \frac{\sqrt{1 - (1-\kappa^{-1})\bar{x}_2^2} - \sqrt{\kappa^{-1}}}{\bar{x}_2(1-\kappa^{-1})}. \quad (\text{B.42})$$

Where here $\kappa = e^{2\eta_k} \bar{x}_2 / \bar{x}_1$ and $\epsilon = p_T / Q$. Both constraints are monotonic with κ , so solving for equality gives the bounds on η_k . The quadratic equations are solved easily and yield

$$\eta_{\min} = -\ln \frac{1 - \bar{x}_2 \sqrt{1 + \epsilon^2}}{\epsilon \sqrt{\bar{x}_1 \bar{x}_2}}, \quad \eta_{\max} = \ln \frac{1 - \bar{x}_1 \sqrt{1 + \epsilon^2}}{\epsilon \sqrt{\bar{x}_1 \bar{x}_2}}. \quad (\text{B.43})$$

These solutions are only physical if

$$\epsilon \leq \frac{\sqrt{1 - \bar{x}_{1,2}}}{\bar{x}_{1,2}} \quad \wedge \quad \eta_{\min} < \eta_{\max}. \quad (\text{B.44})$$

With these constraints, eq. (B.41) becomes

$$\left[\frac{J_\ell(\Phi_{\text{FJ}})}{F_\ell^{\text{corr}}(\Phi_{\text{FJ}})} \right]_{p_T} = \sum_{\ell'} \frac{p_T}{8\pi^2} \int_{\eta_{\min}}^{\eta_{\max}} d\eta_k J_{\ell'}(\bar{\Phi}'_{\text{FJ}}). \quad (\text{B.45})$$

In practice, it is useful to restrict to perform a variable transformation in eq. (B.47) to have a finite integration range. We choose the transform

$$t : (-\infty, \infty) \rightarrow (-1, 1), \quad \eta \mapsto t(\eta) = \tanh(\eta). \quad (\text{B.46})$$

Taking the Jacobian into account, eq. (B.45) becomes

$$\left[\frac{J_\ell(\Phi_{\text{FJ}})}{F_\ell^{\text{corr}}(\Phi_{\text{FJ}})} \right]_{p_T} = \sum_{\ell'} \frac{p_T}{8\pi^2} \int_{t_{\min}}^{t_{\max}} \frac{dt}{1-t^2} J_{\ell'}(\bar{\Phi}'_{\text{FJ}}), \quad (\text{B.47})$$

with the integration bounds given by

$$\begin{aligned} t_{\min} &= \tanh \eta_{\min} = \frac{e^{2\eta_{\min}} - 1}{e^{2\eta_{\min}} + 1}, \\ t_{\max} &= \tanh \eta_{\max} = \frac{e^{2\eta_{\max}} - 1}{e^{2\eta_{\max}} + 1}. \end{aligned} \quad (\text{B.48})$$

C MINNLO_{PS} for colour-singlet plus jet production using 1-jettiness

Here, we briefly review 1-jettiness factorization and the associated evolution equations, and derive the MINNLO_{PS} method based on \mathcal{T}_1 . The steps proceed analogously to the case of \mathcal{T}_0 that was presented in detail in section 3, to which we refer for more details on key steps of the derivation.

C.1 Review of \mathcal{T}_1 factorization and evolution

We begin by reviewing the resummation formalism for 1-jettiness \mathcal{T}_1 [54]. We denote the underlying 1-jet Born process and corresponding momenta as

$$a(q_a) + b(q_b) \rightarrow F(q) + j(q_j), \quad (\text{C.1})$$

where a and b label the incoming partons with momenta q_a and q_b , respectively, j is the parton initiating the outgoing jet with momentum q_j , and F is the colour-singlet final state of total momentum q . For an event with $M \geq 1$ final-state partons, one requires an infrared-safe projection onto the 1-jet configuration in eq. (C.1). The projection determines a 1-jet kinematics of the form in eq. (C.1) with massless reference vectors $q_i^\mu = E_i(1, \vec{n}_i)$,⁹ where the incoming momenta $q_{a,b}$ are always aligned along the beam axes. Following ref. [55], we define \mathcal{T}_1 as

$$\mathcal{T}_1 = \sum_k \min_{i \in \{a,b,j\}} \left\{ \frac{2q_i \cdot p_k}{Q_i} \right\} = \sum_k \min \left\{ \frac{2q_a \cdot p_k}{Q_a}, \frac{2q_b \cdot p_k}{Q_b}, \frac{2q_j \cdot p_k}{Q_j} \right\}, \quad (\text{C.2})$$

⁹If the jet clustering yields massive jets, one can trivially construct massless reference vectors as $q_i^\mu = E_i n_i^\mu$ with $n_i^\mu = (1, \vec{P}_i/|\vec{P}_i|)$, where E_i and \vec{P}_i are the energy and momentum of the jet, respectively.

where the sum runs over all final-state hadronic momenta p_k , and q_i are the Born-like reference momenta as described above. The normalization factors Q_i in eq. (C.2) allow for different definitions of 1-jettiness. Different choices of the Q_i and algorithms for determining the q_i only affect power corrections to the factorization theorem, but not its functional form. For later convenience, we also define normalized directions and their scalar products as

$$\hat{q}_i^\mu = \frac{q_i^\mu}{Q_i}, \quad \hat{s}_{ij} = 2\hat{q}_i \cdot \hat{q}_j = \frac{2q_i \cdot q_j}{Q_i Q_j}. \quad (\text{C.3})$$

Note that all q_i correspond to physical momenta, and hence all $q_i \cdot q_j > 0$.

1-jettiness obeys a factorization theorem in the limit $\mathcal{T}_1 \rightarrow 0$ [54],

$$\begin{aligned} \frac{d\sigma^{\text{sing}}}{d\Phi_{\text{FJ}}d\mathcal{T}_1} &= \sum_{\kappa} \frac{d|\mathcal{M}_{\kappa}|^2}{d\Phi_{\text{FJ}}} H_{\kappa}(\Phi_{\text{FJ}}, \mu) \int dt_a dt_b dt_j B_a(t_a, x_a, \mu) B_b(t_b, x_b, \mu) J_j(t_j, \mu) \\ &\times S_{\kappa} \left(\mathcal{T}_1 - \sum_i \frac{t_i}{Q_i}, \{\hat{q}_i\}, \mu \right). \end{aligned} \quad (\text{C.4})$$

Here, the sum runs over all flavour structures $\kappa \equiv \{a, b, j\}$ contributing to the process in eq. (C.1), and \mathcal{M}_{κ} and H_{κ} denote the corresponding matrix element and hard function, respectively. In eq. (C.4), $B_{a,b}$ are the same beam functions appearing for \mathcal{T}_0 , J_j is the jet function, and S_{κ} is the \mathcal{T}_1 soft function. Note that the jet function only differs between quarks and gluons, while the soft function is sensitive to the full flavour structure κ of the process, as well as the Born reference momenta $\{\hat{q}_i\}$ and the normalization factors Q_i . Performing the same Fourier transform as in eq. (3.7),

$$\begin{aligned} B_i(y, x, \mu) &= \int dt e^{-ity} B_i(t, x, \mu), \\ J_j(y, \mu) &= \int dt e^{-ity} J_j(t, \mu), \\ S_{\kappa}(y, \{\hat{q}_i\}, \mu) &= \int d\mathcal{T} e^{-i\mathcal{T}y} S_{\kappa}(\mathcal{T}, \{\hat{q}_i\}, \mu), \end{aligned} \quad (\text{C.5})$$

eq. (C.4) can be written as

$$\begin{aligned} \frac{d\sigma^{\text{sing}}}{d\Phi_{\text{FJ}}d\mathcal{T}_1} &= \sum_{\kappa} \frac{d|\mathcal{M}_{\kappa}|^2}{d\Phi_{\text{FJ}}} H_{\kappa}(\Phi_{\text{FJ}}, \mu) \int \frac{dy}{2\pi} e^{iy\mathcal{T}_1} B_a \left(\frac{y}{Q_a}, x_a, \mu \right) B_b \left(\frac{y}{Q_b}, x_b, \mu \right) J_j \left(\frac{y}{Q_j}, \mu \right) \\ &\times S_{\kappa}(y, \{\hat{q}_i\}, \mu). \end{aligned} \quad (\text{C.6})$$

In Fourier space, the RGEs of the hard, beam, jet and soft functions are given by

$$\begin{aligned} \frac{d}{d \ln \mu} \ln H_{\kappa}(\Phi_{\text{FJ}}, \mu) &= \gamma_H^{\kappa}(\{q_i\}, \mu), & \frac{d}{d \ln \mu} S_{\kappa}(y, \{\hat{q}_i\}, \mu) &= \gamma_S^{\kappa}(y, \{\hat{q}_i\}, \mu), \\ \frac{d}{d \ln \mu} \ln B_i \left(\frac{y}{Q_i}, x, \mu \right) &= \gamma_B^i \left(\frac{y}{Q_i}, \mu \right), & \frac{d}{d \ln \mu} \ln J_j \left(\frac{y}{Q_j}, \mu \right) &= \gamma_J^j \left(\frac{y}{Q_j}, \mu \right). \end{aligned} \quad (\text{C.7})$$

In eq. (C.7) we have made explicit the flavour index i, j for initial and final state legs for clarity. We write the anomalous dimensions as [118]

$$\begin{aligned}
 \gamma_H^\kappa(\{q_i\}, \mu) &= (n_q C_F + n_g C_A) \hat{\Gamma}_C[\alpha_s(\mu)] \ln \frac{Q^2}{\mu^2} + \gamma_H^\kappa[\{q_i\}, \alpha_s(\mu)], \\
 \gamma_B^i\left(\frac{y}{Q_i}, \mu\right) &= 2\Gamma_C^i[\alpha_s(\mu)] \ln \frac{y\mu^2}{Q y_0} + \gamma_B^i[Q_i, \alpha_s(\mu)] \\
 &= \gamma_J^i\left(\frac{y}{Q_i}, \mu\right), \\
 \gamma_S^\kappa(y, \{\hat{q}_i\}, \mu) &= -2(n_q C_F + n_g C_A) \hat{\Gamma}_C[\alpha_s(\mu)] \ln \frac{y\mu}{y_0} + \gamma_S^\kappa[\{\hat{q}_i\}, \alpha_s(\mu)]. \tag{C.8}
 \end{aligned}$$

Here, as before $y_0 = -ie^{-\gamma_E}$, n_q and n_g denote the number of quarks and gluons for the flavour structure of κ , respectively, and $\hat{\Gamma}_C$ is the colour-stripped cusp anomalous dimension. The noncusp anomalous dimensions read

$$\begin{aligned}
 \gamma_H^\kappa(\{q_i\}, \alpha_s) &= -\hat{\Gamma}_C(\alpha_s) \sum_{i \neq k} (\mathbf{T}_i \cdot \mathbf{T}_k) \ln \frac{2q_i \cdot q_k}{Q^2} + \gamma_H^\kappa(\alpha_s), \\
 \gamma_B^i(Q_i, \alpha_s) &= \Gamma_C^i[\alpha_s(\mu)] \ln \frac{Q^2}{Q_i^2} + \gamma_B^i(\alpha_s), \\
 \gamma_S^\kappa(\{\hat{q}_i\}, \alpha_s) &= \hat{\Gamma}_C[\alpha_s(\mu)] \sum_{i \neq k} (\mathbf{T}_i \cdot \mathbf{T}_k) \ln \frac{2q_i \cdot q_k}{Q_i Q_k} + \gamma_S^\kappa(\alpha_s). \tag{C.9}
 \end{aligned}$$

The \mathbf{T}_i are the colour-charge operators, and the appearing products can be evaluated using

$$\mathbf{T}_i \cdot \mathbf{T}_k = \frac{1}{2}(\mathbf{T}_l^2 - \mathbf{T}_i^2 - \mathbf{T}_k^2), \quad l \neq i, k, \tag{C.10}$$

which follows from colour conservation of the $2 \rightarrow 1$ process. Here, $\gamma_H^\kappa(\alpha_s)$, $\gamma_B^i(\alpha_s)$ and $\gamma_S^\kappa(\alpha_s)$ are the standard noncusp anomalous dimensions, while the logarithmic terms encode the measure dependence. The hard and soft anomalous dimensions are reported in appendix A, whereas the noncusp anomalous dimension of the beam function, which is identical to that of the jet function, read, up to two loops [92–96]

$$\gamma_B^{q(1)} = 3C_F, \tag{C.11}$$

$$\gamma_B^{q(2)} = C_F \left[C_A \left(-20\zeta_3 + \frac{11\pi^2}{18} + \frac{1769}{108} \right) + C_F \left(12\zeta_3 - \pi^2 + \frac{3}{4} \right) - n_f \frac{121 + 6\pi^2}{54} \right],$$

$$\gamma_B^{g(1)} = 4\pi\beta_0, \tag{C.12}$$

$$\gamma_B^{g(2)} = C_A \left[C_A \left(-8\zeta_3 - \frac{11\pi^2}{18} + \frac{548}{27} \right) + \frac{n_f}{27} (3\pi^2 - 92) \right] - C_F n_f.$$

To minimize the logarithms in eq. (C.8), we choose the same canonical resummation scales as in eq. (3.11),

$$\mu_H = Q, \quad \mu_a = \mu_b = \mu_J = \sqrt{\frac{Q y_0}{y}} = \sqrt{\mu_H \mu_S}, \quad \mu_S = \frac{y_0}{y}. \tag{C.13}$$

Furthermore, we also evolve the hard and soft functions such that they are evaluated in terms of $\alpha_s(\mu_B)$. To be precise, we first define the hard, jet and soft functions at their respective canonical scales as

$$\begin{aligned}
 \bar{H}_\kappa(\Phi_{\text{FJ}}, Q) &\equiv H_\kappa(\Phi_{\text{FJ}}, \mu_H = Q) &= \sum_{n=0}^{\infty} \left[\frac{\alpha_s(Q)}{2\pi} \right]^n H_\kappa^{(n)}(\Phi_{\text{FJ}}), \\
 \bar{J}_j\left(\frac{Q}{Q_j}, \mu_J\right) &\equiv J_j\left(\frac{y}{Q_j}, \mu = \mu_J\right) &= \sum_{n=0}^{\infty} \left[\frac{\alpha_s(\mu_J)}{2\pi} \right]^n J_j^{(n)}(Q/Q_j), \\
 \bar{S}_\kappa(\{\hat{q}_i\}, y_0/y) &\equiv S_\kappa(y, \{\hat{q}_i\}, \mu_S = y_0/y) &= \sum_{n=0}^{\infty} \left[\frac{\alpha_s(y_0/y)}{2\pi} \right]^n S_\kappa^{(n)}(\{\hat{q}_i\}),
 \end{aligned} \tag{C.14}$$

where Φ_{FJ} encodes the dependence on the kinematics of the Born F +jet configuration. For clarity, we use the modified symbols \bar{H}_κ and \bar{S}_κ to distinguish these functions from the original hard and soft functions H_κ and S_κ . Importantly, the right-hand side depends on the scale only through the coupling, and do not contain explicit logarithmic terms.¹⁰ We can now evolve these functions to the beam scale similar to eq. (3.14),

$$\begin{aligned}
 \bar{H}_\kappa(\Phi_{\text{FJ}}, Q) &= \bar{H}_\kappa(\Phi_{\text{FJ}}, \mu_B) \exp \left[\int_{\mu_B}^Q \frac{d\mu'}{\mu'} \gamma_{\bar{H}_\kappa}[\Phi_{\text{FJ}}, \alpha_s(\mu')] \right], \\
 \bar{S}_\kappa(\{\hat{q}_i\}, y_0/y) &= \bar{S}_\kappa(\{\hat{q}_i\}, \mu_B) \exp \left[\int_{\mu_B}^{y_0/y} \frac{d\mu'}{\mu'} \gamma_{\bar{S}_\kappa}[\{\hat{q}_i\}, \alpha_s(\mu')] \right],
 \end{aligned} \tag{C.15}$$

where the anomalous dimensions are given by

$$\begin{aligned}
 \gamma_{\bar{H}_\kappa}[\Phi_{\text{FJ}}, \alpha_s(\mu)] &= \frac{d \ln \bar{H}_\kappa(\Phi_{\text{FJ}}, \mu)}{d \ln \mu} = -4\pi\beta_0 \frac{H_\kappa^{(1)}(\Phi_{\text{FJ}})}{H_\kappa^{(0)}(\Phi_{\text{FJ}})} \left[\frac{\alpha_s(\mu)}{2\pi} \right]^2 + \mathcal{O}(\alpha_s^3), \\
 \gamma_{\bar{S}_\kappa}[\{\hat{q}_i\}, \alpha_s(\mu)] &= \frac{d \ln \bar{S}_\kappa(\{\hat{q}_i\}, \mu)}{d \ln \mu} = -4\pi\beta_0 \frac{S_\kappa^{(1)}(\{\hat{q}_i\})}{S_\kappa^{(0)}(\{\hat{q}_i\})} \left[\frac{\alpha_s(\mu)}{2\pi} \right]^2 + \mathcal{O}(\alpha_s^3).
 \end{aligned} \tag{C.16}$$

By making the choice in eq. (C.13) and evolving all functions to the common scale $\mu = \mu_B$, we obtain

$$\frac{d\sigma^{\text{sing}}}{d\Phi_{\text{FJ}} d\mathcal{T}_1} = \sum_\kappa \int \frac{dy}{2\pi} e^{iy\mathcal{T}_1} \mathcal{L}_\kappa(y_0/y) e^{-S_\kappa(y_0/y)}. \tag{C.17}$$

Here, the canonical luminosity is defined as

$$\begin{aligned}
 \mathcal{L}_\kappa(y_0/y) &= \frac{d|\mathcal{M}_\kappa|^2}{d\Phi_{\text{FJ}}} \bar{H}_\kappa(\Phi_{\text{FJ}}, \mu_B) \bar{B}_a\left(\frac{y}{Q_a}, x_a, \mu_B\right) \bar{B}_b\left(\frac{y}{Q_b}, x_b, \mu_B\right) \bar{J}_j\left(\frac{Q}{Q_j}, \mu_B\right) \bar{S}_\kappa(\{\hat{q}_i\}, \mu_B) \\
 &= \sum_{a', b'} \frac{d|\mathcal{M}_\kappa|^2}{d\Phi_{\text{FJ}}} \bar{H}_\kappa(\Phi_{\text{FJ}}, \mu_B) (\bar{C} \otimes f)_a\left(\frac{y}{Q_a}, x_a, \mu_B\right) (\bar{C} \otimes f)_b\left(\frac{y}{Q_b}, x_b, \mu_B\right) \\
 &\quad \times \bar{J}_j\left(\frac{Q}{Q_j}, \mu_B\right) \frac{\bar{S}_\kappa(\{\hat{q}_i\}, \mu_B)}{S(\mu_B)}.
 \end{aligned} \tag{C.18}$$

¹⁰Strictly speaking, $H_\kappa^{(n)}(\Phi_{\text{FJ}})$ also depends on Q through Φ_{FJ} .

In the second step, we divided the \mathcal{T}_1 soft function \bar{S}_κ by the \mathcal{T}_0 soft function S as defined in eq. (3.13), such that the C_{ij} are the same matching coefficients of the beam functions onto the PDFs as in eq. (3.18). The canonical Sudakov form factor is defined as

$$\begin{aligned} \mathcal{S}_\kappa(y_0/y) &= 2 \int_{\sqrt{Qy_0/y}}^Q \frac{d\mu'}{\mu'} \left\{ A_\kappa[\alpha_s(\mu')] \ln \frac{Q^2}{\mu'^2} + B_H^\kappa[\Phi_{\text{FJ}}, \alpha_s(\mu')] \right\} \\ &+ 2 \int_{\sqrt{Qy_0/y}}^{y_0/y} \frac{d\mu'}{\mu'} \left\{ A_\kappa[\alpha_s(\mu')] \ln \frac{(y_0/y)^2}{\mu'^2} + B_S^\kappa[\{\hat{q}_i\}, \alpha_s(\mu')] \right\}. \end{aligned} \quad (\text{C.19})$$

Here, the first exponential is the hard evolution, while the second is the soft evolution. The A and B coefficients are given by

$$\begin{aligned} A_\kappa(\alpha_s) &= \frac{1}{2}(n_q C_F + n_g C_A) \Gamma_C(\alpha_s), \\ B_H^\kappa(\Phi_{\text{FJ}}, \alpha_s) &= \frac{1}{2} \gamma_H^\kappa(\{q_i\}, \alpha_s) - \frac{1}{2} \gamma_{\bar{H}\kappa}(\Phi_{\text{FJ}}, \alpha_s), \\ B_S^\kappa(\{\hat{q}_i\}, \alpha_s) &= \frac{1}{2} \gamma_S^\kappa(\{\hat{q}_i\}, \alpha_s) - \frac{1}{2} \gamma_{\bar{S}\kappa}(\{q_i\}, \alpha_s). \end{aligned} \quad (\text{C.20})$$

Comparing eqs. (C.18) and (C.19) to eq. (3.20), we see that the overall structure of the resummed \mathcal{T}_1 spectrum is very similar to that of \mathcal{T}_0 . The key difference is the explicit dependence of the hard and soft functions and their anomalous dimensions on the flavour channel κ , as well as the additional jet function.

We complete this section by presenting explicit expressions for the jet and soft functions for \mathcal{T}_1 .

\mathcal{T}_1 jet function. The jet function RGE in eq. (C.8) predicts that

$$\begin{aligned} J_i\left(\frac{y}{Q_j}, \mu\right) &= 1 + \frac{\alpha_s(\mu)}{2\pi} \left[\frac{L_j^2}{2} \Gamma_C^{i(1)} + \frac{L_j}{2} \gamma_j^{i(1)} + j_1^i \right] \\ &+ \left(\frac{\alpha_s(\mu)}{2\pi} \right)^2 \left\{ \frac{L_j^4}{8} (\Gamma_C^{i(1)})^2 + \frac{L_j^3}{4} \Gamma_C^{i(1)} \left(\gamma_j^{i(1)} + \frac{4}{3} \pi \beta_0 \right) \right. \\ &\quad \left. + \frac{L_j^2}{2} \left[\Gamma_C^{i(2)} + \Gamma_C^{i(1)} j_1^i + \frac{1}{4} \gamma_j^{i(1)} (\gamma_j^{i(1)} + 4\pi \beta_0) \right] \right. \\ &\quad \left. + \frac{L_j}{2} [\gamma_j^{i(2)} + j_1^i (\gamma_j^{i(1)} + 4\pi \beta_0)] + j_2^i \right\} + \mathcal{O}(\alpha_s^3). \end{aligned} \quad (\text{C.21})$$

Here, we define $L_j = \ln[y\mu^2/(Q_j y_0)]$, and $i = q, g$ distinguishes between quarks and gluons. The cusp anomalous dimension is given in eq. (A.7), the β_n are given in eq. (A.2), and the noncusp anomalous dimensions are provided in eq. (C.11). The jet-function constants j_n^i are known up to three loops [119, 120], and are collected up to two loops in ref. [30]. They are commonly expressed in momentum space, where instead of the logarithms L_j in eq. (C.21) one obtains plus distributions. The conversion between these induces additional

terms. Taking these into account they are given by

$$\begin{aligned}
 j_1^q &= C_F \left(\frac{7}{2} - \frac{\pi^2}{3} \right), \\
 j_2^q &= C_F \left[C_A \left(-\frac{9\zeta_3}{2} - \frac{1}{720}\pi^2 (775 + 37\pi^2) + \frac{53129}{2592} \right) + \frac{(234\pi^2 - 4057) n_f}{1296} \right] \\
 &\quad + C_F^2 \left(-\frac{3\zeta_3}{2} + \frac{61\pi^4}{360} + \frac{205}{32} - \frac{97\pi^2}{48} \right)
 \end{aligned} \tag{C.22}$$

for the quark case, while for gluons they read

$$\begin{aligned}
 j_1^g &= \frac{1}{18} (67 - 6\pi^2) C_A - \frac{5n_f}{9}, \\
 j_2^g &= \frac{C_A^2}{1296} (-9504\zeta_3 + 153\pi^4 - 4344\pi^2 + 40430) + \frac{1}{108} C_A n_f (67\pi^2 - 72\zeta_3 - 760) \\
 &\quad + C_F n_f \left(2\zeta_3 - \frac{55}{24} \right) + \frac{n_f^2}{162} (50 - 3\pi^2).
 \end{aligned} \tag{C.23}$$

The coefficients $J^{(n)}(Q/Q_j)$ in eq. (C.14) are obtained from eq. (C.21) by setting $L_j = \ln(Q/Q_j)$.

\mathcal{T}_1 soft function. The fixed-order structure of the single-differential soft function can be found in ref. [30], where it is expanded as

$$S_\kappa(k, \{\hat{q}_i\}, \mu) = \sum_n \left[\frac{\alpha_s(\mu)}{4\pi} \right]^n \left[S_{\kappa,-1}^{(n)}(\{\hat{q}_i\}) \delta(k) + \sum_{m=0}^{2n-1} S_{\kappa,m}^{(n)} \frac{1}{\mu} \mathcal{L}_n \left(\frac{k}{\mu} \right) \right]. \tag{C.24}$$

Here, the $S_{\kappa,m}^{(n)}$ are those given in ref. [30], which uses different conventions than in this work. We require the Fourier-transformed soft function at its natural scale $\mu = \mu_s = y_0/y$ as defined in eq. (C.14),

$$\begin{aligned}
 \bar{S}_\kappa(\{\hat{q}_i\}, y_0/y) &\equiv S_\kappa(y, \{\hat{q}_i\}, \mu_s = y_0/y) \\
 &= 1 + \frac{\alpha_s(\mu)}{2\pi} S_\kappa^{(1)}(\{\hat{q}_i\}) + \left[\frac{\alpha_s(\mu)}{2\pi} \right]^2 S_\kappa^{(2)}(\{\hat{q}_i\}) + \mathcal{O}(\alpha_s^3).
 \end{aligned} \tag{C.25}$$

Evaluating the Fourier transform using eq. (3.7) and adjusting to our conventions, we obtain

$$\begin{aligned}
 S_\kappa^{(1)}(\{\hat{q}_i\}) &= \frac{1}{2} S_{\kappa,-1}^{(1)}(\{\hat{q}_i\}) - \mathbf{C} \hat{\Gamma}^{(1)} \frac{\pi^2}{6}, \\
 S_\kappa^{(2)}(\{\hat{q}_i\}) &= \frac{7\pi^4}{360} (\mathbf{C} \hat{\Gamma}_C^{(1)})^2 + \mathbf{C} \hat{\Gamma}_C^{(1)} \left[-2\hat{\Gamma}_C^{(1)} \mathbf{L} \zeta_3 - \frac{8}{3} \pi \beta_0 \zeta_3 - \frac{\pi^2}{12} S_{\kappa,-1}^{(1)}(\{\hat{q}_i\}) \right] - \frac{\pi^2}{6} \mathbf{C} \hat{\Gamma}_C^{(2)} \\
 &\quad + (\mathbf{L} \hat{\Gamma}_C^{(1)}) \left[\frac{1}{3} \pi^3 \beta_0 + \frac{\pi^2}{12} (\mathbf{L} \hat{\Gamma}_C^{(1)}) \right] + \frac{1}{4} S_{\kappa,-1}^{(2)}(\{\hat{q}_i\}),
 \end{aligned} \tag{C.26}$$

where $S_{\kappa,-1}^{(2)}(\{\hat{q}_i\})$ can be extracted from refs. [38, 41] (an independent calculation of the two-loop coefficients has been used in ref. [29]) and

$$\mathbf{C} = \sum_{i \in \{a,b,j\}} C_i, \quad \mathbf{L} = \sum_{i \neq k} (\mathbf{T}_i \cdot \mathbf{T}_k) \ln \frac{2q_i \cdot q_k}{Q_i Q_k}. \tag{C.27}$$

C.2 MiNNLO_{PS} formalism based on \mathcal{T}_1

Due to the similarity between the resummed \mathcal{T}_0 and \mathcal{T}_1 formulae, the derivation of the MiNNLO_{PS} method using \mathcal{T}_0 , presented in detail in section 3.2, carries over to the case of \mathcal{T}_1 almost unchanged. Thus, here we only briefly review the key steps, while referring for more details to section 3.2.

The starting point for the MiNNLO_{PS} method is the cumulant of eq. (C.17),

$$\frac{d\sigma^{\text{sing}}(\mathcal{T}_1)}{d\Phi_{\text{FJ}}} = \sum_{\kappa} \int_0^{\mathcal{T}_1} d\mathcal{T}'_1 \int \frac{dy}{2\pi} e^{iy\mathcal{T}'_1} \mathcal{L}_{\kappa}(y_0/y) e^{-S_{\kappa}(y_0/y)}. \quad (\text{C.28})$$

We expand it around $y_0/y \sim \mathcal{T}_1$, i.e. in $L_y = \ln(\mathcal{T}_1 y/y_0) \ll 1$. By keeping only $S_{\kappa}(\mathcal{T}_1)$ exponentiated and expanding all other terms at NNLO accuracy, we obtain [cf. eq. (3.30)]

$$\begin{aligned} \frac{d\sigma^{\text{sing}}(\mathcal{T}_1)}{d\Phi_{\text{FJ}}} &= \sum_{\kappa} e^{-S_{\kappa}(\mathcal{T}_1)} \left[\mathcal{L}_{\kappa}(\mathcal{T}_1) \left(1 - \frac{\zeta_2}{2} [(\mathcal{S}'_{\kappa})^2 - \mathcal{S}''_{\kappa}] - \zeta_3 \mathcal{S}'_{\kappa} \mathcal{S}''_{\kappa} + \frac{3\zeta_4}{16} (\mathcal{S}''_{\kappa})^2 + \frac{\zeta_3}{3} \mathcal{S}'''_{\kappa} \right) \right. \\ &\quad \left. + \mathcal{L}'_{\kappa}(\mathcal{T}_1) (\zeta_2 \mathcal{S}'_{\kappa} + \zeta_3 \mathcal{S}''_{\kappa}) - \frac{\zeta_2}{2} \mathcal{L}''_{\kappa}(\mathcal{T}_1) + \mathcal{O}(\alpha_s^3) \right], \end{aligned} \quad (\text{C.29})$$

where the derivatives are defined in eq. (3.26). Next, we evaluate all derivatives in eq. (C.29) and exponentiate all resulting logarithms, while the remaining terms are absorbed by redefining the luminosity. This yields

$$\frac{d\sigma^{\text{sing}}(\mathcal{T}_1)}{d\Phi_{\text{FJ}}} = \sum_{\kappa} \tilde{\mathcal{L}}_{\kappa}(\mathcal{T}_1) e^{-S_{\kappa}(\mathcal{T}_1)}. \quad (\text{C.30})$$

Defining $\mu_B = \sqrt{Q\mathcal{T}_1}$ and $L_{\mathcal{T}} = \frac{1}{2} \ln(Q/\mathcal{T}_1)$, the modified luminosity is defined similar to eq. (3.40) as

$$\begin{aligned} \tilde{\mathcal{L}}_{\kappa}(\mathcal{T}_1) &= \frac{d|\mathcal{M}_{\kappa}|^2}{d\Phi_{\text{FJ}}} \tilde{H}_{\kappa}(\Phi_{\text{FJ}}, \mu_B) \bar{J}_j \left(\frac{y}{Q_j}, \mu_B \right) \frac{\bar{S}_{\kappa}(\{\hat{q}_i\}, \mu_B)}{S(\mu_B)} \\ &\quad \left[(\tilde{C} \otimes f)_a(x_a, \mu_B) (\tilde{C} \otimes f)_b(x_b, \mu_B) \right. \\ &\quad \left. - \zeta_2 (\hat{P} \otimes f)_a(x_a, \mu_B) (\hat{P} \otimes f)_b(x_b, \mu_B) \right] \\ &\quad - \frac{d|\mathcal{M}_{\kappa}|^2}{d\Phi_{\text{FJ}}} \left(\frac{\alpha_s}{2\pi} \right)^2 c'_{1,1}{}^{\kappa} L_{\mathcal{T}} \left[(\hat{P}^{(0)} \otimes f)_a(x_a, \mu_B) f_b(x_b, \mu_B) \right. \\ &\quad \left. + f_a(x_a, \mu_B) (\hat{P}^{(0)} \otimes f)_b(x_b, \mu_B) \right], \end{aligned} \quad (\text{C.31})$$

where the modified hard function and matching coefficients follow from eq. (3.41),

$$\tilde{H}_{\kappa}(\Phi_{\text{FJ}}, \mu_B) = \bar{H}_{\kappa}(\Phi_{\text{FJ}}, \mu_B) \left[1 + \frac{\alpha_s}{2\pi} c_{1,0}^{\kappa} + \left(\frac{\alpha_s}{2\pi} \right)^2 c_{2,0}^{\kappa} + \mathcal{O}(\alpha_s^3) \right], \quad (\text{C.32})$$

$$\begin{aligned} \tilde{C}_{ij}(x, \mu_B) &= \bar{C}_{ij}(x, \mu_B) \\ &\quad - \left(\frac{\alpha_s}{2\pi} \right)^2 \left[\frac{\zeta_2}{2} (\hat{P}^{(0)} \otimes \hat{P}^{(0)})_{ij}(x) + (c'_{1,0}{}^{\kappa} - \zeta_2 \pi \beta_0) \hat{P}_{ij}^{(0)}(x) \right] + \mathcal{O}(\alpha_s^3). \end{aligned} \quad (\text{C.33})$$

The Sudakov factor is given by

$$\begin{aligned} \mathcal{S}(\mathcal{T}_1) = & 2 \int_{\sqrt{Q\mathcal{T}_1}}^Q \frac{d\mu'}{\mu'} \left[A_\kappa[\alpha_s(\mu')] \ln \frac{Q^2}{\mu'^2} + B_H^\kappa[\Phi_{\text{FJ}}, \alpha_s(\mu')] \right] \\ & + 2 \int_{\sqrt{Q\mathcal{T}_1}}^{\mathcal{T}_1} \frac{d\mu'}{\mu'} \left[A_\kappa[\alpha_s(\mu')] \ln \frac{(\mathcal{T}_0)^2}{\mu'^2} + B_S^\kappa[\{\hat{q}_i\}, \alpha_s(\mu')] \right], \end{aligned} \quad (\text{C.34})$$

where the A_κ coefficients are given in eq. (C.20) and the $B_{H,S}^\kappa$ are defined in eq. (C.20). The constants $c_{n,m}^\kappa$ and $c'_{n,m}^\kappa$ appearing in eqs. (C.31)–(C.32) are identical to those in eq. (3.34), up to changing the A and B coefficients to those in eq. (C.20). In particular, they inherit the dependence of the A_κ and $B_{H,S}^\kappa$ coefficients on the flavour channel κ and the phase space Φ_{FJ} , which is kept implicit.

Open Access. This article is distributed under the terms of the Creative Commons Attribution License ([CC-BY4.0](https://creativecommons.org/licenses/by/4.0/)), which permits any use, distribution and reproduction in any medium, provided the original author(s) and source are credited.

References

- [1] P.F. Monni et al., *MiNNLO_{PS}: a new method to match NNLO QCD to parton showers*, *JHEP* **05** (2020) 143 [Erratum *ibid.* **02** (2022) 031] [[arXiv:1908.06987](https://arxiv.org/abs/1908.06987)] [[INSPIRE](https://inspirehep.net/literature/1908069)].
- [2] P.F. Monni, E. Re and M. Wiesemann, *MiNNLO_{PS}: optimizing 2 → 1 hadronic processes*, *Eur. Phys. J. C* **80** (2020) 1075 [[arXiv:2006.04133](https://arxiv.org/abs/2006.04133)] [[INSPIRE](https://inspirehep.net/literature/2006041)].
- [3] S. Alioli et al., *Matching Fully Differential NNLO Calculations and Parton Showers*, *JHEP* **06** (2014) 089 [[arXiv:1311.0286](https://arxiv.org/abs/1311.0286)] [[INSPIRE](https://inspirehep.net/literature/1311028)].
- [4] S. Alioli et al., *Matching NNLO predictions to parton showers using N³LL color-singlet transverse momentum resummation in geneva*, *Phys. Rev. D* **104** (2021) 094020 [[arXiv:2102.08390](https://arxiv.org/abs/2102.08390)] [[INSPIRE](https://inspirehep.net/literature/2102083)].
- [5] A. Gavardi, M.A. Lim, S. Alioli and F.J. Tackmann, *NNLO+PS W⁺W⁻ production using jet veto resummation at NNLL'*, *JHEP* **12** (2023) 069 [[arXiv:2308.11577](https://arxiv.org/abs/2308.11577)] [[INSPIRE](https://inspirehep.net/literature/2308115)].
- [6] D. Lombardi, M. Wiesemann and G. Zanderighi, *Advancing MiNNLO_{PS} to diboson processes: Zγ production at NNLO+PS*, *JHEP* **06** (2021) 095 [[arXiv:2010.10478](https://arxiv.org/abs/2010.10478)] [[INSPIRE](https://inspirehep.net/literature/2010104)].
- [7] D. Lombardi, M. Wiesemann and G. Zanderighi, *W⁺W⁻ production at NNLO+PS with MINNLO_{PS}*, *JHEP* **11** (2021) 230 [[arXiv:2103.12077](https://arxiv.org/abs/2103.12077)] [[INSPIRE](https://inspirehep.net/literature/2103120)].
- [8] D. Lombardi, M. Wiesemann and G. Zanderighi, *Anomalous couplings in Zγ events at NNLO+PS and improving νν̄γ backgrounds in dark-matter searches*, *Phys. Lett. B* **824** (2022) 136846 [[arXiv:2108.11315](https://arxiv.org/abs/2108.11315)] [[INSPIRE](https://inspirehep.net/literature/2108113)].
- [9] L. Buonocore et al., *ZZ production at nNNLO+PS with MiNNLO_{PS}*, *JHEP* **01** (2022) 072 [[arXiv:2108.05337](https://arxiv.org/abs/2108.05337)] [[INSPIRE](https://inspirehep.net/literature/2108053)].
- [10] S. Zanolini et al., *Next-to-next-to-leading order event generation for VH production with H → b̄b̄ decay*, *JHEP* **07** (2022) 008 [[arXiv:2112.04168](https://arxiv.org/abs/2112.04168)] [[INSPIRE](https://inspirehep.net/literature/2112041)].
- [11] A. Gavardi, C. Oleari and E. Re, *NNLO+PS Monte Carlo simulation of photon pair production with MiNNLO_{PS}*, *JHEP* **09** (2022) 061 [[arXiv:2204.12602](https://arxiv.org/abs/2204.12602)] [[INSPIRE](https://inspirehep.net/literature/2204126)].

- [12] U. Haisch et al., *NNLO event generation for $pp \rightarrow Zh \rightarrow \ell^+ \ell^- b\bar{b}$ production in the SM effective field theory*, *JHEP* **07** (2022) 054 [[arXiv:2204.00663](#)] [[INSPIRE](#)].
- [13] J.M. Lindert et al., *$W^\pm Z$ production at NNLO QCD and NLO EW matched to parton showers with $MinNLO_{PS}$* , *JHEP* **11** (2022) 036 [[arXiv:2208.12660](#)] [[INSPIRE](#)].
- [14] J. Mazzei et al., *Next-to-Next-to-Leading Order Event Generation for Top-Quark Pair Production*, *Phys. Rev. Lett.* **127** (2021) 062001 [[arXiv:2012.14267](#)] [[INSPIRE](#)].
- [15] J. Mazzei et al., *Top-pair production at the LHC with $MinNLO_{PS}$* , *JHEP* **04** (2022) 079 [[arXiv:2112.12135](#)] [[INSPIRE](#)].
- [16] J. Mazzei, A. Ratti, M. Wiesemann and G. Zanderighi, *B-hadron production at the LHC from bottom-quark pair production at NNLO+PS*, *Phys. Lett. B* **843** (2023) 137991 [[arXiv:2302.01645](#)] [[INSPIRE](#)].
- [17] R. Boughezal et al., *Higgs boson production in association with a jet at next-to-next-to-leading order*, *Phys. Rev. Lett.* **115** (2015) 082003 [[arXiv:1504.07922](#)] [[INSPIRE](#)].
- [18] R. Boughezal et al., *Higgs boson production in association with a jet at NNLO using jetiness subtraction*, *Phys. Lett. B* **748** (2015) 5 [[arXiv:1505.03893](#)] [[INSPIRE](#)].
- [19] F. Caola, K. Melnikov and M. Schulze, *Fiducial cross sections for Higgs boson production in association with a jet at next-to-next-to-leading order in QCD*, *Phys. Rev. D* **92** (2015) 074032 [[arXiv:1508.02684](#)] [[INSPIRE](#)].
- [20] X. Chen et al., *NNLO QCD corrections to Higgs boson production at large transverse momentum*, *JHEP* **10** (2016) 066 [[arXiv:1607.08817](#)] [[INSPIRE](#)].
- [21] R. Boughezal, C. Focke, X. Liu and F. Petriello, *W-boson production in association with a jet at next-to-next-to-leading order in perturbative QCD*, *Phys. Rev. Lett.* **115** (2015) 062002 [[arXiv:1504.02131](#)] [[INSPIRE](#)].
- [22] A. Gehrmann-De Ridder et al., *Next-to-Next-to-Leading-Order QCD Corrections to the Transverse Momentum Distribution of Weak Gauge Bosons*, *Phys. Rev. Lett.* **120** (2018) 122001 [[arXiv:1712.07543](#)] [[INSPIRE](#)].
- [23] A. Gehrmann-De Ridder et al., *Precise QCD predictions for the production of a Z boson in association with a hadronic jet*, *Phys. Rev. Lett.* **117** (2016) 022001 [[arXiv:1507.02850](#)] [[INSPIRE](#)].
- [24] R. Boughezal et al., *Z-boson production in association with a jet at next-to-next-to-leading order in perturbative QCD*, *Phys. Rev. Lett.* **116** (2016) 152001 [[arXiv:1512.01291](#)] [[INSPIRE](#)].
- [25] J.M. Campbell, R.K. Ellis and C. Williams, *Driving missing data at the LHC: NNLO predictions for the ratio of $\gamma + j$ and $Z + j$* , *Phys. Rev. D* **96** (2017) 014037 [[arXiv:1703.10109](#)] [[INSPIRE](#)].
- [26] R. Gauld et al., *VH + jet production in hadron-hadron collisions up to order α_s^3 in perturbative QCD*, *JHEP* **03** (2022) 008 [[arXiv:2110.12992](#)] [[INSPIRE](#)].
- [27] H.A. Chawdhry, M. Czakon, A. Mitov and R. Poncelet, *NNLO QCD corrections to diphoton production with an additional jet at the LHC*, *JHEP* **09** (2021) 093 [[arXiv:2105.06940](#)] [[INSPIRE](#)].
- [28] S. Catani and M. Grazzini, *An NNLO subtraction formalism in hadron collisions and its application to Higgs boson production at the LHC*, *Phys. Rev. Lett.* **98** (2007) 222002 [[hep-ph/0703012](#)] [[INSPIRE](#)].

- [29] R. Boughezal, X. Liu and F. Petriello, *N-jettiness soft function at next-to-next-to-leading order*, *Phys. Rev. D* **91** (2015) 094035 [[arXiv:1504.02540](#)] [[INSPIRE](#)].
- [30] J. Gaunt, M. Stahlhofen, F.J. Tackmann and J.R. Walsh, *N-jettiness Subtractions for NNLO QCD Calculations*, *JHEP* **09** (2015) 058 [[arXiv:1505.04794](#)] [[INSPIRE](#)].
- [31] S. Abreu et al., *Quark and gluon two-loop beam functions for leading-jet p_T and slicing at NNLO*, *JHEP* **04** (2023) 127 [[arXiv:2207.07037](#)] [[INSPIRE](#)].
- [32] C.W. Bauer, S. Fleming and M.E. Luke, *Summing Sudakov logarithms in $B \rightarrow X_s \gamma$ in effective field theory*, *Phys. Rev. D* **63** (2000) 014006 [[hep-ph/0005275](#)] [[INSPIRE](#)].
- [33] C.W. Bauer, S. Fleming, D. Pirjol and I.W. Stewart, *An effective field theory for collinear and soft gluons: Heavy to light decays*, *Phys. Rev. D* **63** (2001) 114020 [[hep-ph/0011336](#)] [[INSPIRE](#)].
- [34] C.W. Bauer and I.W. Stewart, *Invariant operators in collinear effective theory*, *Phys. Lett. B* **516** (2001) 134 [[hep-ph/0107001](#)] [[INSPIRE](#)].
- [35] C.W. Bauer, D. Pirjol and I.W. Stewart, *Soft collinear factorization in effective field theory*, *Phys. Rev. D* **65** (2002) 054022 [[hep-ph/0109045](#)] [[INSPIRE](#)].
- [36] C.W. Bauer et al., *Hard scattering factorization from effective field theory*, *Phys. Rev. D* **66** (2002) 014017 [[hep-ph/0202088](#)] [[INSPIRE](#)].
- [37] S. Alioli et al., *N^3LL resummation of one-jettiness for Z-boson plus jet production at hadron colliders*, *Phys. Rev. D* **109** (2024) 094009 [[arXiv:2312.06496](#)] [[INSPIRE](#)].
- [38] J.M. Campbell, R.K. Ellis, R. Mondini and C. Williams, *The NNLO QCD soft function for 1-jettiness*, *Eur. Phys. J. C* **78** (2018) 234 [[arXiv:1711.09984](#)] [[INSPIRE](#)].
- [39] J. Gaunt, M. Stahlhofen and F.J. Tackmann, *The Gluon Beam Function at Two Loops*, *JHEP* **08** (2014) 020 [[arXiv:1405.1044](#)] [[INSPIRE](#)].
- [40] J.R. Gaunt, M. Stahlhofen and F.J. Tackmann, *The Quark Beam Function at Two Loops*, *JHEP* **04** (2014) 113 [[arXiv:1401.5478](#)] [[INSPIRE](#)].
- [41] G. Bell, B. Dehnadi, T. Mohrmann and R. Rahn, *The NNLO soft function for N-jettiness in hadronic collisions*, [arXiv:2312.11626](#) [[INSPIRE](#)].
- [42] S. Alioli et al., *Drell-Yan production at NNLL'+NNLO matched to parton showers*, *Phys. Rev. D* **92** (2015) 094020 [[arXiv:1508.01475](#)] [[INSPIRE](#)].
- [43] S. Alioli et al., *Higgsstrahlung at NNLL'+NNLO matched to parton showers in GENEVA*, *Phys. Rev. D* **100** (2019) 096016 [[arXiv:1909.02026](#)] [[INSPIRE](#)].
- [44] S. Alioli et al., *Precise predictions for photon pair production matched to parton showers in GENEVA*, *JHEP* **04** (2021) 041 [[arXiv:2010.10498](#)] [[INSPIRE](#)].
- [45] S. Alioli et al., *Next-to-next-to-leading order event generation for Z boson pair production matched to parton shower*, *Phys. Lett. B* **818** (2021) 136380 [[arXiv:2103.01214](#)] [[INSPIRE](#)].
- [46] T. Cridge, M.A. Lim and R. Nagar, *$W\gamma$ production at NNLO+PS accuracy in Geneva*, *Phys. Lett. B* **826** (2022) 136918 [[arXiv:2105.13214](#)] [[INSPIRE](#)].
- [47] S. Alioli et al., *Double Higgs production at NNLO interfaced to parton showers in GENEVA*, *JHEP* **06** (2023) 205 [[arXiv:2212.10489](#)] [[INSPIRE](#)].
- [48] S. Alioli et al., *Refining the GENEVA method for Higgs boson production via gluon fusion*, *JHEP* **05** (2023) 128 [[arXiv:2301.11875](#)] [[INSPIRE](#)].
- [49] P. Nason, *A new method for combining NLO QCD with shower Monte Carlo algorithms*, *JHEP* **11** (2004) 040 [[hep-ph/0409146](#)] [[INSPIRE](#)].

- [50] S. Frixione, P. Nason and C. Oleari, *Matching NLO QCD computations with Parton Shower simulations: the POWHEG method*, *JHEP* **11** (2007) 070 [[arXiv:0709.2092](#)] [[INSPIRE](#)].
- [51] S. Alioli, P. Nason, C. Oleari and E. Re, *A general framework for implementing NLO calculations in shower Monte Carlo programs: the POWHEG BOX*, *JHEP* **06** (2010) 043 [[arXiv:1002.2581](#)] [[INSPIRE](#)].
- [52] K. Hamilton, P. Nason, C. Oleari and G. Zanderighi, *Merging H/W/Z + 0 and 1 jet at NLO with no merging scale: a path to parton shower + NNLO matching*, *JHEP* **05** (2013) 082 [[arXiv:1212.4504](#)] [[INSPIRE](#)].
- [53] I.W. Stewart, F.J. Tackmann and W.J. Waalewijn, *Factorization at the LHC: From PDFs to Initial State Jets*, *Phys. Rev. D* **81** (2010) 094035 [[arXiv:0910.0467](#)] [[INSPIRE](#)].
- [54] I.W. Stewart, F.J. Tackmann and W.J. Waalewijn, *N-Jettiness: An Inclusive Event Shape to Veto Jets*, *Phys. Rev. Lett.* **105** (2010) 092002 [[arXiv:1004.2489](#)] [[INSPIRE](#)].
- [55] T.T. Jouttenus, I.W. Stewart, F.J. Tackmann and W.J. Waalewijn, *The Soft Function for Exclusive N-Jet Production at Hadron Colliders*, *Phys. Rev. D* **83** (2011) 114030 [[arXiv:1102.4344](#)] [[INSPIRE](#)].
- [56] I. Moutl et al., *Subleading Power Corrections for N-Jettiness Subtractions*, *Phys. Rev. D* **95** (2017) 074023 [[arXiv:1612.00450](#)] [[INSPIRE](#)].
- [57] I. Moutl et al., *N-jettiness subtractions for $gg \rightarrow H$ at subleading power*, *Phys. Rev. D* **97** (2018) 014013 [[arXiv:1710.03227](#)] [[INSPIRE](#)].
- [58] M.A. Ebert et al., *Power Corrections for N-Jettiness Subtractions at $\mathcal{O}(\alpha_s)$* , *JHEP* **12** (2018) 084 [[arXiv:1807.10764](#)] [[INSPIRE](#)].
- [59] J.R. Gaunt, *Glauber Gluons and Multiple Parton Interactions*, *JHEP* **07** (2014) 110 [[arXiv:1405.2080](#)] [[INSPIRE](#)].
- [60] M.A. Ebert and F.J. Tackmann, *Impact of isolation and fiducial cuts on q_T and N-jettiness subtractions*, *JHEP* **03** (2020) 158 [[arXiv:1911.08486](#)] [[INSPIRE](#)].
- [61] S. Catani and M. Grazzini, *QCD transverse-momentum resummation in gluon fusion processes*, *Nucl. Phys. B* **845** (2011) 297 [[arXiv:1011.3918](#)] [[INSPIRE](#)].
- [62] B. Andersson, G. Gustafson, L. Lonnblad and U. Pettersson, *Coherence Effects in Deep Inelastic Scattering*, *Z. Phys. C* **43** (1989) 625 [[INSPIRE](#)].
- [63] K. Hamilton et al., *Matching and event-shape NNDL accuracy in parton showers*, *JHEP* **03** (2023) 224 [*Erratum ibid.* **11** (2023) 060] [[arXiv:2301.09645](#)] [[INSPIRE](#)].
- [64] G. Bewick, S. Ferrario Ravasio, P. Richardson and M.H. Seymour, *Logarithmic accuracy of angular-ordered parton showers*, *JHEP* **04** (2020) 019 [[arXiv:1904.11866](#)] [[INSPIRE](#)].
- [65] M. Dasgupta et al., *Parton showers beyond leading logarithmic accuracy*, *Phys. Rev. Lett.* **125** (2020) 052002 [[arXiv:2002.11114](#)] [[INSPIRE](#)].
- [66] J.R. Forshaw, J. Holguin and S. Plätzer, *Building a consistent parton shower*, *JHEP* **09** (2020) 014 [[arXiv:2003.06400](#)] [[INSPIRE](#)].
- [67] Z. Nagy and D.E. Soper, *Summations of large logarithms by parton showers*, *Phys. Rev. D* **104** (2021) 054049 [[arXiv:2011.04773](#)] [[INSPIRE](#)].
- [68] G. Bewick, S. Ferrario Ravasio, P. Richardson and M.H. Seymour, *Initial state radiation in the Herwig 7 angular-ordered parton shower*, *JHEP* **01** (2022) 026 [[arXiv:2107.04051](#)] [[INSPIRE](#)].

- [69] F. Herren et al., *A new approach to color-coherent parton evolution*, *JHEP* **10** (2023) 091 [[arXiv:2208.06057](#)] [[INSPIRE](#)].
- [70] M. van Beekveld et al., *PanScales parton showers for hadron collisions: formulation and fixed-order studies*, *JHEP* **11** (2022) 019 [[arXiv:2205.02237](#)] [[INSPIRE](#)].
- [71] M. van Beekveld et al., *PanScales showers for hadron collisions: all-order validation*, *JHEP* **11** (2022) 020 [[arXiv:2207.09467](#)] [[INSPIRE](#)].
- [72] J.M. Campbell et al., *NLO Higgs Boson Production Plus One and Two Jets Using the POWHEG BOX, MadGraph4 and MCFM*, *JHEP* **07** (2012) 092 [[arXiv:1202.5475](#)] [[INSPIRE](#)].
- [73] S. Alioli, P. Nason, C. Oleari and E. Re, *Vector boson plus one jet production in POWHEG*, *JHEP* **01** (2011) 095 [[arXiv:1009.5594](#)] [[INSPIRE](#)].
- [74] ATLAS collaboration, *Measurement of the transverse momentum distribution of Drell-Yan lepton pairs in proton-proton collisions at $\sqrt{s} = 13$ TeV with the ATLAS detector*, *Eur. Phys. J. C* **80** (2020) 616 [[arXiv:1912.02844](#)] [[INSPIRE](#)].
- [75] CMS collaboration, *Measurements of differential Z boson production cross sections in proton-proton collisions at $\sqrt{s} = 13$ TeV*, *JHEP* **12** (2019) 061 [[arXiv:1909.04133](#)] [[INSPIRE](#)].
- [76] PARTICLE DATA GROUP collaboration, *Review of Particle Physics*, *PTEP* **2020** (2020) 083C01 [[INSPIRE](#)].
- [77] NNPDF collaboration, *Parton distributions from high-precision collider data*, *Eur. Phys. J. C* **77** (2017) 663 [[arXiv:1706.00428](#)] [[INSPIRE](#)].
- [78] A. Buckley et al., *LHAPDF6: parton density access in the LHC precision era*, *Eur. Phys. J. C* **75** (2015) 132 [[arXiv:1412.7420](#)] [[INSPIRE](#)].
- [79] G.P. Salam and J. Rojo, *A Higher Order Perturbative Parton Evolution Toolkit (HOPPET)*, *Comput. Phys. Commun.* **180** (2009) 120 [[arXiv:0804.3755](#)] [[INSPIRE](#)].
- [80] T. Sjöstrand et al., *An introduction to PYTHIA 8.2*, *Comput. Phys. Commun.* **191** (2015) 159 [[arXiv:1410.3012](#)] [[INSPIRE](#)].
- [81] P. Skands, S. Carrazza and J. Rojo, *Tuning PYTHIA 8.1: the Monash 2013 Tune*, *Eur. Phys. J. C* **74** (2014) 3024 [[arXiv:1404.5630](#)] [[INSPIRE](#)].
- [82] M. Grazzini, S. Kallweit and M. Wiesemann, *Fully differential NNLO computations with MATRIX*, *Eur. Phys. J. C* **78** (2018) 537 [[arXiv:1711.06631](#)] [[INSPIRE](#)].
- [83] S. Catani and B.R. Webber, *Infrared safe but infinite: Soft gluon divergences inside the physical region*, *JHEP* **10** (1997) 005 [[hep-ph/9710333](#)] [[INSPIRE](#)].
- [84] P.F. Monni, E. Re and P. Torrielli, *Higgs Transverse-Momentum Resummation in Direct Space*, *Phys. Rev. Lett.* **116** (2016) 242001 [[arXiv:1604.02191](#)] [[INSPIRE](#)].
- [85] W. Bizon et al., *Momentum-space resummation for transverse observables and the Higgs p_{\perp} at $N^3LL+NNLO$* , *JHEP* **02** (2018) 108 [[arXiv:1705.09127](#)] [[INSPIRE](#)].
- [86] O.V. Tarasov, A.A. Vladimirov and A.Y. Zharkov, *The Gell-Mann-Low Function of QCD in the Three Loop Approximation*, *Phys. Lett. B* **93** (1980) 429 [[INSPIRE](#)].
- [87] S.A. Larin and J.A.M. Vermaseren, *The Three loop QCD Beta function and anomalous dimensions*, *Phys. Lett. B* **303** (1993) 334 [[hep-ph/9302208](#)] [[INSPIRE](#)].
- [88] G. Billis, M.A. Ebert, J.K.L. Michel and F.J. Tackmann, *A toolbox for q_T and 0-jettiness subtractions at N^3LO* , *Eur. Phys. J. Plus* **136** (2021) 214 [[arXiv:1909.00811](#)] [[INSPIRE](#)].

- [89] G.P. Korchemsky and A.V. Radyushkin, *Renormalization of the Wilson Loops Beyond the Leading Order*, *Nucl. Phys. B* **283** (1987) 342 [[INSPIRE](#)].
- [90] S. Moch, J.A.M. Vermaseren and A. Vogt, *The three loop splitting functions in QCD: The nonsinglet case*, *Nucl. Phys. B* **688** (2004) 101 [[hep-ph/0403192](#)] [[INSPIRE](#)].
- [91] A. Vogt, S. Moch and J.A.M. Vermaseren, *The Three-loop splitting functions in QCD: The Singlet case*, *Nucl. Phys. B* **691** (2004) 129 [[hep-ph/0404111](#)] [[INSPIRE](#)].
- [92] S. Fleming, A.K. Leibovich and T. Mehen, *Resumming the color octet contribution to $e^+e^- \rightarrow J/\psi + X$* , *Phys. Rev. D* **68** (2003) 094011 [[hep-ph/0306139](#)] [[INSPIRE](#)].
- [93] T. Becher, M. Neubert and B.D. Pecjak, *Factorization and Momentum-Space Resummation in Deep-Inelastic Scattering*, *JHEP* **01** (2007) 076 [[hep-ph/0607228](#)] [[INSPIRE](#)].
- [94] T. Becher and M.D. Schwartz, *Direct photon production with effective field theory*, *JHEP* **02** (2010) 040 [[arXiv:0911.0681](#)] [[INSPIRE](#)].
- [95] I.W. Stewart, F.J. Tackmann and W.J. Waalewijn, *The Quark Beam Function at NNLL*, *JHEP* **09** (2010) 005 [[arXiv:1002.2213](#)] [[INSPIRE](#)].
- [96] C.F. Berger et al., *Higgs Production with a Central Jet Veto at NNLL+NNLO*, *JHEP* **04** (2011) 092 [[arXiv:1012.4480](#)] [[INSPIRE](#)].
- [97] R.V. Harlander, *Virtual corrections to $g g \rightarrow H$ to two loops in the heavy top limit*, *Phys. Lett. B* **492** (2000) 74 [[hep-ph/0007289](#)] [[INSPIRE](#)].
- [98] T. Gehrmann, T. Huber and D. Maitre, *Two-loop quark and gluon form-factors in dimensional regularisation*, *Phys. Lett. B* **622** (2005) 295 [[hep-ph/0507061](#)] [[INSPIRE](#)].
- [99] S. Moch, J.A.M. Vermaseren and A. Vogt, *Three-loop results for quark and gluon form-factors*, *Phys. Lett. B* **625** (2005) 245 [[hep-ph/0508055](#)] [[INSPIRE](#)].
- [100] P.A. Baikov et al., *Quark and gluon form factors to three loops*, *Phys. Rev. Lett.* **102** (2009) 212002 [[arXiv:0902.3519](#)] [[INSPIRE](#)].
- [101] R.N. Lee, A.V. Smirnov and V.A. Smirnov, *Analytic Results for Massless Three-Loop Form Factors*, *JHEP* **04** (2010) 020 [[arXiv:1001.2887](#)] [[INSPIRE](#)].
- [102] T. Gehrmann et al., *Calculation of the quark and gluon form factors to three loops in QCD*, *JHEP* **06** (2010) 094 [[arXiv:1004.3653](#)] [[INSPIRE](#)].
- [103] K.G. Chetyrkin, B.A. Kniehl and M. Steinhauser, *Decoupling relations to $O(\alpha_s^3)$ and their connection to low-energy theorems*, *Nucl. Phys. B* **510** (1998) 61 [[hep-ph/9708255](#)] [[INSPIRE](#)].
- [104] Y. Schroder and M. Steinhauser, *Four-loop decoupling relations for the strong coupling*, *JHEP* **01** (2006) 051 [[hep-ph/0512058](#)] [[INSPIRE](#)].
- [105] K.G. Chetyrkin, J.H. Kuhn and C. Sturm, *QCD decoupling at four loops*, *Nucl. Phys. B* **744** (2006) 121 [[hep-ph/0512060](#)] [[INSPIRE](#)].
- [106] G. Kramer and B. Lampe, *Two Jet Cross-Section in e^+e^- Annihilation*, *Z. Phys. C* **34** (1987) 497 [*Erratum ibid.* **42** (1989) 504] [[INSPIRE](#)].
- [107] T. Matsuura and W.L. van Neerven, *Second Order Logarithmic Corrections to the Drell-Yan Cross-section*, *Z. Phys. C* **38** (1988) 623 [[INSPIRE](#)].
- [108] T. Matsuura, S.C. van der Marck and W.L. van Neerven, *The Calculation of the Second Order Soft and Virtual Contributions to the Drell-Yan Cross-Section*, *Nucl. Phys. B* **319** (1989) 570 [[INSPIRE](#)].

- [109] S. Moch, J.A.M. Vermaseren and A. Vogt, *The quark form-factor at higher orders*, *JHEP* **08** (2005) 049 [[hep-ph/0507039](#)] [[INSPIRE](#)].
- [110] D.A. Dicus and S.S.D. Willenbrock, *Radiative Corrections to the Ratio of Z and W Boson Production*, *Phys. Rev. D* **34** (1986) 148 [[INSPIRE](#)].
- [111] R. Hamberg, W.L. van Neerven and T. Matsuura, *A complete calculation of the order $\alpha - s^2$ correction to the Drell-Yan K factor*, *Nucl. Phys. B* **359** (1991) 343 [[INSPIRE](#)].
- [112] W.-L. Ju and M. Schönherr, *The q_T and $\Delta\phi$ spectra in W and Z production at the LHC at $N^3LL'+N^2LO$* , *JHEP* **10** (2021) 088 [[arXiv:2106.11260](#)] [[INSPIRE](#)].
- [113] M.A. Ebert, B. Mistlberger and G. Vita, *N-jettiness beam functions at N^3LO* , *JHEP* **09** (2020) 143 [[arXiv:2006.03056](#)] [[INSPIRE](#)].
- [114] R. Kelley, M.D. Schwartz, R.M. Schabinger and H.X. Zhu, *The two-loop hemisphere soft function*, *Phys. Rev. D* **84** (2011) 045022 [[arXiv:1105.3676](#)] [[INSPIRE](#)].
- [115] P.F. Monni, T. Gehrmann and G. Luisoni, *Two-Loop Soft Corrections and Resummation of the Thrust Distribution in the Dijet Region*, *JHEP* **08** (2011) 010 [[arXiv:1105.4560](#)] [[INSPIRE](#)].
- [116] A. Hornig et al., *Non-global Structure of the $\mathcal{O}(\alpha_s^2)$ Dijet Soft Function*, *JHEP* **08** (2011) 054 [*Erratum ibid.* **10** (2017) 101] [[arXiv:1105.4628](#)] [[INSPIRE](#)].
- [117] D. Kang, O.Z. Labun and C. Lee, *Equality of hemisphere soft functions for e^+e^- , DIS and pp collisions at $\mathcal{O}(\alpha_s^2)$* , *Phys. Lett. B* **748** (2015) 45 [[arXiv:1504.04006](#)] [[INSPIRE](#)].
- [118] T. Becher and M. Neubert, *Infrared singularities of scattering amplitudes and N^3LL resummation for n-jet processes*, *JHEP* **01** (2020) 025 [[arXiv:1908.11379](#)] [[INSPIRE](#)].
- [119] R. Brüser, Z.L. Liu and M. Stahlhofen, *Three-Loop Quark Jet Function*, *Phys. Rev. Lett.* **121** (2018) 072003 [[arXiv:1804.09722](#)] [[INSPIRE](#)].
- [120] P. Banerjee, P.K. Dhani and V. Ravindran, *Gluon jet function at three loops in QCD*, *Phys. Rev. D* **98** (2018) 094016 [[arXiv:1805.02637](#)] [[INSPIRE](#)].